Chapter 2

THE ENERGY GAP OF CLUSTERS NANOPARTICLES, AND QUANTUM DOTS

Klaus Sattler
Department of Physics and Astronomy, University of Hawaii, Honolulu, Hawaii, USA

Contents

Handbook of Thin Films Materials, edited by H.S. Nalwa
Volume 5: Nanomaterials and Magnetic Thin Films

ISBN 0-12-512913-0/$35.00

1. INTRODUCTION

The energy gap between valence and conduction band is of fundamental importance for the properties of a solid. Most of a material's behavior, such as intrinsic conductivity, optical transitions, or electronic transitions, depend on it. Any change of the gap may significantly alter the material's physics and chemistry. This occurs when the size of a solid is reduced to the nanometer length scale. Therefore, the science and the technology of nanomaterials needs to take into account a bandgap, which is different from that of the bulk.

The aim of the research in this field is to determine experimentally and theoretically the dependence of the energy gap for particles, which are reduced in size to the nanometer range. In addition, effects such as structural changes, lattice contraction, atomic relaxation, surface reconstruction, surface passivation, or strain induced by a host material, can change the gap. We consider nanoparticles of metals, semiconductors, and carbon, with sizes typically smaller than 10 nm, which is the range where size effects become observable. The quantum size effect (QSE) predicts the formation of a bandgap with decreasing particle size for metals and widening of the intrinsic gap for semiconductors.

For clusters of simple metals, two models are used for their description: the tight-binding (molecular orbit) model and the electron-shell model. They can lead to different bandgaps for small clusters and they can lead to different critical sizes for the cluster-to-bulk transition. For divalent metals, a bandgap is expected to open with decreasing particle size due to narrowing and shift of energy bands. The critical size where this transition occurs has been determined by various groups.

For transition and noble metals, a bandgap opens for small cluster sizes and varies strongly with the cluster size. Both, tight-binding and electron-shell approaches have been used theoretically.

The bandgap for semiconductor quantum dots is usually quite well described by an extended effective mass approximation (EMA). This describes a bandgap, which gradually increases for smaller sized particles. It is illustrated in Figure 1. which shows calculated optical band energies for silicon crystallites with respect to their diameter. Experimental bandgap data from photoemission and photoluminescence studies as well as pseudopotential calculations [1] are given in Figure 2.

For very small clusters of semiconductors, the EMA does apply. The basic approach to cluster properties is to start from the atom, and calculate the gap with increasing cluster size. For clusters containing just a few atoms, surface passivation would change their intrinsic properties significantly. Therefore, the properties of a pristine cluster have to be studied with the assumption of a bare surface. Most often, the clusters do not have the bulk atomic structure. One finds for instance that not the diamond structure but rather the close-packed structure gives the global minimum of small silicon clusters. A covalent-metallic transition is predicted which leads to a bandgap for silicon clusters much smaller than the 1.1-eV bulk gap.

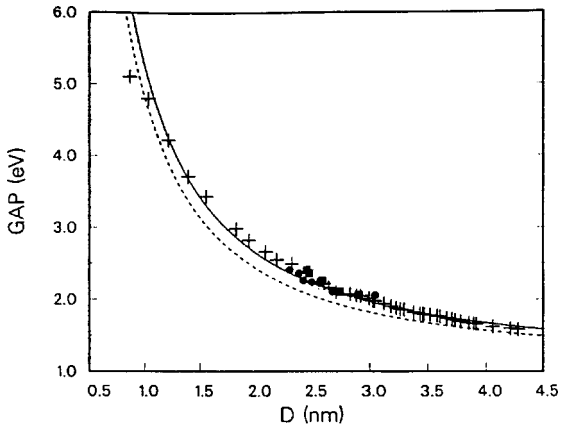

Fig. 1. Calculated optical bandgap energies for silicon crystallites dependent on their diameter [122]. The continuous line is an extrapolation by a $d^{-1.39}$ power law. The dashed curve includes the Coulomb energy between the electron and the hole. The black dots and the squares are experimental results [391]. Reproduced with permission from [122], copyright 1992, American Institute of Physics. Reproduced with permission from [391], copyright 1988, American Physical Society.

Nanoparticles can be produced in many ways and environments. Free clusters and particles are usually generated by cooling of a vapor in contact with an inert gas or during supersonic expansion. Clusters and particles can also be grown on solid supports after atomic vapor has been deposited. A scanning tunneling microscopy (STM) image of a supported silicon cluster is shown in Figure 3. It has a diameter of 2.5 Å and is surrounded by the clean graphite surface, imaged atom by atom.

Morphology and crystalline structure of nanoparticles can be studied by electron microscopy, diffraction methods,

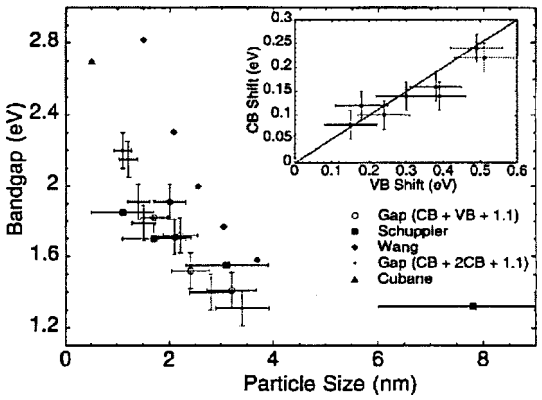

Fig. 2. Bandgap of silicon particles as a function of particle size [1]. Photoelectron data are given by the open and filled circles; the photoluminescence data of Schuppler et al. [586] for oxidized silicon particles is given with the filled squares; the pseudopotential calculation of Wang and Zunger [587] is given with the filled diamonds and the cubane data are given by the filled triangle. The inset shows the conduction band shift versus the valence band shift. Reproduced with permission from [1], copyright 1998, American Physical Society. Reproduced with permission from [586], copyright 1995, American Physical Society. Reproduced with permission from [587], copyright 1996, American Physical Society.

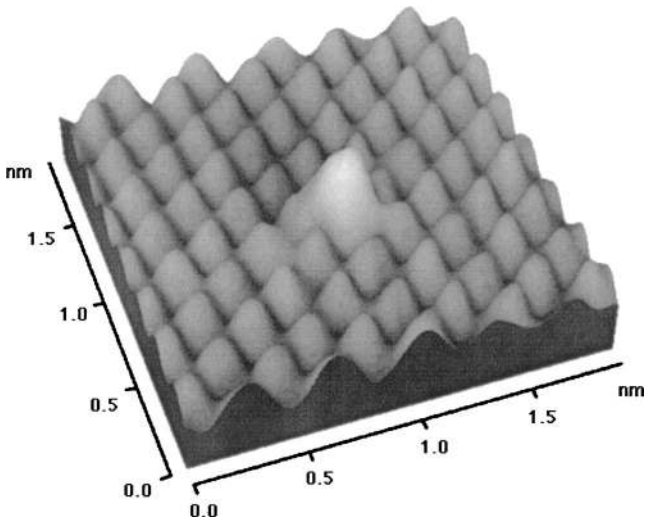

Fig. 3. STM image of a 2.5-Å silicon cluster supported on the substrate of highly oriented pyrolytic graphite (HOPG) [48]. Reproduced with permission from [48], copyright 2000, American Physical Society.

surface reactivity, and Raman spectroscopy. The question is if the particles are fragments of the crystalline bulk or if they have their own atomic structure. Silicon and germanium nanoparticles formed as deposits or composite materials typically show nearly spherical geometries in high-resolution transmission electron microscopy (HRTEM) for particles having diameters as large as 200 nm [2–4]. Frequently, micrographs reveal lattice fringes corresponding to the crystalline diamond phases, such as the {111} interplanar spacings of 0.31 nm for Si and 0.33 nm for Ge. The atomic spacing can critically influence the electronic structure of the particles. A change to reduced lattice constant was observed for Ge particles of diameter less than 4 nm [3]. A nanoparticle with a diamond crystal structure is shown in Figure 4.

For silicon particles, a structural transformation is predicted for smaller sizes. In molecular dynamic studies, Si_n cluster growth follows nondiamond structure up to $n = 2000$ (ca. 4 nm diameter) at which point crossover to a diamond growth pattern occurs [5]. Large crystalline Si and Ge particles, with $d > 50$ nm have their Raman peaks unchanged when the size is varied [2]. Therefore, the critical size for structural transfomation of silicon particles is probably around 4 nm.

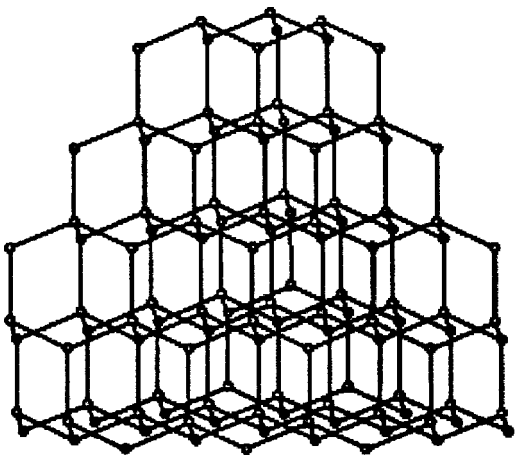

Fig. 4. Model of a 120-atom silicon cluster with a diamond-type crystal structure.

Small carbon clusters and nanoparticles can have amorphous, graphitic, diamond, or cage structures. In addition, mono- and polycyclic rings, chains, and other low-density structures are possible. We will report bandgap measurements on vapor-grown (amorphous) carbon particles as a function of size.

There is no strict distinction in literature between the terms "clusters, nanoparticles, and quantum dots." However, often "clusters" are used for agglomerates of very few atoms, "nanoparticles" are used for larger agglomerates (usually of metals or carbon), and "quantum dots" are used for semiconductor particles and islands where quantum confinement of charge carriers or excitons determines their properties.

In the following sections, we give the status of research of the bandgap and we consider possible applications of the particles for optoelectronic and other uses.

2. EXPERIMENTAL TECHNIQUES

2.1. Optical Spectroscopy

A method for probing the band structure of semiconductors is to measure the optical absorption or luminescence spectrum. In the absorption process, a photon of known energy excites an electron from a lower to a higher energy state. For determination of the fundamental gap, band-to-band transitions are probed. However, because the transitions are subject to selection rules, the determination of the energy gap from the "absorption edge" of the luminescence peak is not a straightforward process.

Because the momentum of a photon is very small compared to the crystal momentum, the optical process should conserve the momentum of the electron. In a direct-gap semiconductor, momentum-conserving transition connects states having the same k-values. In an indirect bandgap, semiconductor momentum is conserved via a phonon interaction. Although a broad spectrum of phonons is available, only those with the required momentum change are usable. These are usually the longitudinal- and the transverse-acoustic phonons. In addition, the indirect process is a two-step event. Therefore, indirect optical processes have very low transition probabilities.

Clusters and nanoparticles of a semiconductor may be optically active even though the bulk material is not. This can have various reasons: The energy band structure and the phonon distribution can be entirely different for clusters compared to the crystalline bulk. Clusters have localized states that are not present in the bulk. The transition from an upper to a lower energy state may proceed via one or more localized intermediate states. The intermediate steps may or may not be radiative. Yet, they have a profound effect on the actual efficiency of the radiative transition.

Nanoparticles have many of their atoms at surface positions. A surface is a strong perturbation to any lattice, creating many dangling bonds. These unsaturated bonds are energetically unfavorable. The particles can lower their free energy by side- and back-bonding of these bonds. For silicon and germanium particles, this can be at the cost of giving up the sp^3-hybridization. Therefore, the sp^3-characteristics of the diamond-like bulk may not be present for these small particles.

A high concentration of deep and shallow levels can occur at the surface of nanoparticles, and these may act as electron-hole recombination centers. The distribution of surface states is discontinuous for small clusters, but can be continuous for nanoparticles, where the surface consists of several facets. When electrons or holes are within a diffusion length of the surface, they will recombine, with transitions through a continuum of states being nonradiative.

Optical spectroscopy studies of nanoparticles demonstrate their atomlike discrete level structure by showing very narrow transition line widths [6–11]. Optical techniques probe the allowed transitions between valence band and conduction band states for nanoparticles which do not have defect or impurity states in the energy gap. Interpretation of optical spectra often is not straightforward and needs correlation with theoretical models [12–14].

Photoluminescence peak energies were found to increase with decreasing particle size, for instance from ~1.3 to 1.6 eV for Si nanocrystals that decrease in size from 5 to 2 nm [15]. Nanocrystalline silicon films showed optical bandgaps of 1.9 to 2.4 eV [16]. The photoluminescence results from various studies are plotted in Figure 5 [17]. For Ge nanocrystals, blue photoluminescence was observed [18].

The bandgap of semiconductor clusters depends strongly on their atomic structure. Fullerenes, for instance, have bandgaps strongly varying with size and pentagon–hexagon arrangements. Amorphous carbon (a-C) has a bandgap of typically between 0.4 and 0.7 eV and can behave like a semiconductor. In some samples of a-C, energy gaps up to 3 eV were observed [19]. There is a significant bandgap variation for differently prepared a-C samples. This is related to varying microscopic mass densities and described theoretically by microcrystalline and cluster models [20]. Tetrahedral amorphous carbon (ta-C) contains more than 80% sp^3-bonded carbon [21]. Clusters and rings with sp^2-coordination in the otherwise amorphous material have been suggested to model this material. A gap of ~2 eV is found for ta-C [22].

Thin films have been prepared that consist of 5- to 50-nm-sized Si crystallites embedded in an amophous silicon matrix [23]. The silicon crystallites are embedded in films of SiO_2 glasses [24, 25]. Semiconductor-doped glasses (SDG) have large nonlinear susceptibilities for optical transitions near their optical bandgap and a fast electron-hole recombination time of psec order. Bandgaps of Si particles in SiO_2 in the range 1.2 to 1.5 eV have been observed and depend on the film preparation [24].

In early studies of photoluminescence (PL), surface defects were often considered to control the optical properties of quantum dots [26–32]. Work [7, 33–38] on CdSe QDs however suggests that the near-edge emission (which leads to the determination of the bandgap) is determined by their core, and not by the surface structure.

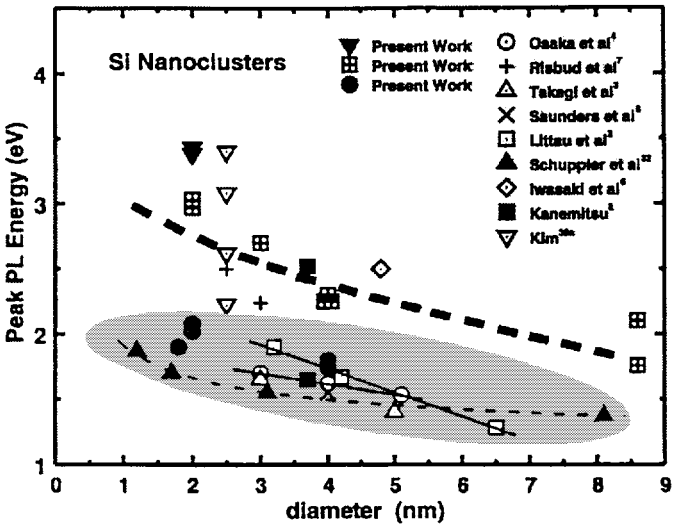

Fig. 5. Summary of data on peak luminescence versus silicon particle size, after Wilcoxon, Samara, and Provencio [17] with data from Osaka et al. [588], Risbud, Liu, and Shackelford [589], Takagi et al. [267], Saunders et al. [590], Littau et al. [269], Schuppler et al. [402], Iwasaki, Lda, and Kimura [591], Kanemitsu [592], and Kim [367].

2.2. Scanning Tunneling Spectroscopy

Historically, tunneling spectroscopy with metal-insulator-metal (MIM) tunnel junctions was first demonstrated by Giaever [39]. His MIM tunneling experiment provided a direct measurement of the energy gap of superconductors, which was a critical evidence for the Bardeen-Cooper-Schrieffer (BCS) theory of superconductivity.

A systematic method of obtaining local tunneling spectra with STM was developed by Feenstra, Thompson, and Fein [40]. It is an extension of the tunneling junction experiment of Giaever. Scanning tunneling spectroscopy (STS) is complementary to topographic imaging by STM. It can be accomplished in a number of ways. Most STS studies today are performed with constant tip-sample separation at a fixed location on the surface. This is accomplished by momentarily interrupting the feedback controller and then ramping the applied voltage over the desired interval while simultaneously measuring the tunneling current. If no spatial resolution is required and a large flat area is investigated, the method is straightforward [41]. However, if one wants to correlate the tunneling spectra with the local surface structure, the I–V measurement must be performed together with the topography measurement. While the tip is scanning over the sample surface, a map of tunneling spectra is generated.

Scanning tunneling spectroscopy has been applied extensively to determine the electronic structure of semiconductors [42–44], superconductors [45], and metals [46]. STS is used to study solid surfaces and thin films [47] as well as adsorbed

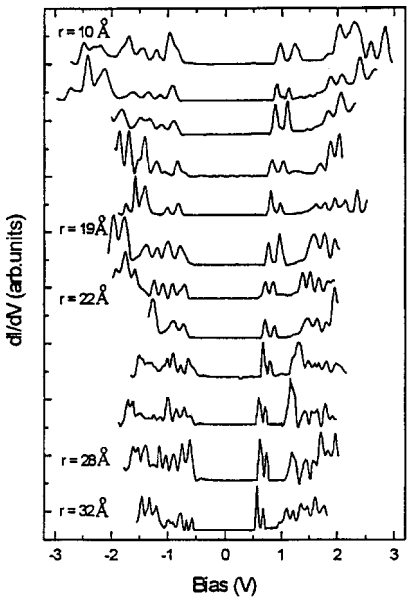

Fig. 6. Size evolution of *dI/dV* versus *V* characteristics of InAs quantum dots, measured by scanning tunneling spectroscopy [49]. Reproduced with permission from [49], copyright 2000, American Physical Society.

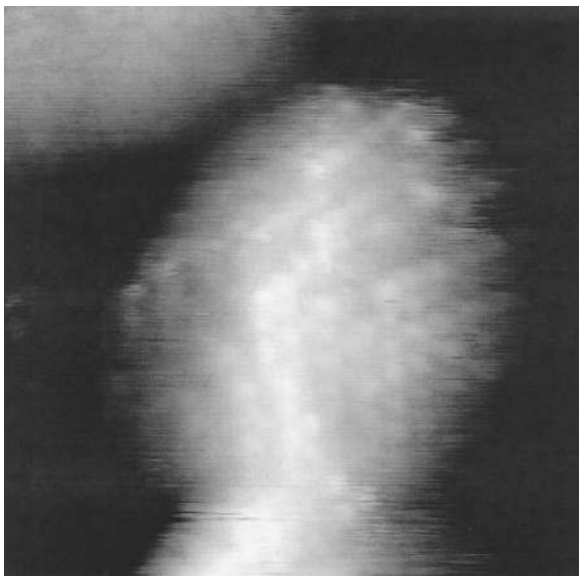

Fig. 7. An 11×11-nm STM image of a palladium particle, with atomic resolution [475]. Reproduced with permission from [475].

clusters [48, 49], fullerenes [50, 51], and molecules [52–54]. STS studies were reported for semiconductor quantum dots such as Si [48], CdS [55], CdSe [56, 57], InAs [49, 58] and others [59–61]. In addition, tunneling spectra of metal quantum dots have been obtained [62, 63]. A sequence of STS spectra is shown in Figure 6 for quantum dots of InAs [49].

STS theory has its focus mostly on the relationship between I–V curves and the local density of states (LDOS) [64–71]. Most calculations used the assumption of imaging at low bias voltage and were following the theory of Tersoff and Hamann [64]. In some theoretical treatments, this has been extended to finite bias voltages [72–74]. An STS theory has been developed specifically for semiconductors [75], since they need a treatment different from the one for metals [76, 77].

Scanning tunneling microscopy can be used to obtain the atomic structure of particles. This is illustrated in Figure 7, which shows an STM image of a palladium particle with atomic resolution. The combined use of STM and atomic force microscope (AFM) [78, 79] can also give information about the interplay between atomic and electronic structure. The STM probes the density of states (DOS) of a sample at the Fermi level E_F (if a small bias voltage of a few millivolts is applied). The AFM probes the total DOS of the valence electrons, over a relatively wide energy range. This can lead to differences in the images obtained from the two methods. For instance, when assembled nanoparticles are imaged, and there are low-energy grain boundaries between the particles, these boundaries usually have different DOS at E_F, well seen in STM imaging. Therefore, the particles are individually imaged by STM. The AFM however is not sensitive to small DOS variations at E_F and therefore does not well resolve particles with low-energy grain boundaries. This has been seen in experimental studies of nanophase materials [79].

As expected from the Bardeen formula (derived for MIM tunnel junctions) [80], the tip density of states (DOS) plays an equal role as the sample DOS in determining the tunneling spectra. In an STS experiment, the goal is to obtain the DOS of the sample, and one requires a tip with a constant, structureless DOS. When the tip is a metal, there is a sharp onset of the tunneling current when the bias voltage exceeds half the gap energy and this is independent of the tip DOS. This argument has been used by Giaever and many others for the determination of bandgaps in tunnel junctions and it applies to gap studies of nanoparticles by STS as well.

For nanoparticles, a gap may appear in the I–V curve which is not related to the electronic structure. If the particle charges up, a Coulomb blockade gap may be the dominant I–V feature around zero bias [81–83]. This gap is size dependent, increasing with smaller particle diameter [84]. Single-electron charging has also been studied for molecules in STS experiments [85].

The effect of the Coulomb blockade can be seen from the appearance of supported clusters in STM images. On a gray scale image, a supported cluster usually appears brighter than the substrate. If the substrate in an STM image is set to a gray level, a cluster appears white. If however the cluster is charged, the tunneling current is blocked and the cluster appears black.

STS has been used to study the interplay between single-electron tunneling (SET) and quantum-size effects. This can experimentally be observed when the charging energy of the particle by a single electron is comparable to the electronic level separation, and both are larger than $k_B T$ [50].

In optical spectroscopy, the bandgap is determined from allowed transitions between valence and conduction band states in the particle. In tunneling experiments, on the other

hand, the discrete levels in a particle's valence and conduction band are probed separately. Therefore, STS provides complimentary information on the electronic structure of the particles.

3. THEORY

3.1. Methods and Results for Metal Clusters

The electronic structure of metal clusters is calculated within two theoretical ab initio approaches: density functional calculations in the local-density approximation (LDA) [86] and Hartree-Fock configuration interaction (HFCI) calculations [87]. The LDA gives accurate ground state properties for neutral and charged clusters, but does not well describe excited states. Simulated annealing [86] can be used together with LDA to find the atomic structure of a cluster in the ground state. The calculations can yield the vertical detachment energies (VDE) of metal clusters which are related to the electron affinity [88]. The HFCI method yields electronic ground and excited states of neutral and charged metal clusters. The optimum geometry of a cluster can only be determined for very small sizes because the calculations for larger clusters require too much computer time.

For metal clusters with highly delocalized valence electrons, the electronic-shell model can be applied [89]. It assumes that the valence electrons of each atom in the cluster become free electrons confined by the boundaries of the cluster. For spherical clusters, the eigenstates are electronic shells with defined angular momentum. Shell closings occur at $n = 2, 8, 18, 20, 34, 40, \ldots$ electrons which lead to magic numbers for alkali metal clusters with these n-values. With increasing cluster size, the 1s, 1p, 1d, 2s, 1f,…shells become successively occupied.

The shell model neglects the core potentials of the atoms in the cluster. It uses the jellium model, which considers the positive charges of the atoms being smeared out to a homogeneous background. Therefore, the model is not used to determine properties which are related to the atomic structure of the clusters.

While metal clusters with closed electron shells are spherical, the clusters with open electronic shells are deformed from the spherical shape. In theory, this deformation has been studied within the jellium approach [90–95], with ab initio calculations [96–98], and tight-binding models [99, 100]. The clusters are deformed due to the Jahn–Teller effect [101, 102]. The deformations have effects on the electron-shell energies [101].

Ab initio molecular dynamics calculations were used to study the deformations of Na clusters at high temperatures (500–1100 K) [103]. A large highest occupied molecular orbital–lowest unoccupied molecular orbital (HOMO–LUMO) gap of 1.1 eV was found for the closed-shell cluster Na_8. This gap is unchanged at 550 K, where the cluster is liquid-like. In the open-shell Na_{14} the deformation opens a gap which remains in the liquid state. The liquid Na_{14} cluster favors axially deformed shapes, with two isomers, prolate and oblate. The deformation is driven by the opening of the HOMO–LUMO gap. Among three isomers for Na_{14}, prolate, oblate, and spherical, the prolate isomer has the lowest energy and the highest HOMO–LUMO gap (0.4 eV). When the Na_{14} cluster is heated to 1100 K, the cluster structure oscillates between different isomers and the time-averaged level density no longer shows a pronounced HOMO–LUMO gap.

The shell model is not restricted to alkali metal clusters. Electron detachment energies of Pb_n^- ($n = 24$–204) [104] for instance are well described by local-density approximation in the spherical jellium model.

The simplest atomic structure is the linear chain. For linear arrangement of metal atoms, one usually obtains HOMO–LUMO gaps which oscillate between odd and even numbers of atoms per cluster. This is illustrated in Figure 8, which gives the orbital energy distributions of linear Cu_n clusters [105] (up to $n = 10$).

Transition metal clusters are particularly interesting for studies of the formation of the bulk band structure with increasing particle size. Transition metal atoms include both localized 3d-electrons and delocalized 4s-electrons. It can be expected that these states have a very different cluster size dependence. Cu, for example, has the atomic structure $3d^{10}4s$. Like the alkali atoms, Cu has a single s-electron outside a closed shell. The 3d-states however lie just below the 4s-states in energy and are expected to influence the cluster properties. In bulk Cu, the 3d-states contribute significantly to the density of states at the Fermi level, which leads to the very high electrical conductivity of Cu. In Cu clusters, the 4s-states are delocalized and therefore show strong discontinuous size-dependent variations, whereas the 3d-band evolves monotonically with cluster size. The calculated density of states for Cu_8 and Cu_{20} clusters is shown in Figure 9.

In photoemission experiments, the electron affinities for Cu clusters have been studied as a function of cluster size [106–108]. A multitude of distinct features was observed in the spectra [108] and attempts were made to explain these features theoretically [109–111].

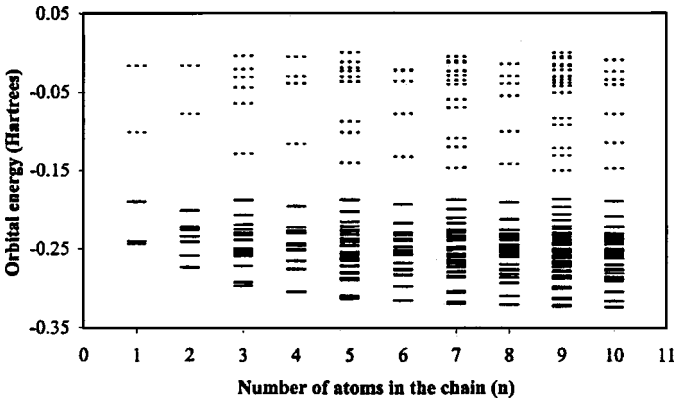

Fig. 8. Occupied (continuous line) and unoccupied (dashed line) energy levels for linear Cu atomic chain [105]. Energies in the neighborhood of the HOMO and LUMO are shown. Reproduced with permission from [105], copyright 1999, American Chemical Society.

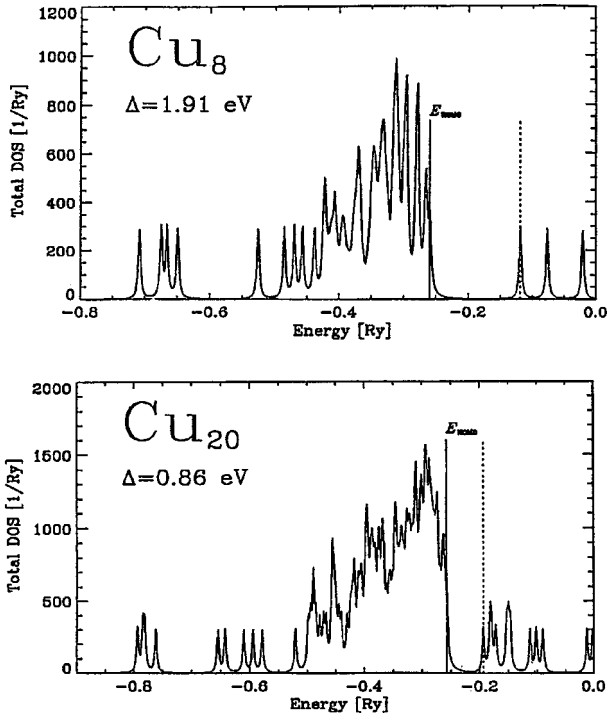

Fig. 9. Total electronic density of states calculated for the two closed-shell clusters Cu_8 and Cu_{20} in their lowest energy structures [102]. Reproduced with permission from [102], copyright 1994, American Physical Society.

Clusters from noble metals exhibit similarities to simple metal clusters with respect to their electronic structures. This is well illustrated with tight-binding calculations for Cu clusters ($n = 2$–95) [102] (Figure 10). The clusters have large HOMO–LUMO gaps with the magic (electron) numbers $n = 2, 8, 18, 20, 34$, which are the numbers known from the spherical shell model. Shell closures result in particularly large HOMO–LUMO gaps for these clusters. The theoretical and experimental values for Cu_8 coincide very well, 1.91 [102] and 1.93 eV [112], respectively. A lower value of $E_g = 1.33$ eV for Cu_8 was also calculated [113]. For the closed-shell Cu_{20} cluster, $E_g = 0.83$ eV is obtained. The typical band features of bulk Cu are not yet evolved for Cu_{20}.

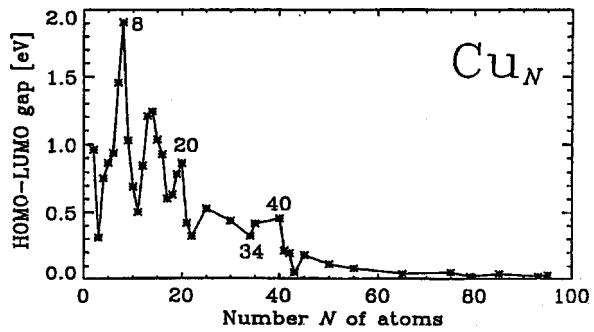

Fig. 10. HOMO–LUMO gap calculated for Cu clusters versus size [102]. Reproduced with permission from [102], copyright 1994, American Physical Society.

The same general characteristics for the electron level structure of Cu clusters has been obtained from several studies [102, 114, 115]. In contrast to the bulk, Cu clusters exhibit an almost complete s–d-band separation. Low lying occupied valence states have s-character, whereas the higher occupied levels have predominantly d-character. The states directly at the HOMO and the unoccupied states have mostly s–p-character with minor d-contributions. This shows that the atomic d-electrons form a narrow d-band in the clusters with the extended s–p-states being located in separate energy regions, below and above the d-band. Hybridization between these two band characters is found to be small. The molecular orbitals of the extended states are associated with the states of the electron-shell model. An s- and d-band separation similar to that for Cu clusters has also been obtained in calculations of surface slab model clusters Ni_{20} and Ni_{51}, where the HOMO was found to have s-character [116]. We note that bulk Cu and Ni is characterized by completely overlapping s- and d-bands.

3.2. Methods and Results for Semiconductor Clusters

Early theoretical studies of semiconductor particles used the effective mass approximation (EMA) [117–119]. This approach can sometimes be successful in fitting luminescence data [120]. The EMA assumes that the semiconductor bands are parabolic and that the kinetic energies of electrons and holes can be expressed in terms of their effective masses, m_e and m_h. Direct bandgap semiconductors have parabolic bands at the top of the valence band and the bottom of the conduction band. Therefore, the EMA gives a good estimate of the bandgap in large clusters of direct gap materials. The approximation is not accurate for states away from the point, or for indirect bandgap semiconductors.

Early calculations using EMA assumed an infinite potential step at the cluster surface, and applied perturbation theory to solve the Schroedinger equation with the effective mass (EM) Hamiltonian. The calculated exciton energies agree qualitatively with the experiment for larger clusters, but are usually too large for small clusters [118, 119]. Calculations with a more realistic finite potential step at the surface have given results in much better agreement with the experiment [121].

First-principles and semiempirical theories show that the EMA-derived bandgap of semiconductor particles is overestimated. The gap-to-diameter dependence is still described by an inverse power law, but with a smaller exponent [122]. Another applied method is an empirical pseudopotential theory, which has been used for nanoparticles by imposing a boundary condition on the pseudopotential solution for an infinite lattice [123–125]. There is better agreement with experiments compared to EMA, but the method does not include surface effects, as an infinite potential step is required at the surface. Yet, the surface of nanoparticles may influence or may even dominate the particle properties. Many experiments, as, for example, time-resolved fluorescence measurements [29], or electrooptical Stark effect measurements [126] show the

surface trapping of excited charge carriers. Such results cannot be explained by models, which account for size quantization alone but ignore the surface. Green's function recursion within the tight-binding approximation was also used to estimate bandgaps and exciton energies of nanoparticles [127]. The method models the atomic structure of clusters realistically and can be used to study surface effects.

Theoretically, small silicon clusters were first proposed to be fragments of the crystalline bulk [128, 129]. The clusters were assumed to have a diamond structure with nonrelaxed surface atoms. Such tetrahedral-bond-network (TBN) clusters have many dangling orbitals and very low average coordination numbers. In further studies, crystalline structures were shown either to correspond to high-energy local minima or to be highly unstable [130–134]. Ab initio electronic structure calculations have been used to predict lowest energy structures for Si clusters in the size range 2–14 atoms [130, 131, 135–144]. Raghavachari [130, 139], Raghavachari and Logovinsky [140], and Raghavachari and Rohlfing [141] have used (uncorrelated) Hartree–Fock (HF) wave functions to optimize the cluster structures. Tomanek and Schlüter [142, 143] have used a local-density functional (LDF) method, Pacchioni and Koutecky [131] and Balasubramanian [135, 136] performed configuration interaction (CI) calculations, and Ballone et al. [137] used simulated annealing techniques for geometry optimization. All of these calculations are largely in agreement as to the equilibrium structures for very small silicon clusters.

4. METALS

4.1. Alkali Metal Clusters

Clusters of metal atoms encompass the evolution of collective properties from an atom to a solid. In particular, the development of metallicity with increasing size is a fascinating field to study [145]. The free atom has sharp and well-separated electronic energy levels, which undergo major changes once the atoms are assembled to clusters. With increasing particle size, the HOMO–LUMO gap becomes gradually narrower and finally vanishes. A nonmetal–metal transition occurs as a function of size. Experimentally, the closure of the gap is observed in the shrinking difference between ionization potential and electron affinity. The Kubo effect (the quantum size effect, QSE) describes the discrete levels in small systems. Yet, the QSE is a continuum approach, which breaks down at very small particle sizes.

A number of experimental [146] and theoretical [147–151] studies of alkali clusters have been performed. The alkali metals have simple electronic structures as they have energy bands very similar to those of free electrons. For alkali metal clusters, two theoretical models are used for describing their electronic properties. The jellium model has been successful for the calculation of mass spectra and optical spectra [152, 153]. The valence electrons are treated as completely free, only confined to a spherical box with a constant positive background. The model leads to a shell structure for the electrons (electron-shell model), For other properties, quantum chemical calculations [147–149] were successfully used (molecular orbit model). They are expensive in theoretical input and computing time, but lead to the best results for very small clusters with less than about 50 atoms. The two models yield different bandgap behavior as a function of particle size. An overlap of the two theories has been achieved by including pseudopotentials to the jellium calculation [150].

4.2. Noble and Transition Metal Clusters

For metal particles, the quantum-size effect (QSE) predicts the opening of a gap with decreasing size. Experiments usually show HOMO–LUMO gaps much smaller than predicted by the QSE. In addition, the nonmetal to metal transition seems to occur at quite small cluster sizes. For example, while Pt clusters with up to six atoms revealed nonzero energy gaps [154], 60-atom Pt clusters showed zero-energy gaps [155]. For Ni clusters with $n < 20$, ab initio molecular orbit calculations yield HOMO–LUMO gaps up to 0.25 eV, approaching zero at about $n = 16$ [156]. Studies of photodetachment spectroscopy [157] suggest that the electronic structure of Ni clusters approaches the bulk limit for $n > 14$, while measurements of vertical ionization potentials [158] put this limit beyond $n = 100$. Structural, electronic, and magnetic properties are strongly correlated for transition metal clusters such as Ni_n [159].

In a study of vanadium clusters V_n ($n < 65$), three size regions of spectral evolution were observed: molecular-like behavior for $n = 3$–12, transition from molecular to bulklike for $n = 13$–17, and gradual convergence to bulk for $n > 17$ with bulk behavior at about $n = 60$ [157]. For Mn clusters, the strong dependence of the gap on the cluster structure was demonstrated. For Mn_5, there are several isomers whose energies lie very close to the energy of the ground state but with the HOMO–LUMO gap varying between zero and 2.63 eV [160]. For Cu_{13}, a gap of 0.36 eV was calculated [161]. This value is smaller than the experimental results of about 0.7 eV [109]. In the range $4 \leq n \geq 30$, the gaps for Cu clusters vary between 0.25 and 1.4 eV but do not approach zero at $n = 30$ [109] (Fig. 11). The density of states for Cu clusters has almost fully converged to the bulk DOS for $n \approx 500$ [102]. Theoretical studies of Al clusters with $n \leq 15$ show strong discontinuous size-dependent gap variations (between 0.2 and 1.2 eV) [162] (Fig. 12). They roughly agree with earlier theoretical studies where HOMO–LUMO gaps in the range 0.4 to 2 eV were found for Al clusters up to $n = 13$ [163]. The gap was calculated to be close to zero for Al clusters with $n \geq 54$ [163] (Fig. 13). For small Ag_n ($n = 2-6$), the HOMO–LUMO gaps were experimentally determined: 6.5 eV (Ag_2), 3.8 eV (Ag_3), 5.0 eV (Ag_4), 4.2 eV (Ag_5), 5.1 eV (Ag_6) [164]. An odd–even effect in these values is visible.

Aluminum clusters show a strong magic number tendency for $n = 13$ [165, 166]. Therefore, the gap for Al_{13}has typically a much greater value compared to the other clusters in this size range [163]. A gap of 1.89 eV was obtained by photoemission for anions of Al_{13}, dramatically exceeding the gaps of

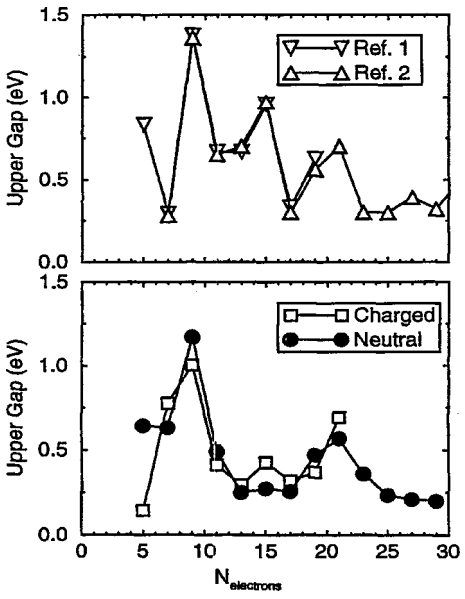

Fig. 11. Gap between the two upper electronic levels for odd-electron clusters. Upper panel: experimental results on Cu_n^- [593, 594]. Lower panel: calculations for neutral and negatively charged Cu_n^- clusters. The data are plotted as a function of the odd-electron number [109].

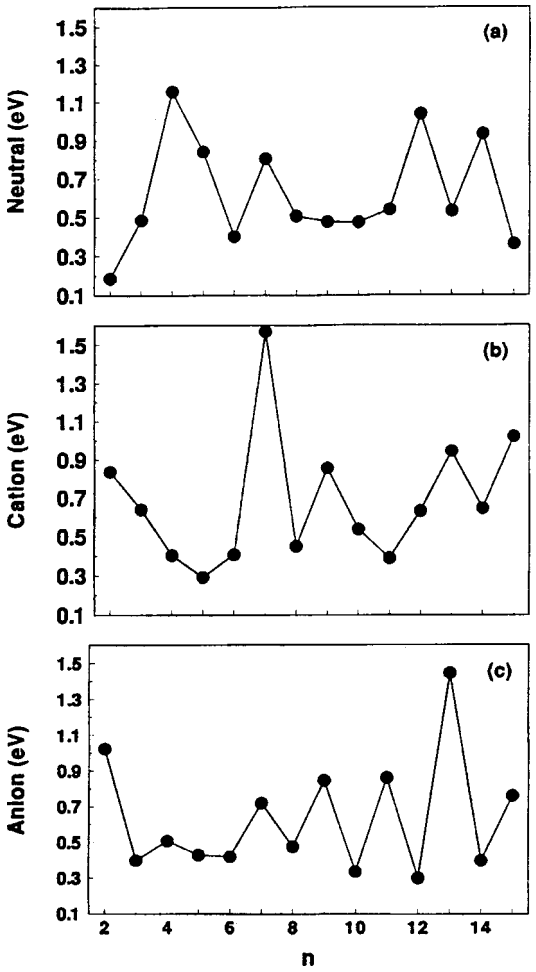

Fig. 12. HOMO–LUMO gap calculated for (a) neutral, (b) positively charged, and negatively charged Al clusters [162]. Reproduced with permission from [162], copyright 1999, American Institute of Physics.

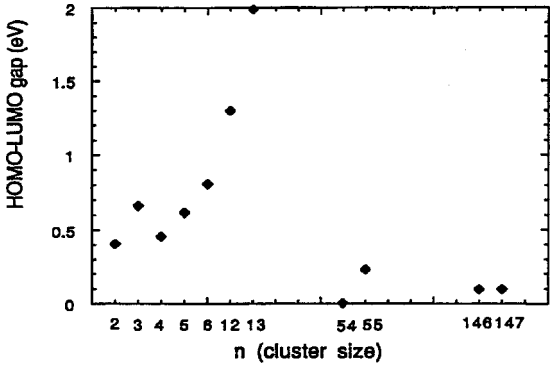

Fig. 13. HOMO–LUMO gap calculated for neutral Al clusters [163]. Reproduced with permission from [163], copyright 1993, American Physical Society.

0.25 and 0.32 eV of Al_{12} and Al_{14}, respectively [167]. Angle-resolved photoemission studies indicate that the nonmetal to metal transition for Pd particles is at about 25 Å [168]. Photoelectron spectroscopy studies of Ti_n ($n = 3-65$) yield electron affinities (EA) which increase monotonically toward the bulk work function starting from Ti_8 [169]. The EAs of the larger clusters are well described by the spherical drop model. This suggests that titanium clusters become metallic at $n \approx 8$. A number of first-principles studies were performed for small Ni clusters but with large discrepancies in the calculated ionization potentials [156]. Such discrepancies arise from the particular choice of geometries, interatomic spacing, atomic basis functions, approximations in the exchange-correlation potentials, and the treatment of the core electrons.

Scanning tunneling spectroscopy has been applied to determine the HOMO–LUMO gap of metal clusters. The tunneling conductance through the clusters decreases markedly for a range of bias voltages around zero and for small enough clusters. Pd, Ag, Cd, and Au clusters with diameters greater than 1 nm show the zero-gap characteristics of the bulk metals in STS experiments [170]. Below 1 nm, an energy gap opens, and its value increases with smaller cluster sizes. Energy gaps up to 70 meV were measured. These are much smaller than the gap values obtained from calculations.

Metal clusters usually have an atomic structure which is different from that of the bulk. Studies by scanning transmission electron diffraction (STED) showed that Pd clusters with diameters less than 20 Å prefer the non-fcc (face-centered cubic) icosahedral over the standard fcc bulk structure [171]. On the other hand, studies of Cu clusters with extended X-ray absorption fine structure (EXAFS) indicated fcc structure even for clusters with about 13 atoms [172]. For Au, Pt, Rh, Ni, and Ag clusters, the fcc bulk structure seems to be favored over the icosahedral structure for a diameter bigger than about 20 Å [173, 174].

The reactivity of small clusters with simple molecules can vary significantly with cluster size [175–184]. Features in the electronic structure of the bare clusters can be obtained from measurements of vertical detachment energies (approximately giving the electron affinities) and the ionization potentials [177, 185–188]. The reactivities of neutral Nb and Fe clusters

with H_2 were found to correlate with their ionization potential [185, 189]. This shows that the reactivity of a cluster is linked to its electronic structure. Various models have been proposed for the size-dependent reactivity. The most obvious explanation is the promotion of an electron from the cluster to the antibonding state of the attached molecule [190]. Other models have emphasized the details of the electronic structure of the clusters [191]. In studies of photoelectron spectra of Fe, Co, and Ni clusters, it was found that the size dependence of reactivity with H_2 molecules correlates well with the HOMO–LUMO gap variation [186].

The reactivity of metal clusters with inert gases such as argon and krypton can be very similar to those with hydrogen [192]. In addition, the measured reactivities can be almost independent of the charge state of the clusters (neutral, positive, negative) [176, 178, 182, 189]. This suggests that the electron transfer model, based on the reactivity correlation with the electronic structure needs to be replaced by an alternative model in some cases. The geometry of the clusters may instead determine the adsorption characteristics. It has been considered in some cases to be responsible for the reactivity of metal clusters [193, 194].

Magic number clusters are highly stable due to electronic or geometric shell closings. They have high binding energies per atom, large ionization potentials, and wide HOMO–LUMO gaps. This is well seen with Nb clusters, which show shell closings for Nb_8, Nb_{10}, and Nb_{16}. These magic clusters are relatively unreactive for hydrogen absorption [195]. The reactivity pattern for Nb clusters are roughly independent on the charge state of the clusters, with Nb_n^+, Nb_n^-, and Nb_n^0 giving similar results. This indicates that the geometrical structure of the clusters might be important for their chemical activity. The dependence of HOMO–LUMO gaps for Nb clusters is shown in Figure 14.

For a comparison of theory with experiments, one needs to take into account that neutral, positively and negatively charged clusters may have different atomic and electronic structures. This has been illustrated with calculations for Al_n [162], Cu_n [196], and others. For example, while the bandgap for the anion Al_{13} of 1.5 eV is much higher than the gaps of 0.3 and 0.4 eV gaps for Al_{12} and Al_{14}, respectively, $n = 13$ is much less magic for the neutral and positively charged clusters. Another magic Al cluster is Al_7, but only if positively charged. Gaps of 1.6, 0.40, and 0.45 eV were calculated for Al_7^+, Al_6^+ and Al_8^+, respectively.

Structural isomers may also differ considerably in their electronic properties. This has been shown by a number of theoretical studies, for instance for Co_n (n =1–8) [197], Cu_n (n =2–5) [196], Cu_n ($n \leq 9$) [111], Al_5 [198], and others. Various isomers of Na_{19}^+ lead to very different photoabsorption spectra [199].

Bond-length contraction is another effect, which has an influence on cluster properties. Metal clusters usually have reduced interatomic distances compared to the bulk metals. The bond-length contraction $\Delta R/R$ becomes very pronounced for clusters with just a few atoms. This is illustrated in calculations of rhodium clusters with $\Delta R/R = 17\%$ (Rh_2), 10.9% (Rh_3), 7.4% (Rh_4), 5.8% (Rh_6) and 4.0% (Rh_{12}) [200]. Average interatomic distances and coordination numbers for Ni_n (n = 3–23) have been calculated [201] and are shown in Figure 15. For Pd clusters, several theoretical studies predict a

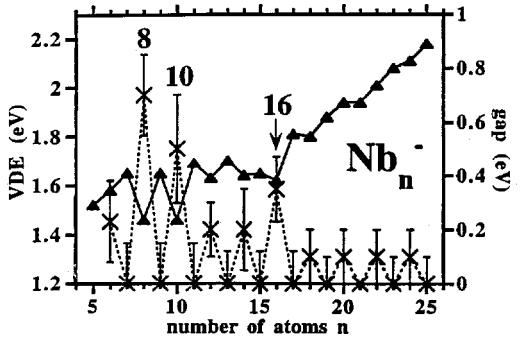

Fig. 14. Vertical detachment energies (triangles, left scale) and HOMO–LUMO gaps (crosses, right scale), extracted from photoelectron spectra of Nb_n^- clusters [195]. Reproduced with permission from [195], copyright 1998, American Institute of Physics.

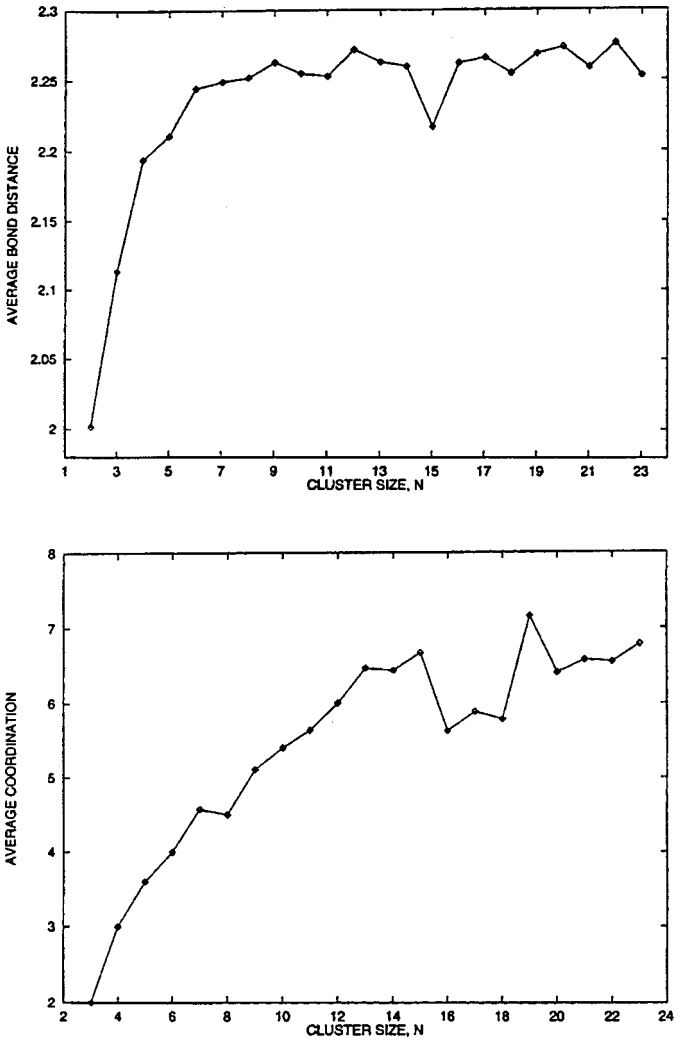

Fig. 15. Average interatomic distances and coordination numbers calculated for Ni clusters [201]. Reproduced with permission from [201], copyright 1997, American Chemical Society.

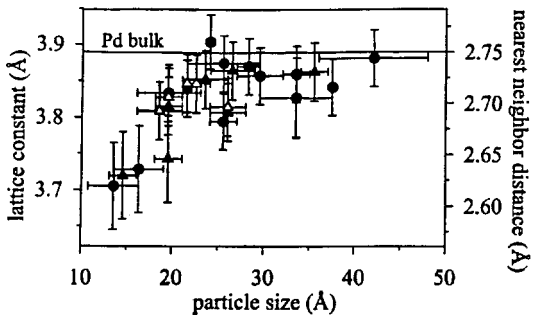

Fig. 16. Atomic spacings in supported Pd clusters as a function of cluster size evaluated from electron diffraction patterns [206]. Reproduced with permission from [206], copyright 1999, American Chemical Society.

decrease of the lattice constant with a decreasing cluster size [202–205]. An experimental study on Pd particles in the size range 15–45 Å showed a lattice constant reduction of about 5% [206] (Fig. 16). A reduction in lattice constant has also been observed for Ta and Pt clusters [207, 208]. In general, a cluster may be viewed as bulk matter under pressure.

Another consideration is the interaction with the substrate for supported clusters. It has been studied for several metal clusters and substrates: Cu_4, Ag_4, Ni_4, and Pd_4 on MgO [209], Cu_n ($n \leq 13$) on MgO [210], Cr_n on Ru(001) [211], Cu_n and Au_n on Cu(001) [212], Al_n on highly oriented pyrolytic graphite (HOPG) [213] and Pd_n on HOPG [214]. Some of these substrates may strongly influence a cluster's atomic and electronic structure [211, 212]. Size-selected clusters can completely change their free atomic structure, after softly landing on the support. This has been illustrated for Cu and Au clusters (with $n = 13$ and 55), which become flat after deposition on a (1×1)O/Ru(001) substrate and stay in a metastable configuration when the substrate is kept at low temperature [212]. The clusters then show a high degree of epitaxy on the substrate lattice.

Platinum clusters adsorbed on HOPG affect the area around the adsorption site by inducing periodic charge density modulations (PCDM) [215]. This can occur for relatively strong particle-substrate interaction. The particle is surrounded by superstructures, which decay exponentially away from the adsorption site. These structures result from a local distortion of the periodic charge density of the substrate.

Nanoparticles of metals may emit light when stimulated by electron injection. For semiconductor particles, photon emission is mostly due to interband transitions and can be used to determine bandgaps. For metal particles, however the luminescence is originated by the collective excitation of the electron gas leading to a Mie plasmon resonance [216]. The peak position of the plasmon resonance for Ag particles shows a pronounced blueshift with decreasing particle size with a $1/d$ behavior (d-cluster diameter). This is caused by intrinsic size effects of the particles.

Metal clusters in beams can be used for scientific studies but their amounts are usually to small for industrial applications. In addition, supported nanoparticles [214, 217–219] are limited to scientific studies. Other techniques, such as solution-phase synthesis [220] have been applied for metal particles with high (macroscopic) quantities. Additionally, metal nanoparticles (Pt, Pd, Ag, Au) were synthesized in polymer matrices [221]. The large scale production of nanopowders allows their application in nanotechnology.

4.3. Divalent Metal Clusters

A transition from van der Waals to metallic bonding is expected for divalent metal clusters (e.g., Be_n, Mg_n, Hg_n) as a function of size. The atoms of these elements have a closed-shell s^2-atomic configuration and a fairly large sp-promotion energy E_{sp} (e.g., $E_{sp}(\mathrm{Hg}) \sim 6$ eV, $E_{sp}(\mathrm{Be}) \sim 4$ eV, where $E_{sp} = E(s_1p_1) - E(s_2)$. Therefore, one expects the smaller clusters to be insulating and bonded through weak, mainly van der Waals-like forces. In contrast, the corresponding bulk materials are strongly bound (e.g., $E_{coh}(\mathrm{Hg}) = 0.67$ eV, $E_{coh}(\mathrm{Be}) = 3.32$ eV) and have metallic properties which result from the overlap between the s- and p-bands. Consequently, a strong qualitative change in the nature of the chemical bonding (from van der Waals to metallic) should take place with increasing size. For Hg_n a transition from van der Waals to metallic bonding has been estimated to occur in the range $20 < n < 50$ [222].

The first experiments which confirmed (to some extent) the expectations were ionization energy studies, performed on beams of Hg clusters [223]. Metallic behavior was reached at $n = 80$–100. Similar results have been obtained from autoionizaton resonance energy measurements [224]. Studies of photoelectron spectra on Hg clusters revealed a much bigger cluster size of $n = 400 \pm 30$ for bandgap closure [225] (Fig. 17).

Electron-shell and supershell effects, originally observed in mass spectra of monovalent-metal sodium clusters [226, 227], were later also found for divalent metal clusters [228]. The electron-shell structure was identified for Hg clusters containing up to 1500 valence electrons.

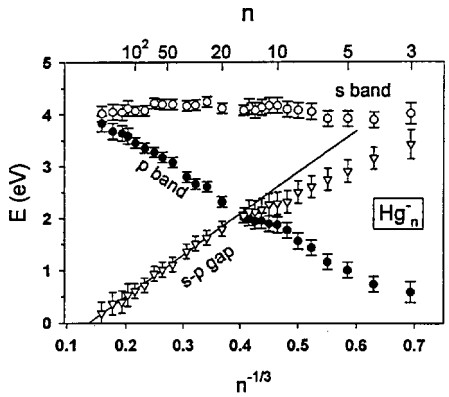

Fig. 17. The size dependence of the binding energies of the 6s-HOMO (open circles) and the 6p- (full circles) electrons in the photoelectron spectra of Hg anion clusters. The s–p-bandgap is the difference between these values (open triangles). The solid line is a linear fit to the bandgap in the range $n = 50$–250, and extrapolates to zero at about $n = 400$ [225]. Reproduced with permission from [225], copyright 1998, American Chemical Society.

5. SEMICONDUCTORS

5.1. Binary Semiconductor Nanocrystals

The properties of binary semiconductor nanocrystals and quantum dots (QDs) have received much attention in the past, following the pioneering work of Efros and Efros [117] and Ekimov, Efros, and Onushchenko [229], Brus [119], and Weller et al. [230]. Many size-dependent phenomena have then been observed in the following years [231–233]. These include light emission from silicon nanocrystals and porous silicon [234], and bandgap tunability in the nanoparticles [235].

The systematic investigation of II–VI quantum dots (ZnS, CdS, CdSe, etc.) began with Brus' work using solution-phase synthesis [236]. It also was inspired by a theoretical work which showed that the linear and resonant nonlinear optical properties exhibit the greatest enhancement when the nanoparticle radius R is much smaller than the Bohr radius of the exciton (a_B) in the corresponding bulk material [237]. Deviation of properties are expected for semiconductor QDs in the strong-confinement limit, where $R/a_B \ll 1$. The Bohr radii of excitons vary strongly between different semiconductors: 10 Å (CuCl), 60 Å (CdSe), 200 Å (PbS), 340 Å (InAs), 460 Å (PbSe), 540 Å (InSb).

The electronic spectra of PbS, PbSe, and PbTe QDs are simple, with energy gaps that can be much larger than the gaps of the parent bulk materials (which are 0.2–0.4 eV for the lead salts). In contrast, the energy level structure of II–VI and III–V QDs are much more complicated, with closely spaced hole levels and valence band mixing [6] which complicates the study of these materials.

Particles of Cd_3P_2 are found to be strongly size quantized [238]. This is seen from a 1.5-eV blueshift of the first electronic transition for 27-Å particles compared to the bulk bandgap of 0.5 eV. The shift is explained by quantum confinement of the exciton. The radius of the exciton is 180 Å, as calculated from the effective masses of the electron ($0.05m_0$) and the hole ($0.4m_0$) and the high frequency dielectric constant ($\sim$15). The large increase in the gap is due to the restriction of the large exciton to the 27-Å sized particle.

The electronic structure and the luminescence of II–VI nanopowders and quantum dots has been studied by several groups [11, 29, 239–244]. Many articles concerning the distribution of electronic states have appeared in literature [127, 231, 232, 245–248]. In addition to optical spectroscopy, conductance spectroscopy was used to study the bandgap [57].

Photoelectron spectroscopy of cluster beams is now an established method to study the electronic structure. The electron affinity of cluster anions as a function of size can be studied via photodetachment [249]. Such beam experiments are restricted to small sizes (for instance $Ga_nP_n^-$ ($n = 1$–9) [249] or $In_nP_n^-$ ($n = 1$–13) [250]) but allow studying both stoichiometric and nonstoichiometric clusters.

The physical properties of the larger nanoparticles are dominated by the confinement of electrons [251]. For CdSe particles, a widening HOMO–LUMO gap was observed in optical absorption and band-edge emission (photoluminescence) studies [235, 241]. From another study, the size dependence of the gap for CdSe particles is given in Figure 18 [252]. Absorption and emission spectra of InP quantum dots show similar dependence [253] illustrated in Figure 19 [254]. Although the experiment and the QSE theory agree reasonably well at large sizes, theory diverges from the experimental values for small sizes ($d < 7$ nm). This may be due to the nonparabolicity of the bands at higher wave vectors and the finite potential barrier at the surface of the particles. Tight-binding calculations can yield better agreement for the smaller sizes [127, 245].

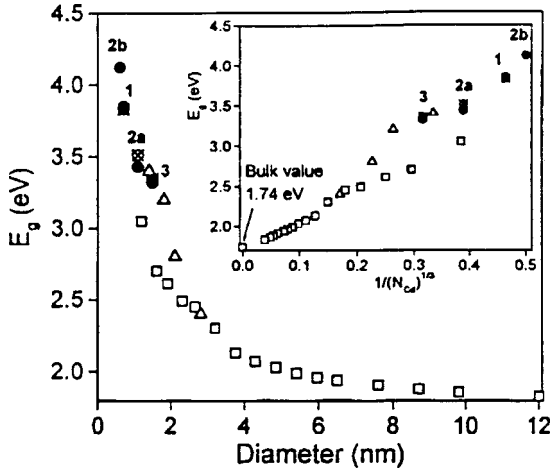

Fig. 18. Size dependence of the bandgap of CdSe particles [252]. Filled circles are taken from Soloviev et al. [252], squares and triangles are taken from Murray, Noms, and Bawendi [235] and Rogach et al. [595]. The inset displays for the same data the dependence of the gap on $1/(N_{Cd})^{1/3}$, with N_{Cd} being the number of Cd atoms.

The effective mass approximation gives $1/R^2$ for the dependence of the bandgap on the radius of nanoparticles. However, it usually overestimates E_g. For PbS particles, for instance, the

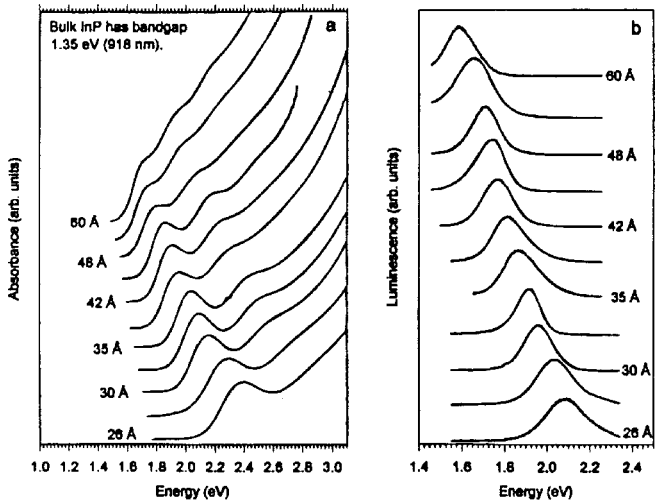

Fig. 19. Optical absorption and emission spectra of InP quantum dots as a function of diameter [254]. Reproduced with permission from [254], copyright 1998, American Chemical Society.

energy gap increases as $\sim 1/R^{1.3}$ for $R \geq 2.5$ nm [255]. For the very small sizes, the bandgap is usually not described by a simple R-dependence but rather changes discontinuously. This is shown in the gaps of stoichiometric Ga_nAs_n clusters ($n =$ 2–6) which were determined using first-principle pseudopotential calculations: 5.8 eV (Ga_2As_2), 5.7 eV (Ga_3As_3), 4.3 eV (Ga_4As_4), 5.1 eV (Ga_5As_5), and 4.8 eV (Ga_6As_6) [256].

Williamson et al. [257] studied the conditions under which the bandgaps of free standing and embedded semiconductor quantum dots are direct or indirect. The results are obtained from experimental and theoretical investigations of quantum dots and quantum wells. It is found that free dots of CdSe, InP, and InAs have direct bandgaps for all sizes, while the direct bulk gap of GaAs and InSb dots becomes indirect below a critical size. Dots embedded in a direct gap host matrix either stay direct (InAs/GaAs at zero pressure) or become indirect at a critical size. Direct gap dots in an indirect gap host have a transition to indirect gap for sufficiently small particles (GaAs/AlAs and InP/GaP quantum well) or are always indirect (InP/GaP dots, InAs/GaAs above 43-kbar pressure and GeSi/Si dots). Theoretical studies predict a change from an indirect to a direct semiconductor for particles smaller than ~2 nm [258, 259] for GaP.

The bandgap in a bulk semiconductor depends on the temperature. Studies generally report that this dependency is similar for nanoparticles and the bulk [260]. The variation may be slightly weaker [261] in nanoparticles of varying size. The response of the bandgap to temperature can be measured in optical experiments by the temperature coefficients dE_g/dT of lowest electron-hole pair energies. For PbS and PbSe quantum dots, it was found that dE_g/dT decreases with decreasing dot size by more than an order of magnitude from the bulk value and even becomes negative (below ~3 nm) [262]. This shows that nanoparticles of semiconductors can have their electron levels frozen, i.e., with no or little response to a change of temperature. Such weak temperature dependence is expected for atomic-like levels. The observation is explained with the characteristics of quantum dots and nanoparticles: With a decrease in size, the continuum states of the bulk semiconductor transform gradually to the discrete states of the particle. This has effects on the thermal expansion of the lattice, the thermal expansion of the wave function envelope, the mechanical strain, and the electron-phonon coupling. The localized states respond little to variations of interatomic distances and angles.

Semiconductor particles are starting to find applications due to their delta-function-like density of states and their photoluminescence. However, the luminescence often is quenched above 300 K, at temperatures where the devices still have to function. This illustrates that besides having the bandgap well adjusted to a particular application, the matrix elements for the optical transitions may play a decisive role. Thermal escape of carriers to nonradiative recombination centers such as surface and interface states or other electron acceptors can drastically reduce carrier recombination rates [263]. The effect of temperature on the photoluminescence of semiconductor particles has well been studied [264].

Particles in solid host materials are protected from ambient air exposure. The embedded particles can show effects very similar to those of the free particles. For example, GaAs particles in Vycor glass show the typical nonlinear optical properties due to quantum confinement [265].

5.2. Silicon and Germanium Clusters

The early work of silicon clusters was inspired by studies of cluster beams. Such clusters are produced under high vacuum conditions and consequently do not have their surface bonds saturated. In the early 1990s, there was a new development for nanostructured silicon. Bulk silicon, when electrochemically etched, was made porous and was found to show photoluminescence in the visible range [266]. Soon the new effect was attributed to silicon nanowires or particles present in the porous structure. Indeed, STM studies of the porous silicon surface show the presence of nanoparticles (Fig. 20). It was supported by the observation that individual silicon particles showed photoluminescence [267–274]. The Si particles have been synthesized by liquid-solution-phase growth [275, 276], from silane via slow combustion [277], microwave plasma [267], chemical vapor deposition [25], gas evaporation [278–281], sputtering or ablation [24], ultrasonification of porous silicon [282, 283] and various other techniques.

This development led to an intense scientific activity to understand both the increase of the bandgap (made responsible for the luminescence in the visible range due to interband transitions), and the observed high transition probability. The silicon particles, responsible for the photoluminescence, were considered to have their surface bonds passivated, in accordance with the experimental conditions during the production of porous silicon. Indeed, unpassivated silicon clusters did not emit any light after UV excitation [274]. Therefore, interest in

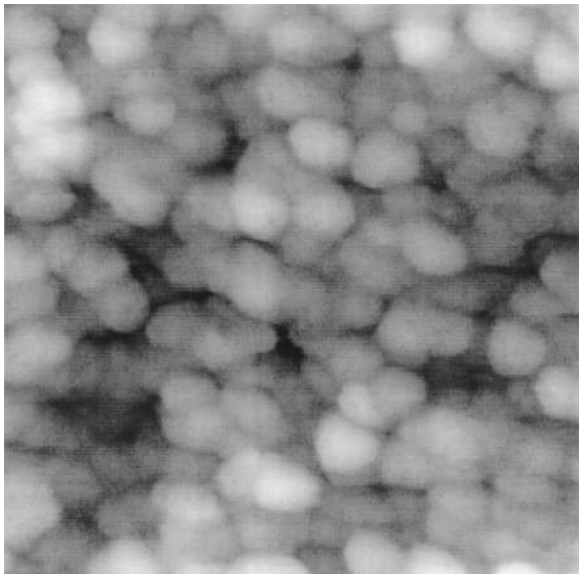

Fig. 20. AFM image (656×656 nm) of light-emitting porous silicon [475]. Reproduced with permission from [475].

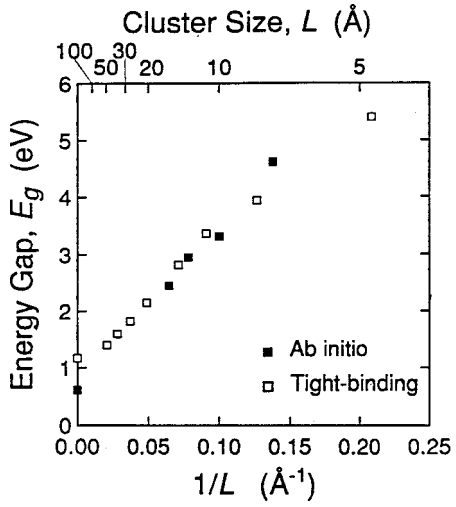

Fig. 21. Size dependence of the energy gap of hydrogenated silicon clusters; results from ab initio [287] and tight-binding calculations [596].

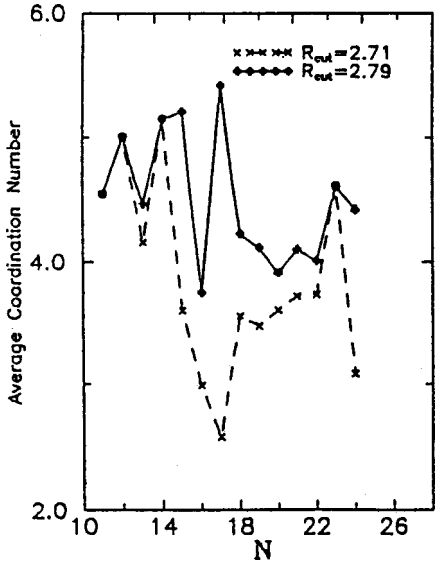

Fig. 22. Size dependence of the average coordination number calculated for small silicon clusters (with different distance cutoffs) [302]. Reproduced with permission from [302], copyright 1995.

coming years moved away from pristine to passivated silicon clusters. Most of the work concentrated on hydrogen passivated [1, 284–290] (Fig. 21) and on oxidized silicon clusters [291–294].

Since the discovery of room-temperature visible photoluminescence in silicon nanocrystals [267] and porous silicon [266], the size dependence of the energy gap of Si nanostructures has been discussed extensively [287, 295–297]. The quantum-size effect, resulting in a blueshift of the energy gap with decreasing size, was widely believed to be at the heart of the novel optical properties of porous silicon [1, 267, 298–300]. The energy gap was found to increase significantly with decreasing size, for instance between 1.3 and 2.5 eV for particles of 5 to 1 nm in size [1]. The experimental data often were described by the effective mass approximation (EMA). An inverse power law for the bandgap behavior as a function of size is predicted by EMA and leads to very large bandgaps for particles of small size. Different exponents in the power law have been discussed [301].

Obviously, simple models like the effective mass approximation are not applicable to pristine silicon clusters. EMA is a continuum approach, which does not consider the complexity of the atomic structure, the unsaturated surface, and the significant changes in hybridization, which can occur when the size of the pristine particles is reduced.

$(Si)_n$ with just a few atoms ($n < 10$) were theoretically found to have compact cubooctahedral or icosahedral structure. The average coordination number for silicon clusters with $n = 12$–24 tends to lie above the coordination number 4 of the bulk diamond structure [302] (Fig. 22). Theoretical results [143, 303–307] predicting the compact structure for small Si clusters have been confirmed experimentally by Raman spectroscopy [308] and anion photoelectron spectroscopy [309]. The close-packed structure is typical for metallic rather than covalent systems. As bulk silicon is a semiconductor, a major change in the electronic properties can therefore be expected with size reduction. The critical size n^* for a transition from covalent to metallic bonding was estimated, but with very different values: $n^* = 100$–1000 [143] and $n^* = 50$ [303].

Electronic structure and bandgap are reasonably well known for porous silicon and large passivated Si particles [287, 288, 310–314]. However, the HOMO–LUMO gap of small, unpassivated Si clusters is much less understood.

Gaps between zero and several electron volts were predicted for small unpassivated silicon clusters. For example, a zero gap or close to zero gap was theoretically obtained for Si_{28} [315] (Fig. 23), Si_{29} to Si_{45} [316] (Fig. 24), while gaps of 1.2 eV for Si_{20} [317] and Si_{46} [318] and 0.3–3 eV for Si_3-Si_{11} [143] were calculated (Fig. 25).

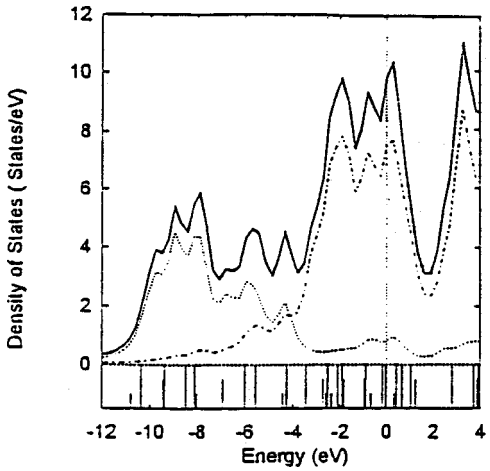

Fig. 23. Electronic density of states and eigenvalue distribution for an Si_{28} cluster. Dotted and dashed lines denote the partial densities of states for 3s and 3p, respectively, [315]. Reproduced with permission from [315], copyright 1995, American Physical Society.

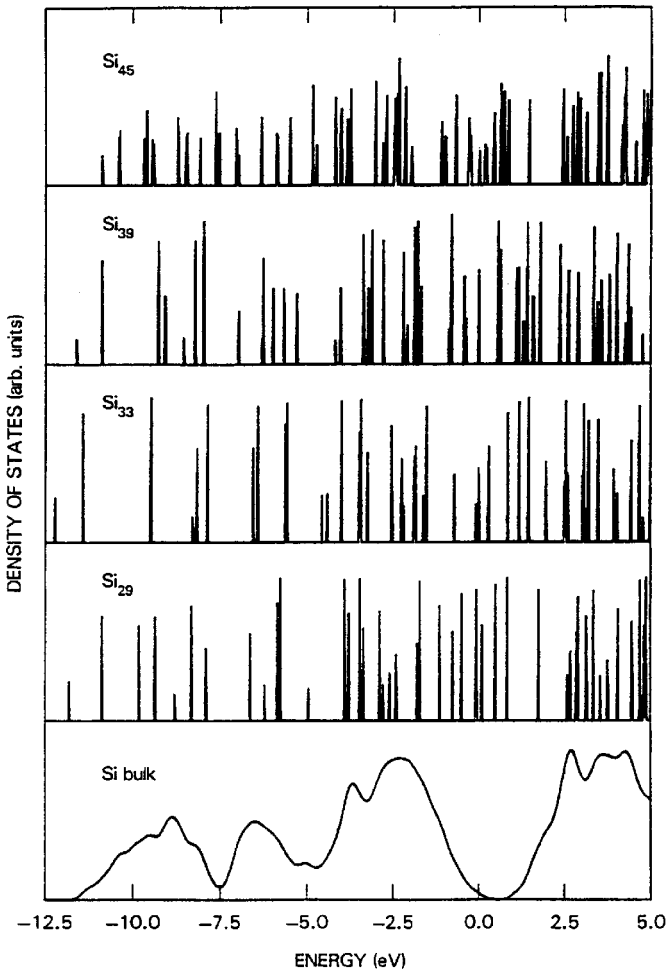

Fig. 24. Electron level distribution calculated for Si_{29}, Si_{33}, Si_{39}, and Si_{45}, in comparison with the density of states of bulk silicon [316]. Reproduced with permission from [316], copyright 1996, Trans Tech Publications.

For medium-sized silicon clusters, with up to several hundred atoms per cluster various atomic structures have been proposed [303, 315, 319–322] and the HOMO–LUMO gap was calculated to depend strongly on the assumed atomic structure [320, 323]. Due to the relatively large number of atoms, semiempirical techniques such as the interatomic force field method [324] were used instead of ab initio techniques. In this size range, there seems to be a structural transformation. Jarrold and Constant [325] found that clusters up to ~27 atoms have a prolate shape while larger clusters have more spherical shapes. Other abrupt changes in properties of medium-sized Si clusters have been observed in photoionization measurements, at $n^* = 20$–30 [326]. A structural transformation at n^* would imply a sudden change of the electric polarizabilities of the clusters. In a theoretical study of Si_n with 10–20 atoms [327] the polarizability is found to be a slowly varying function of n. This indicates that n^* might be greater than 20. Photoelectron spectroscopy of Si cluster anions ($n = 10$–20) [328] yielded HOMO–LUMO gaps to scatter discontinuously between 0.6 and 2.1 eV (Fig. 26).

Clusters may have disordered structures if produced by fast cooling of a molecular beam or vapor [2]. The atoms do not have the time to find low-energy positions. The atomic structure of such particles therefore can be significantly different from both the bulk and the nanocrystal structures [329]. The electronic structure and the bandgap of amorphous silicon clusters (a-Si_n) have been calculated with a tight-binding approximation [284]. A comparison of the size dependence of the HOMO-LUMO gap for amorphous bare (a-Si_n), H-passivated (a-Si_n), and crystalline (c-Si) particles is shown in Figure 27. A strong blueshift with size reduction is predicted for all three types of particles.

The size-dependent bandgap of Ge nanoparticles has been calculated over a wide size range, from 12 to 1 nm, and the bandgap was found to change gradually from 1 to 4 eV, respectively, [330]. We note that 12-nm Ge particles would have a gap much larger than the bulk gap of 0.6 eV. Indeed, there are many reports of strong visible photoluminescence in germanium nanocrystals [3, 18, 331–340]. If interband transitions are responsible for the luminescence, the bandgaps of the Ge particles have to be several electron volts wide.

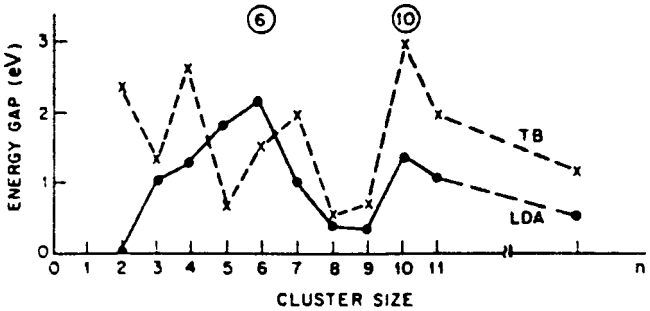

Fig. 25. HOMO–LUMO gaps calculated for Si clusters; results from local-density functional (solid line) and tight-binding (dashed line) results) [143]. Reproduced with permission from [143], copyright 1987, American Physical Society.

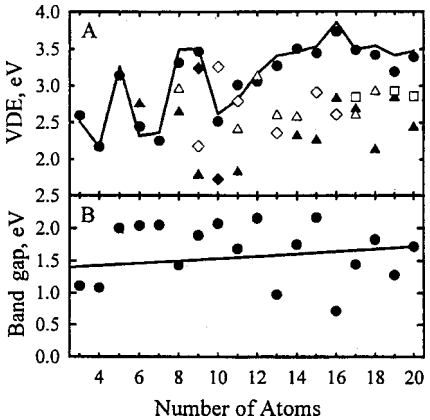

Fig. 26. (A) Vertical detachment energies (VDE) of Si_n anions; the solid line is measured with photoelectron spectroscopy. The symbols mark values calculated for silicon clusters of various structures. (B) Bandgaps calculated for lowest energy neutral Si clusters [328]. Reproduced with permission from [328], copyright 2000, American Physical Society.

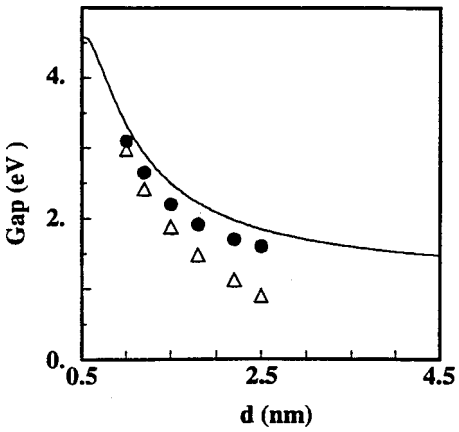

Fig. 27. HOMO–LUMO gap of amorphous clusters compared to crystallites: amorphous bare Si_n (empty triangle), hydrogen passivated Si_n (filled circle), and crystallites (full line) [284]. Reproduced with permission from [284], copyright 1997, American Physical Society.

Gap calculations within the effective mass model yield such wide gaps but quantitatively disagree with the optical results [335, 341]. Additionally, the tight-binding calculations for Ge particle gaps by Niquet et al. [330] are inconsistent with the experiments.

The blue–green photoluminescence is observed with little change in color for particles from about 2 to 15 nm [335, 341]. This would imply a bandgap of about 2 eV, independent of the particle size. Photoelectron spectroscopy studies have revealed HOMO–LUMO gaps for Ge_n clusters ($n = 4$–34) which do not show a blueshift in this size range but rather scatter around the bulk value of 0.6 eV [342] (Fig. 28). It indicates that the observed photoluminescence radiation is not due to the size-dependent quantum confinement but rather to surface or defect state transitions.

A wide spread of energy gaps is predicted for structural isomers of clusters with the same size. For example, calculations of germanium clusters with different atomic structures give gap values of 0.1–1.35 eV for Ge_8, 0–1.84 eV for Ge_9, and 1.13–2.64 eV for Ge_{10} [288].

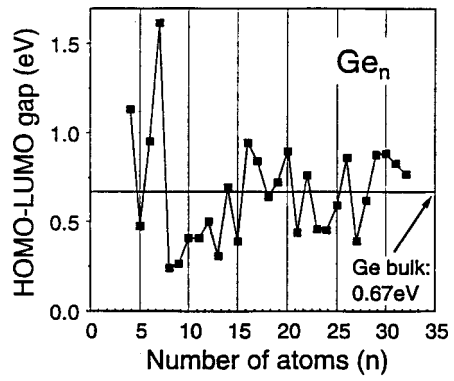

Fig. 28. HOMO–LUMO gaps of Ge clusters obtained from photoelectron spectroscopy (PES). The line at 0.67 eV indicates the energy gap of bulk Ge [342]. Reproduced with permission from [342], copyright 1998, Elsevier Science.

6. UNPASSIVATED SILICON PARTICLES

6.1. Particle Preparation

In the following, we show tunneling spectroscopy studies [48] determining the energy gap of pristine silicon particles over a size range where major size-dependent changes are expected. Using STM and STS as local probes allows studying individual clusters. STM is used to image the clusters and the surrounding support and to determine cluster sizes and shapes. STS is used to measure the energy gap.

The clusters were grown on highly oriented pyrolytic graphite (HOPG) upon submonolayer deposition of silicon vapor. The deposition was done by direct current (dc) magnetron sputtering of silicon in ultra-high vacuum (UHV) base pressure. Clusters form after surface diffusion by quasi-free growth on the inert substrate. After the deposition, the samples were transferred to the STM chamber (1×10^{-10} Torr) without braking vacuum. Since local STS of clusters is not feasible at room temperature due to the thermal drift, voltage-dependent STM [343] was the STS method of choice. It has been shown that local STS and voltage-dependent STM give comparable results for spectra of an adsorbate [343].

At submonolayer coverage, small clusters are formed on the support, well separated from each other. An area of pure graphite typically surrounds a particle (Fig. 29). Once an Si cluster was selected, a series of STM images at different bias voltages was recorded. If the cluster has a gap and the bias voltage is tuned to be within the gap, there are no states available for tunneling. Accordingly, the cluster is "invisible" until the bias voltage is high enough to allow tunneling into the "conduction band" or out of the "valence band" of the cluster. In the constant-current mode, this is reflected by the apparent height Δz of the clusters as it varies with the bias voltage. The equivalent measurement in the constant-height mode is the difference ΔI in tunneling current on the substrate and on the cluster. Each series of STM images yields a plot of ΔI as a function of V. Clusters in the size range from a few angstroms to a few nanometers were analyzed. For long exposure and high currents, nanoscale silicon wires can be grown [344].

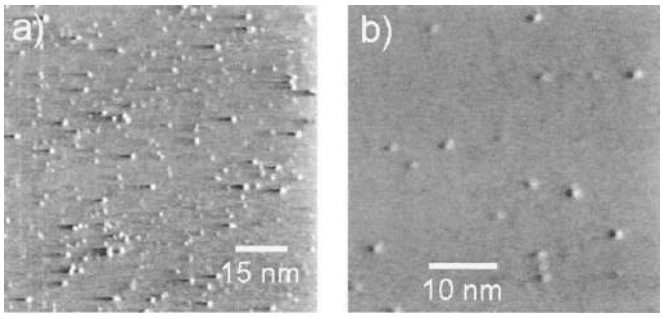

Fig. 29. Pristine silicon particles on HOPG, generated by vapor deposition in UHV [389]. Reproduced with permission from [389].

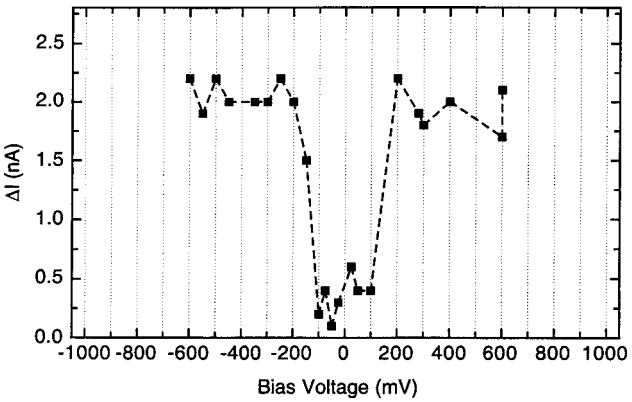

Fig. 30. $\Delta I(V)$ plot of a 2.5-Å silicon cluster. ΔI is the difference between the tunneling currents measured with the tip located on top of the cluster or on the substrate [48]. Reproduced with permission from [48], copyright 2000, American Physical Society.

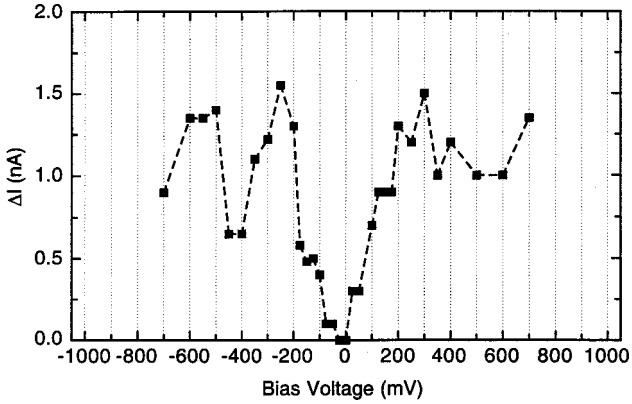

Fig. 32. $\Delta I(V)$ plot of a 9-Å silicon cluster [48]. Reproduced with permission from [48], copyright 2000, American Physical Society.

The well-known nonreactive nature of HOPG and the observed low sticking coefficients for many atoms and molecules (at room temperature) shows that chemisorption is not a process to occur for silicon clusters adsorbed on HOPG. This is supported by studies [345] reporting high scattering yields of Si_n^+ and Si_n^- ($n = 5$–24) impinging on HOPG. Impinging Si clusters have very low sticking probability and are easily reemitted. If the clusters are formed at the substrate, they are kept on the support by physisorption due to small electrostatic dipole forces.

6.2. Gap Measurement of Si Particles by STS

In Figures 30–33 $\Delta I(V)$ curves for several silicon clusters are displayed. They have in common that a bandgap is visible around zero bias. Figure 31, for example, shows the $\Delta I(V)$ curve for a 10-Å cluster. A bandgap with steep edges can be seen. The plot is taken with data points typically 25 mV apart. ΔI is zero in the gap region since the cluster completely vanishes in the STM image. There are no accessible states in the cluster and the tunneling electrons pass through the cluster without interaction. Accordingly, only the substrate is visible in the STM image. The gap is nearly symmetric around zero bias. Outside of the gap, the ΔI values fluctuate due to quality differences of the STM images. For positive bias voltages, electrons tunnel from the tip to the sample and vice versa for negative bias voltages. ΔI values are observed to be higher in the positive than in the negative bias range. This shows that the cluster has a higher state density at the conduction band edge compared to the valence band edge. The states are difficult to identify, as the electronic features of small silicon clusters are little known.

In Figure 34 the energy gap of the analyzed clusters is plotted versus the cluster size. In the range between 15 and 40 Å, only clusters with zero gap are observed. For smaller clusters, zero gaps are found as well but nonzero gaps predominate. Below 15 Å, the gaps tend to increase with decreasing cluster size. The largest gap recorded is 450 meV, for clusters with 5 and 8.5 Å. There is a significant scatter of the data points in the small size range. Clusters of similar size can have very different energy gaps. For example, at 8 ± 1 Å a zero-gap cluster and one with a 250-meV gap is found.

The size of a cluster was determined with an error bar of typically $\pm$ 10%. For a spherical cluster, one can relate a

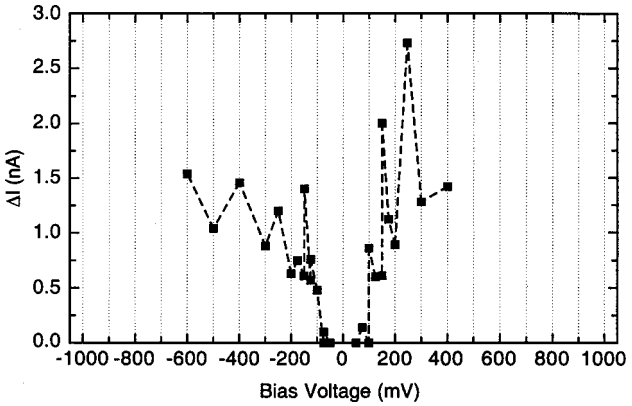

Fig. 31. $\Delta I(V)$ plot of a 10-Å silicon cluster [48]. Reproduced with permission from [48], copyright 2000, American Physical Society.

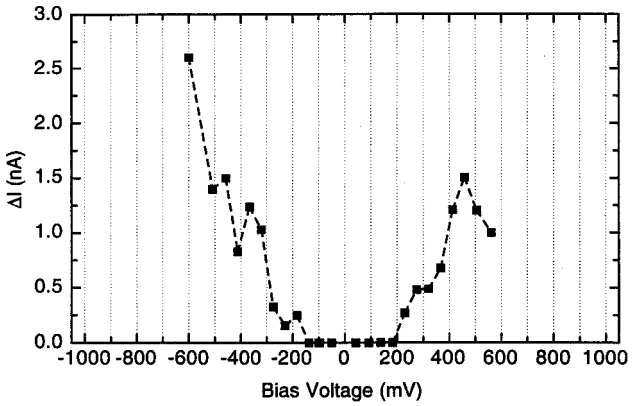

Fig. 33. $\Delta I(V)$ plot of a 8.5-Å silicon cluster [48]. Reproduced with permission from [48], copyright 2000, American Physical Society.

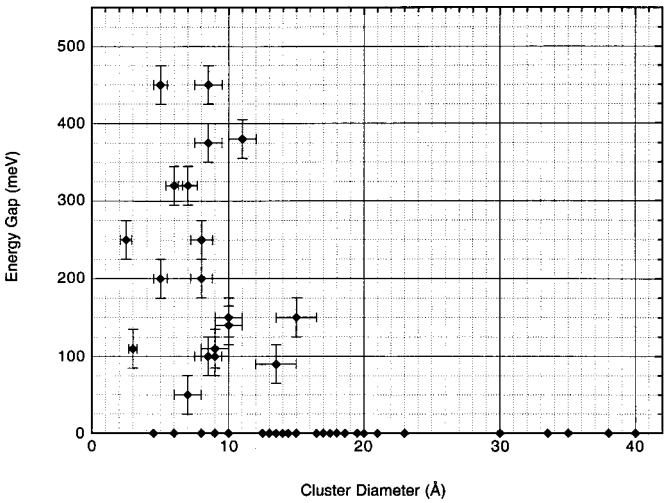

Fig. 34. Energy gap values from STS measurements as a function of silicon cluster size [48]. Reproduced with permission from [48], copyright 2000, American Physical Society.

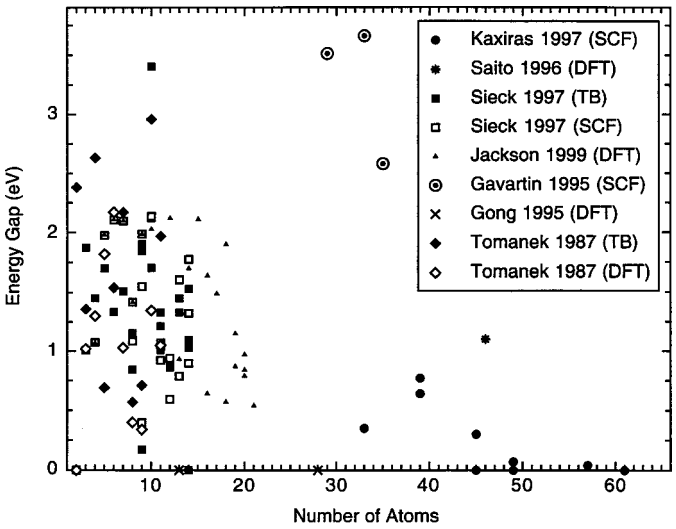

Fig. 35. Calculated energy gaps for pristine silicon clusters using density functional theory (DFT) [143, 302, 315, 317, 327], tight-binding (TB) methods [143, 349], or self-consistent-field (SCF) algorithms [349–351].

given diameter to the number of atoms using the expression $d(n) = (3/4\pi\rho)^{1/3} n^{1/3}$, where ρ is the mass density and n is the number of atoms in the cluster. Using the mass density of bulk silicon, one obtains $d(n) = 3.3685 n^{1/3}$ (Å). It follows that 26 atoms are in a spherical 10-Å Si cluster. ~~Some~~ 9- and 11-Å Si clusters contain $n = 19$ and 35 atoms, respectively. These small-sized clusters have properties depending strongly on their size. One atom more or less may have a pronounced effect on the cluster's electronic structure. Therefore, the energy gap can strongly differ for clusters of similar size. In the STS experiment, one does not determine the number of atoms in a cluster but rather the diameter. In the uncertainty window of $\pm 10\%$, there are clusters with slightly different numbers of atoms. Such a spread in the number of atoms per cluster explains the observed scatter of gap data.

The gaps for clusters smaller than 15 Å lie far below the value of silicon bulk or the enhanced values due to the quantum-size effect. To check whether clusters with very large gaps are present, we applied bias voltages up to $\pm$ 2.5 V. Therefore, clusters with gaps up to 5 eV could have been detected.

The results are surprising at first. Bulk silicon has a bandgap of 1.1 eV and one may expect it to be much higher for small particle sizes due to the quantum-size effect. For surface passivated silicon clusters, this has in fact been confirmed both experimentally [1, 269, 273, 274, 291–294, 296, 346, 347] and theoretically [122, 284, 285, 287, 288, 290, 295, 301, 348] with gaps up to 4 eV. The STS results show that the gaps of unpassivated and passivated silicon clusters are entirely different.

Theoretical results about the HOMO–LUMO gaps of silicon clusters show strong variations, depending on calculation methods, assumptions, and types of approaches. A variety of calculated gaps is shown in Figure 35. They have been obtained by density functional theory (DFT) [143, 302, 315, 317, 327], tight-binding methods [143, 349], or self-consistent-field (SCF) algorithms [349–351]. Over the range from Si_2 to Si_{61}, clusters with zero bandgaps are found, as well as clusters with gaps up to 3.5 eV.

On the extended surface of bulk silicon, the density of dangling bonds is known to be high. It is a consequence of the strong directional properties of the sp^3-hybrids and the missing neighbors at the surface. The same can be expected for unpassivated silicon clusters. Each dangling bond contributes a partially filled surface state.

Since they are partially filled, the surface states associated with the dangling bonds are located in the energy gap around the Fermi level. This has been well demonstrated for the surface of bulk silicon using a number of methods including tunneling spectroscopy [352–354]. These experiments show that surface states mostly fill the bandgap of the unpassivated silicon surface. For clusters of silicon, with unpassivated surfaces, a similar situation can be expected. In fact, a calculation of Si_{29}, Si_{87}, and Si_{357} shows density of states with zero-energy gap between HOMO and LUMO [355]. The passivated clusters, Si_{29} H_{36}, Si_{87} H_{76}, and Si_{357} H_{204}, however show the broad bandgaps of 3.44, 2.77, and 1.99 eV, respectively, just as expected for particles in this size range. Evidently, the zero gap of the pristine particles originates from the surface states.

The surface of bulk silicon has a high density of extra states which are located in the fundamental bandgap [356] and tend to form surface state bands [357, 358]. The ideal bulk surface of silicon reconstructs to a variety of complicated atomic arrangements, as, for example, the 7×7 reconstruction of the (111) crystal facet [359]. This reduces some of the dangling orbitals but still leaves many extra states in the gap. Local tunneling spectroscopy measurements show substantial tunneling currents even at very low bias, indicating a high density of states near the Fermi energy [353]. Zero bandgap, due to the

metallic surface state density, has also been observed in combined photoemission and inverse photoemission studies [360].

Two transport mechanisms explain the conducting properties of the cluster surface. For high density, the surface states overlap forming a conduction band. The cluster surface then shows the transport properties of a metal. For lower state density, thermally activated hopping between the localized surface states leads to the observed conducting behavior. At ∼15 Å, corresponding to $n^* \sim 90$ atoms per cluster, a major change in the cluster properties occurs. The energy gap suddenly opens up and subsequently widens for smaller clusters. This change to nonzero energy gaps shows a transformation of the electronic structure of the clusters. We associate it with the covalent-metallic transformation suggested previously for silicon clusters by several groups. Accordingly, large silicon clusters are sp^3-hybridized with strong covalent bonds and rigid bond angles giving rise to high surface state density. Around a critical size n^*, the sp^3-nature of the bonds gradually changes to hybridization other than sp^3 or even to the atomic s- and p-configurations. In fact, ab initio calculations show that sp^3 is not the favored hybridization for small silicon particles. The change of the electronic structure at the critical size also means a change in the atomic structure of the clusters. Below n^*, the clusters are not fragments of the bulk anymore but rather have their cluster-specific structures. These are close-packed structures resembling those of metals. In this sense, one may say that at n^* a covalent-metallic transition occurs.

Some of the studied silicon clusters exhibit zero-energy gaps even below n^*. These clusters have the surface state configurations similar to those above n^*. It shows that the transition at $N^* = 90$ does not occur for all silicon clusters. Some clusters have sp^3-coordinated bonds even at very small size. They coexist with the compact clusters as structural isomers. This is not surprising because silicon bonds are very strong and many isomers are stable at room temperature. The observation of various bandgaps for similarly sized clusters is also a consequence of the analysis of individual clusters using STM and STS.

A silicon cluster of 15-Å diameter contains about 90 atoms, with the bulk structure of silicon being assumed for the volume density. This critical size of $n^* = 90$ can be compared to the widely different theoretical estimates ($n^* = 30 - 4000$) [132, 142, 303, 361, 362]. A covalent-metallic transition has been postulated but it has previously not been observed. Yet, there are some indications for such a transition. Chemical reactions of Si_n^+ show significant changes in the chemisorption probabilities at $n = 29 - 36$ (for O_2 adsorption) [363]. The dissociation energy of Si_n^+ starts to deviate from the smooth size behavior below about $n = 40$ [364]. The photoionization threshold suddenly has a drop at $n \sim 20 - 30$ [326]. We note that these experiments have been performed on charged clusters or by transfer from neutral to charged. The stability and structure of neutral and charged silicon clusters however may be different.

The highest observed gap (∼450 meV) in the STS experiment is less than half the bulk value. Interestingly, the gap of surface states of Si (111) (2×1) was found to be in this range (450 meV) [357]. A similar result has been obtained from studies of silicon clusters in beams, where the bandgaps were found to be far below the 1.1-eV gap of bulk silicon [365].

6.3. Coulomb Blockade of Si Particles

Quantum dots of silicon and germanium can show Coulomb blockade and single-electron tunneling effects. These have been studied in particular with respect to the fabrication of a quantum dot transistor [366–370]. Coulomb blockade oscillations have also been studied for (10-nm diameter) silicon nanowires within a metal-oxide-semiconductor field-effect transistor (MOSFET) [371].

Single-electron tunneling (SET) was observed in conductance spectroscopy for metal particles [372, 373–375]. The SET studies on metal particles were done at low temperatures, at 4 K [84, 376] and 77 K [61, 377]. A Coulomb staircase in the I–V characteristics was also observed for CdSe particles at 77 K [61]. In some tunneling studies of quantum dots, sub-Kelvin temperatures were applied [378–380]. In these systems, the single-electron charging energy is substantially larger than the level spacing. Low temperatures are required for these particles to show the characteristic Coulomb gaps.

Electrochemically it was demonstrated that gold particles in solution show Coulomb-staircase charging behavior [381]. Incremental charging was also found for a molecule using an STM at room temperature [85]. Silicon particles on HOPG can also show Coulomb blockade at room temperature [371, 382–388].

In Figure 36 an STM image is shown with both, "white" and "black" dots on the "gray" background of the substrate.

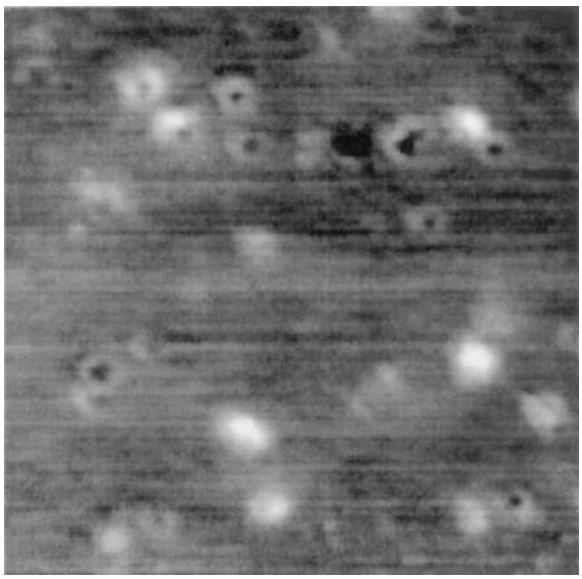

Fig. 36. A 29×29-nm STM image of silicon particles adsorbed on HOPG. Some of the particles appear black due to Coulomb blockade of the tunneling current [487]. Reproduced with permission from [487], Fig. 37. Reproduced with permission from [50], copyright 1996, American Institute of Physics.

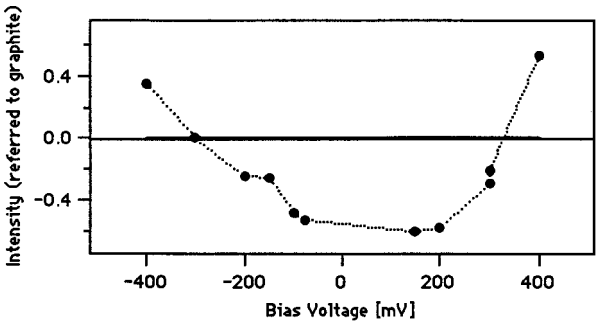

Fig. 37. $\Delta I(V)$ plot for a silicon particle which shows Coulomb blockade. The intensity of the cluster referred to graphite is below zero in a bias voltage range of about 600 mV due to Coulomb blockade [597]. Reproduced with permission from [597].

The white dots are due to silicon particles, which are conductive for the tunneling electrons. The black dots however, block the tunneling electrons because they are insulating and charged by single electrons. The white halo around the black dots indicates that the surface of the Si particles is conducting. This is expected for particles with unpassivated surface bonds. Electron transfer between tip and substrate can occur through the conducting surface of the particles. One finds that the core of these particles is insulating while the surface is conducting.

In Figure 37 the STS plot for a black cluster is given. For values above and below the zero line, the cluster appears white or black, respectively. The voltage range where the particle appears black gives the value of the Coulomb gap. The plot was taken from a 13-Å silicon particle. It shows a Coulomb energy gap of 640 meV [389].

7. PASSIVATED SILICON PARTICLES

7.1. Pristine versus Passivated Silicon Clusters

While reconstruction leads to a reduction of surface dangling bonds, it does not eliminate them completely. Therefore, the reconstructed silicon surface still contains a large number of dangling bonds and shows strong chemical reactivity. The bulk silicon surface is oxidized rapidly under ambient conditions. The reactivity of silicon clusters is reduced [363] compared to the bulk and the reduction depends on the size of the particles. In fact, magic Si clusters where found with weak interaction strength [390]. For such clusters, most (or even all) of the dangling bonds have disappeared by backhanding and relaxation.

What a difference the surface passivation makes was illustrated in a calculation of pristine silicon clusters and their hydrogenated counterparts [355]. The pristine clusters show a density of states with zero-energy gaps between HOMO and LUMO. The passivated clusters show wide bandgaps up to 3.4 eV.

Passivated silicon particles have been investigated experimentally and theoretically [289, 391–398]. The diamond structure is stabilized by the hydrogen passivation and therefore the bulk crystal structure has been applied to the smallest silicon clusters [289].

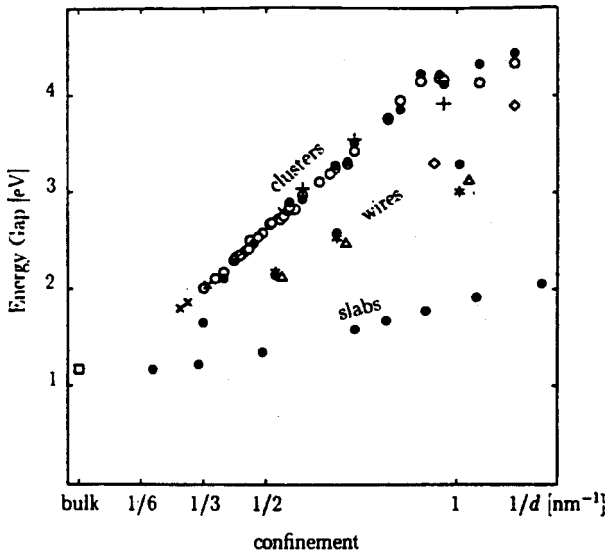

Fig. 38. Energy gap calculated for H-terminated slabs (two-dimensional), wires (one-dimensional) and clusters (zero-dimensional) (after Delley and Stelgmeier [290]). Data are plotted for studies by Delley and Steigmeier [290, 301], Delley, Steigmeir, and Auderset [598], Wang and Zunger [295], Hirao, Uda, and Murayama [599], Mintmire [600], Read et al. [601], and Buda, Kohanoff, and Parrinello [409].

H-passivated silicon wires were also studied [399]. Clusters, wires, and slabs of silicon show the same qualitative behavior with a blueshift of the bandgap with decreasing size [290] (Fig. 38). Large energy gaps have been reported, such as 4.6–2.45 eV for 7.3–15.5 Å [287], 5.3–1.7 eV for 5 to 50 Å [400] and ~5 to ~2 eV for 10 to 27 Å [288] hydrogenated silicon particles. Often, the purpose of the research was the interest in understanding the visible photoluminescence of porous silicon (π-Si) [287, 297, 311, 401–412].

The quantum efficiency and the stability of the luminescence depend on the passivation of the grains and the grain boundaries in porous silicon (π-Si). The π-Si material can significantly be improved by passivation with oxygen through rapid thermal processing [31, 413]. The porous silicon structure can be envisioned as small units remaining in the lattice after electrochemical edging. These units where first considered to be silicon nanowires [266] and later to be rather nanoparticles. In both cases, their surface is passivated as it was exposed to the ions in the acid during the electrochemical process. The atomic structure of both partticles and wires is usually assumed to be the diamond structure of the bulk. This structure is stabilized by the surrounding atoms of the host and by the passivation of the dangling bonds. It is usually not the equilibrium structure of the corresponding free nanoparticle or nanowire.

The passivation of the surface is often debated with respect to the luminescence. Bulk silicon is an indirect bandgap semiconductor with no optical activity. In the crystalline bulk material, the momentum conservation rules have to be fulfiled. In a nanoparticle however, the strict rules may be lifted due to disorder and surface effects.

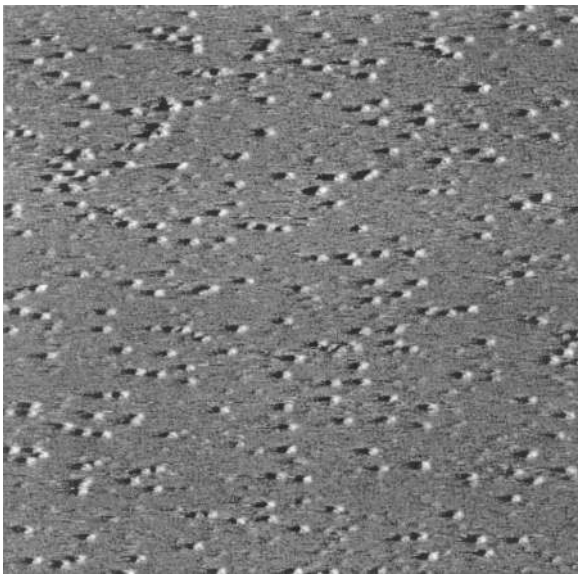

Fig. 39. STM image (152×152 nm) of hydrogenated silicon particles on HOPG [389]. Reproduced with permission from [389].

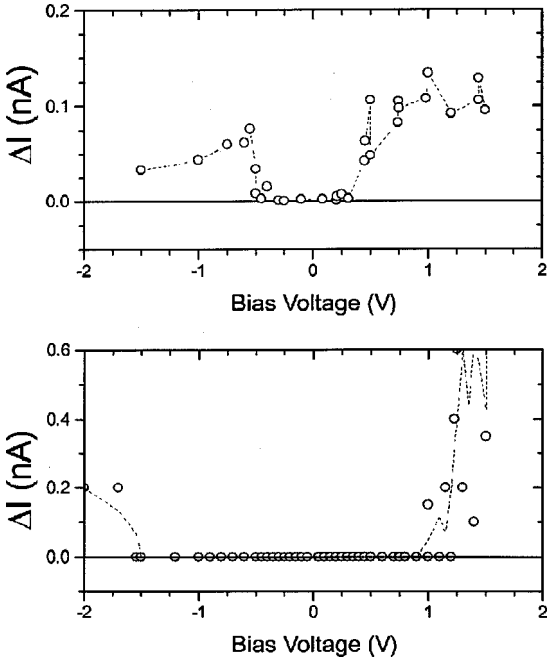

Fig. 40. $\Delta I(V)$ plots of two hydrogenated silicon clusters (a) 6.8 Å, (b) 9.8 Å [389]. Reproduced with permission from [389].

Passivation with hydrogen removes dangling bonds at the surface of the particles. Passivation with oxygen has further consequences for the particles. For instance, the silicon atoms at the surface may become inactive for luminescence once a layer of silicon dioxide has formed. Then, after a particle is oxidized it can appear with smaller diameter compared to the original pristine particle [272].

7.2. Energy Gap Studies of H-Passivated Si Particles

Dangling bond states are localized states in the bulk bandgap. If they are removed by passivation, the gap measured in the STS study should drastically increase. Passivation of surface states is achieved after particle formation by exposing the surface to foreign atoms. In studies of H-passivated silicon particles by STM–STS [389], atomic hydrogen gas was used for surface passivation of silicon particles. H atoms are obtained when igniting a plasma by applying a 1-kV dc voltage to very sharp tips in close proximity to the grounded sample holder. Figure 39 shows an STM image of silicon particles which have been grown on the graphite support in UHV and subsequently passivated with atomic hydrogen. Figure 40 shows $\Delta I(V)$ curves for two hydrogenated clusters. The 6.8- and 9.8 Å diameter particles have energy gaps of 0.9 and 2.4 eV, respectively. These values are far greater than the gap values, which were measured by STS for the pristine particles. It shows that dangling surface states were removed by passivation with hydrogen.

8. NANOWIRES OF SILICON

8.1. Nanowires with Various Geometries

Semiconductor wires thinner than 100 nm are attracting much attention because of their fascinating quantum properties. They may be used for developing one-dimensional quantum wire high speed field-effect transistors and light-emitting devices with extremely low power consumption. Sakaki [414] calculated, that for one-dimensional GaAs channels the electron mobility exceeds 10^6 cm^2/V at low temperature, which is more than 1 order of magnitude larger than the calculated electron mobility of a two-dimensional electron gas [415]. The effect of quantum confinement in quantum wires (QWRs) has been evidenced in the luminescence [416–418], two-photon optical absorption [419], inelastic light scattering [420], and various other studies. It is obvious that impurity scattering and boundary effects become increasingly important when the width of the QWRs is reduced. Additionally, the atomic structure of the QWRs is fundamentally important for their overall properties. In many studies, the atomic structure of QWRs has been assumed to be the same as in the crystalline bulk.

In addition to theoretical studies of electronic and optical properties [399], a number of experimental studies have been reported for Si QWRs: transmission electron microscopy [421], electron transport [422], photoluminescence [423, 424], infrared-induced emission [425], Raman spectroscopy [423, 426]. The atomic structure of the wires in these studies however was not known and was assumed to be either amorphous or the diamond structure of the bulk. This may be justified when the wires are formed by methods like lithography and orientation dependent etching [427]. It may not apply to self-forming quantum wires, which were grown freely by vapor condensation.

Crystalline silicon does not have the tendency to grow in one dimension, as there is no preferential direction associated with the diamond-type lattice. The formation of sp^3-bonds

in silicon leads to fourfold coordination with four equivalent directions for growth. This is in contrast to carbon, which can also occur in sp^1- and sp^2-configurations and therefore has various forms of one-dimensional structures. As small clusters, carbon grows in the form of linear chains or monocyclic rings. It also grows in the form of nanotubes [428]. Such quasi-one-dimensional structures are of great interest for scientists and engineers due to their exceptional quantum properties not found in the three-dimensional bulk.

Due to the technological importance, efforts have been made to produce nanometer scale silicon wires in a controlled manner, using common semiconductor processing steps [429–432]. Columns with small diameters have been found after electrochemical treatment of Si wafers with hydrofluoric acid [266, 433]. There has been much discussion about whether quantum confinement in these wires explains the visible photoluminescence of porous silicon.

Individual nanowires of silicon have been produced by a number of research groups [427, 430, 431, 434–445], for example, by natural masking [435], lithography [427, 441], wet-chemical etching [431, 437] and vapor–liquid–solid growth [438]. These methods use growth techniques, which lead to natural surface passivation of the wires, usually by oxidation. Silicon is very easily oxidized, because the diamond-type crystal structure leads to a high density of dangling bonds at the surface.

8.2. Fullerene-Structured Si Nanowires

In an article [344], the formation of fullerene-structured silicon nanowires was reported. The results of this work are shown in this chapter.

The nanowires were grown from the atomic vapor in ultra-high vacuum and analyzed by scanning tunneling microscopy (STM). Such an STM image (114×114 nm) is displayed in Figure 41. The picture shows several bundles with 20–30 wires per bundle. The nanowires are more than 100-nm long, with diameters from 3 to 7 nm. The width of the wires is uniform in each bundle.

For structural consideration of vapor grown silicon nanowires, one may start from the requirement of a distinct wire axis, and keep bond angles close to the bulk ones. Additionally one may apply the topological restrictions that only five- and six-membered rings occur. This leads to the construction of several linear polyhedric networks:

(a) Si_{12}-cage polymer structure (12 atoms per unit cell).
(b) Si_{15}-cage polymer structure (10 atoms per unit cell).
(c) Si_{20}-cage polymer structure (based on the I_h dodecahedron, 30 atoms per unit cell).
(d) Si_{24}-cage polymer structure (based on the $D6d$ icosahedron, 36 atoms per unit cell).

The suggested structures are shown in Figure 42. All models have a stacking of Si cages in common, in the center of which lies the wire axis. While these lattices deviate from the diamond-structured bulk, tetrahedral configuration of the Si atoms is maintained.

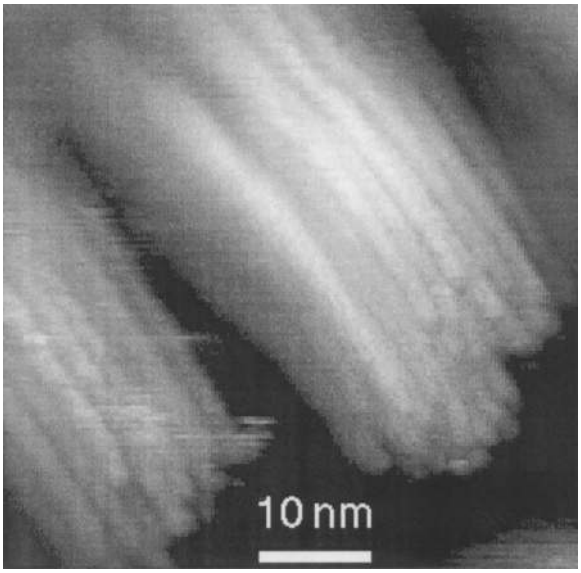

Fig. 41. Bundles of vapor-grown silicon nanowires, imaged by STM [344]. Reproduced with permission from [344], copyright 1999, American Physical Society.

In structure "a" (C_{3v} symmetry), the axis of the wire passes through the centers of buckled Si_6-rings. Two adjacent rings are connected by three bonds and form an Si_{12} cage. This cage represents the unit cell, which is repeated every 6.31 Å. The surface of the wire consists of buckled hexagons.

Structure "b" (C_{5v} symmetry) consists of planar pentagons, joined through five outward oriented interstitial atoms. Two pentagons together with the interstitial atoms form a cage. The

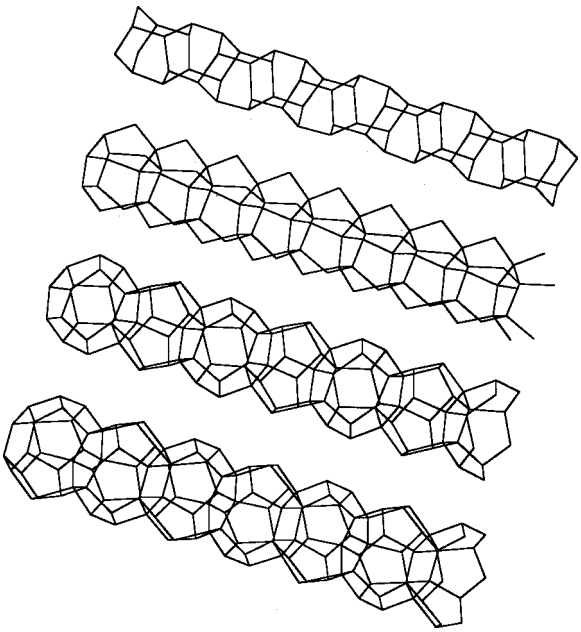

Fig. 42. Four models of nanowire core structures, as polymers of Si_{12}–, Si_{15}–, Si_{20}–, and Si_{24}– cages [344]. Reproduced with permission from [344], copyright 1999, American Physical Society.

unit cell of this structure contains 10 atoms and the repeat distance is 3.84 Å. The surface of the wire consists of buckled hexagons.

Structure "c" (C_{5v} symmetry) is built from Si_{20}-cages. These dodecahedra (I_h symmetry) are the smallest possible fullerene structures, consisting of 12 pentagons. In the wire structure, two adjacent cages share one pentagon. The 30 atoms of one and a half such cages build the unit cell, which is repeated every 9.89 Å. Pentagons make up the surface net of this wire.

Structure "d" (C_{6v} symmetry) is similar to structure c, only that Si_{24}-cages (D_{6d} symmetry) are used as building blocks. These units contain 12 pentagons and 2 hexagons. The hexagons are shared by two adjacent cages and are concentric to the wire axis. The unit cell consists of 36 atoms and the lattice parameter is 10.03 Å. The surface of the wire consists of pentagons.

The Si_{20} and Si_{24} cages correspond to the smallest fullerenes. Si_{20} is a 12-hedron consisting entirely of pentagons. It has six equivalent fivefold symmetry axes. The fullerenic 13-hedron (Si_{22}) does not exist. The fullerenic 14-hedron (Si_{24}) has twofold linear (30°-twisted) coordination.

To find the most stable of the proposed structures, their binding energies and HOMO–LUMO gaps were calculated. The PM3 self-consistent-field molecular orbit (SCFMO) theory derived by Stewart [446] was applied. The calculations show energy gaps between 1.8 and 3.2 eV (Fig. 43) for nanowires containing up to 60 atoms. The wires are between ~4 Å (structure a) and 10 Å (structure d) thick. The gap

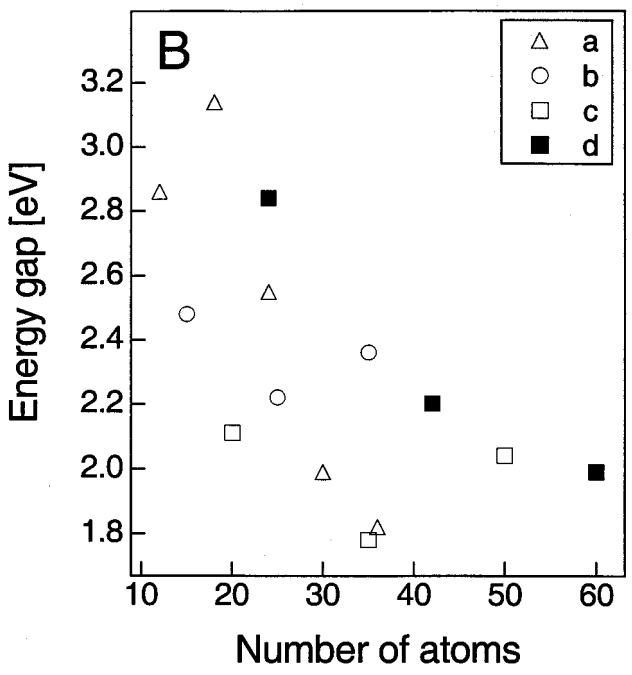

Fig. 43. PM3-calculated energy gaps as a function of size for the four wire structures [344]. Reproduced with permission from [344], copyright 1999, American Physical Society.

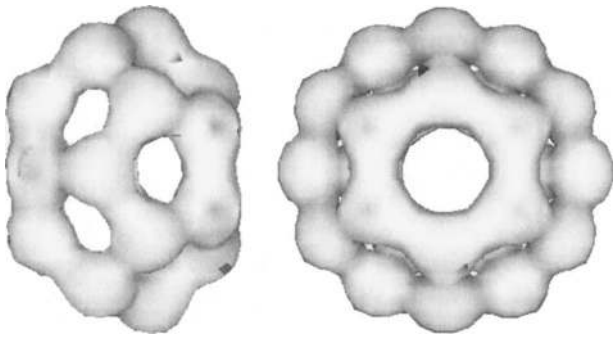

Fig. 44. Charge density isosurface of the fullerenic Si_{24} cluster [344]. Reproduced with permission from [344], copyright 1999, American Institute of Physics.

becomes rapidly smaller with increasing length of the wire. For a given size, the energy gap of structure d is largest.

For small length, structure d has the highest binding energy. The Si_{24} fullerene cage is thermodynamically favorable over the other structures, and also has a symmetry axis specified for preferential addition of further cages. Therefore, the Si_{24}-based wire may have the best chance to form.

Among the four considered configurations, structure d has the highest binding energy per atom and the largest energy gap. If energetics is responsible for the wire formation in its early stage, then structure d should grow preferentially. Once the Si_{24}-based polymer has formed, the wire may continue to add layer by layer, further increasing its diameter.

Dodecahedral Si_{20} clusters were predicted to be stable, using a model potential for an sp^3-hybridized atom [129]. It has been argued that these clusters may not be found isolated in experiments because the dangling bonds (on the cages' outer surfaces) would make them "unextractable" [317] from other silicon material. Fullerenic Si_{20} units were synthesized as bulk body-centered cubic (bcc) solids, with additional Si atoms at half the interstitial sites (three sites per Si_{20}), leading to a silicon lattice with $(Si_3Si_{20})_2 = Si_{46}$ units [54]. Such hollow silicon materials may have novel properties. In fact, superconductivity was found in the $Na_2Ba_6Si_{46}$ phase [447].

In Figure 44, the charge density distribution of Si_{24} is shown, as obtained from the PM3 analysis. The left side of the figure gives a side view with the pentagonal-type surface. The axis for wire growth goes through the two hexagons on the opposite sides of the cluster. The hexagons are rotated by 30° relative to each other. On the right side of the figure, the cluster is viewed from the wire axis.

9. CARBON PARTICLES

9.1. Electronic Structure of Carbon Particles

The fast growing technological importance of carbon-based nanostructures is well known [448]. From the backbones of organic molecules to particulates in air pollution [449, 450] or diamond-like films, carbon is crucial to the stability and the properties of many natural and artificial structures. In fact,

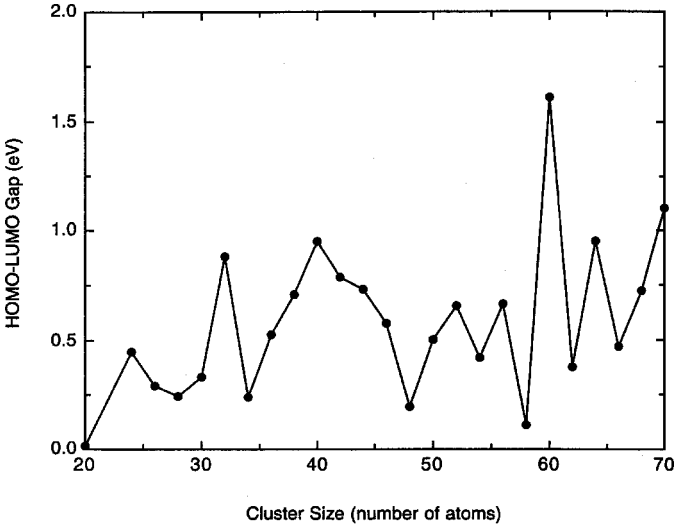

Fig. 45. HOMO–LUMO gap, calculated for fullerene-structured Si_{20} to Si_{70} clusters [461]. Reproduced with permission from [461], copyright 1992, American Institute of Physics.

an infinite number of covalent carbon structures may exist with either diamond-like (sp^3), graphite-like (sp^2), linear (sp), or mixed (sp^3/sp^2, sp^2/sp, sp^3/sp) bonding. The "flexibility" in the s–p-hybridization makes carbon unique leading to the enormously large variety of hydrocarbon molecules. However, this flexibility in bond type becomes a difficult issue if small clusters of elemental carbon are considered. Many metastable isomeric structures are possible, each having a pronounced minimum in the potential-energy hypersurface [451, 452]. Fullerenes are a well-studied class of such isomers, but they form only a small fraction of the overall possibilities. While carbon clusters with up to about 30 atoms in the ground state are believed to be linear chains, monocyclic or polycyclic rings [453], the atomic structures and properties of the larger (nonfullerene) clusters are little known.

Graphite and some forms of amorphous carbon [454] are semimetallic with zero bandgaps. If carbon particles are reduced in size to a level where quantum effects become important, large energy gaps may appear [145, 455]. Indeed, energy gaps of up to 8.5 eV have been predicted for carbon clusters with fewer than 10 atoms [456]. Using high-resolution electron energy loss spectroscopy (EELS) a semimetal to semiconductor transition has been found for noncrystalline, graphite-like carbon particles with diameters of about 1 nm [457].

Simulation studies obtained the value of 2.2 eV [458] for C_{60} and gaps below 2 eV for cages composed of 24 to 80 atoms [459–461]. In another theoretical study of fullerenes from C_{20} to C_{70} [461] the HOMO–LUMO gaps vary between 0.015 (C_{20}) to 1.61 eV (C_{60}). This variation is discontinuous

Table I. Energy Gaps for Carbon Clusters

Reference	Year	Clusters	Energy Gap	Methods
Pitzer and Clementi [580]	1959	$C_2, \ldots, C_{10}$	Increasing with decreasing size	LCAO calculations
Liang and Schaefer [456]	May 1990	C_4, C_6, C_8, C_{10}	C_4: 8.14 eV C_6: 7.2 eV C_8: 6.6 eV C_{10}: 6.19 eV	SCF and CISD (single and double configuration interaction)
Liang and Schaefer [456]	September 1990	C_{10}, isomers	C_{10}: 8.47 eV	ab initio quantum mechanical method with SCF, CISD
Feng, Wang, and Lerner [582]	1990	C_{60}, isomers	5.4 eV	Intermediate neglect of differential overlap (INDO), INDO/CI
Zhang et al. [461]	1992	C_{20}, $C_{24}, \ldots, C_{70}$	Refer to graph	Tight-binding molecular dynamics and geometry optimization
Woo, Kim, and Lee [460]	1993	C_{50}, C_{60}, C_{70}, C_{80}	C_{50}: 0.5 eV C_{60}: 2.2 eV C_{70}: 1.55 eV C_{80}: 0.3–0.4 eV	Empirical tight-binding energy calculations
Wang et al. [583]	1993	C_{60}, C_{70}	Values around 2–3 eV	Analytical quasi-particle energy calculations
Endredi and Ladik [584]	1993	C_{60}	8.31 eV	Density functional theory
Tomanek [585]	1995	C_{60}	2.2 eV	Linear combination of atomic orbitals (LCAO) method
Yao et al. [51]	1996	C_{60}	1.8 eV	STM experiment

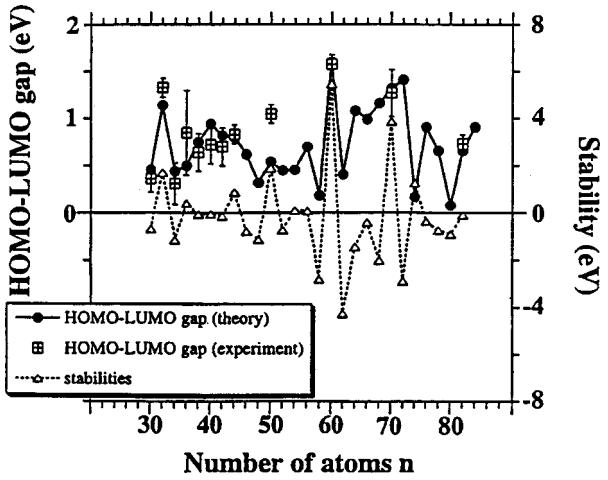

Fig. 46. HOMO–LUMO gaps for fullerenes derived from photoelectron spectra, as well as theoretical gap and stability data [464]. Reproduced with permission from [464], copyright 1998, American Physical Society.

with respect to the cluster size (Fig. 45). A comparison of theoretical results for energy gaps of carbon particles is given in Table I.

Several groups have determined the HOMO–LUMO gap experimentally by scanning tunneling spectroscopy. For C_{60}, a gap of 1.8 eV was determined [51]. The importance of charging effects has been used to explain a small observed gap value of 0.7 eV for STS of C_{60} [50]. Various gap values (0.8, 1.3, and 1.4 eV) were determined for C_{60} clusters at different adsorption sites of the Si(111) 7×7 substrate [462]. For C_{36}, a gap of 0.8 eV was obtained by STS [463]. Photoelectron spectroscopy has been used to study free fullerenes. HOMO–LUMO gaps between zero and 1.6 eV were determined for C_{30} to C_{82}, and the size dependence was found to change discontinously with cluster size [464] (Fig. 46).

9.2. Bandgap Studies of Carbon Particles

In this chapter, we show STS results for carbon clusters [465] with diameters between 4 and 1100 Å. Voltage-dependent STM was used as the STS method.

Figure 47 shows STM images of a 5.5 Å carbon cluster at different bias voltages. For this cluster, the complete sequence consists of 36 images in the bias range from -1.0 to $+1.0$ V. Six of these images, with bias voltages of -550, -275, -225, $+225$, $+275$, and $+550$ mV are displayed in the upper panel of Figure 47. While the cluster appears bright at -550 mV, it is less bright at -275 mV and it is no longer visible at -225 and at $+225$ mV. It reappears again at $+275$ mV. The lower panel of Figure 47 shows cross sections of the images. The difference ΔI between the currents with the tip on the cluster and on the bare substrate is a measure of the density of states of the cluster.

ΔI values as a function of the bias voltage are shown for three different clusters in Figure 48. Each data point corresponds to an STM image. Distinct electronic structure features are observed, varying with size. For some of the clusters, a small asymmetry of the current-voltage plots with respect to zero bias was observed. Such shifts may be due to the presence of a contact potential between the cluster and the substrate, which is superimposed to the applied bias voltage [466]. The interaction of carbon clusters with the HOPG substrate is negligible [467, 468]. This is seen from the fact that the clusters are easily moved by the STM tip and often are even picked up.

Energy gaps of 650, 450, and 150 meV are found for clusters with diameters of 4, 5.5, and 7.5 Å, respectively. The cluster diameters and energy gaps are plotted in Figure 49. The results show close to zero-energy gaps for large clusters. At about 15 Å, an energy gap opens.

To understand the observed size behavior of the energy gap, the effective mass approximation (EMA) is used. For a spherical well, the solutions to the Schrödinger equation are given by spherical Bessel functions. If the potential well is infinite, the

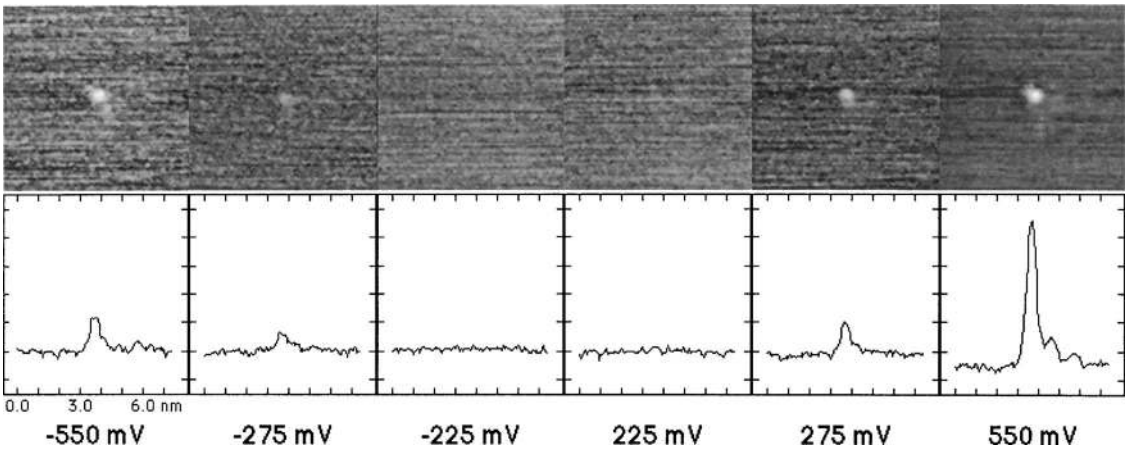

Fig. 47. STM images (upper panel) and profiles (lower panel) of a carbon cluster at different bias voltages. The cluster is 5.5 Å in diameter [465]. Reproduced with permission from [465], copyright 1999, Elsevier Science.

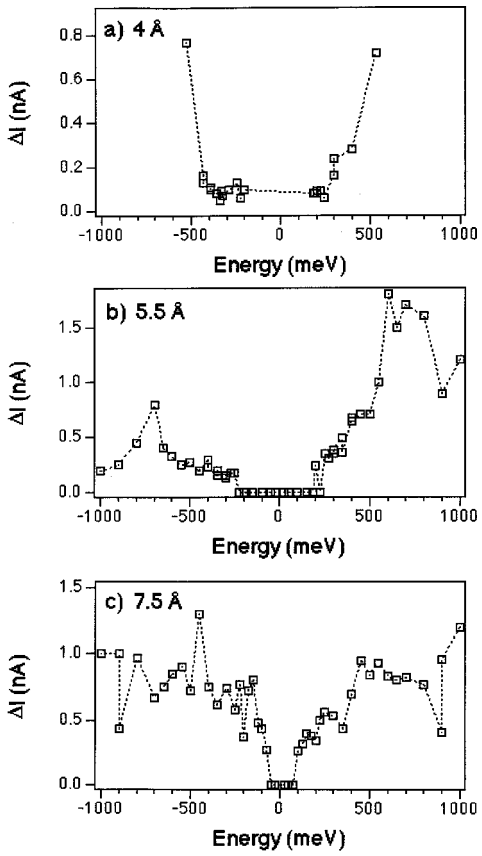

Fig. 48. $\Delta I(V)$ plots for three different clusters. (a) A 4-Å cluster with an energy gap of 300 meV, (b) a 5.5-Å cluster with an energy gap of 450 meV, (c) a 7.5-Å cluster with a 150-meV gap [465]. Reproduced with permission from [465], copyright 1999, Elsevier Science.

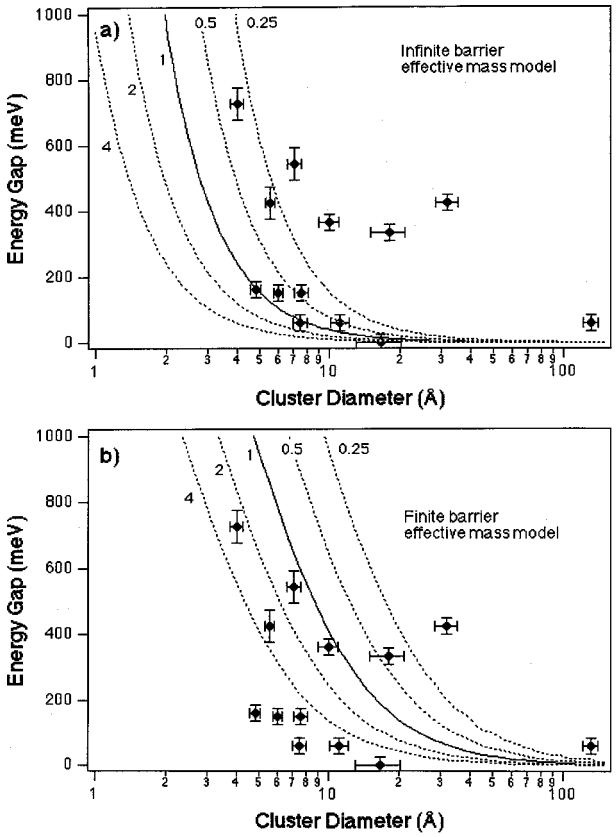

Fig. 49. Energy gaps for carbon clusters of different size; (a) experimental data and infinite barrier effective mass model fit (solid line is for $m^*/m = 1$), (b) experimental data and finite barrier effective mass model fit [465]. Reproduced with permission from [465], copyright 1999, Elsevier Science.

wave function vanishes at this barrier and the energy eigenvalues are determined from the zeros of the Bessel functions. This leads to a size-dependent shift of the energy gap, which scales with the inverse square of the diameter d.

In Figure 49a, this result is plotted for different effective masses. The curves show a significant opening of the energy gap for particle sizes below about 100 Å. Only for very high effective masses, do the curves get close to the observed gap values. Therefore, it appears that the "infinite barrier effective mass model" does not well describe the particle properties.

The infinite barrier approach does not take into account the finite ionization potential of the clusters. It can be introduced by considering a finite potential well. In this case, electrons have a nonzero probability to move out into an area surrounding the particle. For clusters, due to their small sizes, the spill-out of the electron density significantly affects their overall properties [290, 469]. The radial wave function exhibits an oscillatory behavior in the internal region and a decreasing exponential behavior in the external region. If V_0 is the depth of the well, the energies E of bound states are within $-V_0$ and zero. For convenience, we introduce the parameters $k = \{2m^*(V_0 + E)\}^{1/2}$ (inside) and $\kappa = \{2m^*|E|\}^{1/2}$ (outside). The internal and external solutions join smoothly at the boundary only for those k and κ at which the transcendental equation $\mathrm{ctg}(kd/2) = -\kappa/k$ holds. The resulting energy gap values are smaller than in the infinite wall approximation, as can be seen in Figure 49b. Again, the curves for different effective masses are plotted. It is found that in the size regime of interest the energy gaps are not sensitive to the depth of the potential well. Essentially the same results are obtained for $V_0 = 5$ eV and for $V_0 = 8$ eV.

The experimental gap data do not follow a single curve in Figure 49. There is a spread of gaps even for the same cluster size. This is not surprising as in this small size range (below about 15 Å) the individual atomic structures and bond conditions become crucial. For small clusters, size-dependent properties are discontinuous. In addition, as small covalent clusters are stable in a large number of isomeric structures, a wide range of energy gaps is expected for the same clusters size.

10. THIN FILMS OF PARTICLES

10.1. Formation and Properties

Nanoparticles, produced in vacuum, by an aerosol or liquid phase techniques, can form thin compact films after deposition on a support material. Narrow particle size distributions

($<\sim 5\%$) can be obtained. Several groups have studied ordered superlattices of crystalline metal [470, 471] and semiconductor particles [472–474].

Another technique is the deposition of atomic vapor on an inert substrate. The particles form on the substrate by quasi-free growth, diffuse at the substrate, and form a granular solid film. By using appropriate generation conditions, one can achieve quite narrow size distributions. Depending on the substrate temperature and on the cluster-substrate interaction, the film thickness can be more or less uniform. Layer-by-layer growth for particle films can be achieved.

Nanoparticle films are interesting from many points of view. They still may have many properties of the free nanoparticles. The coupling between the particles however leads to interface formation, which can result in changes of electronic and optical properties. The particles in the films can form ordered lattices with translational symmetry. The particles in gold particle films on mica, for instance, are ordered in a zigzag pattern [475]. The type of order can be due to the coupling to the substrate or due to the interaction between the particles. For spherical symmetric particles of metal atoms, one can expect close-packed structures. The type of structure however can differ over macroscopic regions. Often, the nanoparticle films have ordered areas in the nano-to-micrometer size range.

Silicon nanoparticle films have been studied by several groups concerning their structural [16], electrical [476], electronic [477–479], and optical properties [480–482]. The films were produced from particles deposited after laser ablation of silicon [476], magnetron sputtering [483, 484], laser induced decomposition of SiH_4 [480] and a few other techniques [355, 485, 486].

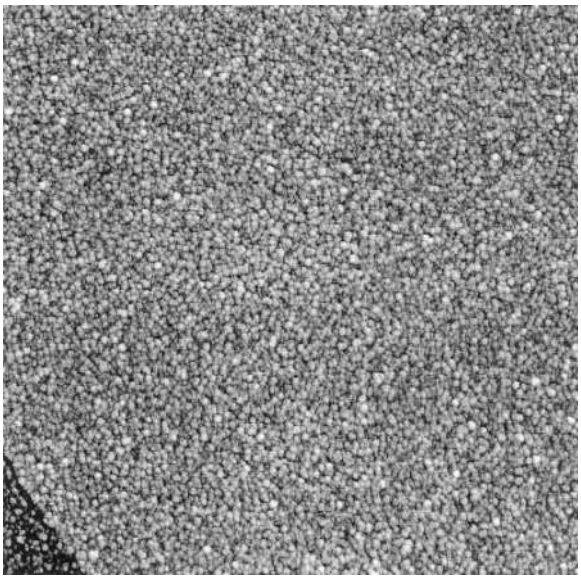

Fig. 50. An 820×820-nm STM image of a thin film of silicon particles [487]. Reproduced with permission from [487], to be published.

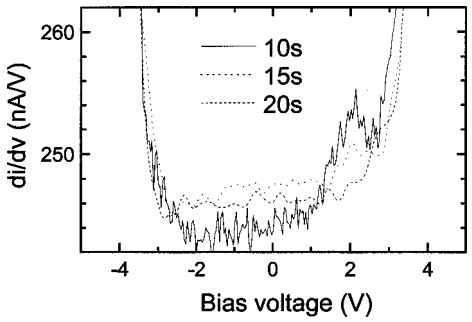

Fig. 51. A di/dV curve for a thin film of silicon particles taken by STS [487]. Reproduced with permission from [487], to be published.

10.2. Bandgap Studies of Si Particle Films

An image of a silicon particle film, grown by vapor condensation on highly oriented pyrolytic graphite (HOPG), is shown in Figure 50 [487]. The silicon nanoparticles were grown upon deposition of several monolayers of atomic silicon using magnetron sputtering. By removing some of the particles in small areas, using high tunneling currents, we determined that the films are between one and three layers thick.

In Figure 51 dI/dV curves are shown taken on several of these films produced under different conditions. All di/dV curves show a peak at a positive bias of about 2 V. Very likely, this peak is not a band structure feature. Therefore, one obtains bandgap of about 3.5 eV. This value is relatively large compared to the gap expected for free 5-nm silicon particles. It suggests that the coupling between the particles can alter their electronic structure and that the interface has an important influence on the film properties. These films have been grown from pristine silicon particles, which are expected to be highly reactive after formation. They strongly couple with their neighbors once they are consolidated. The dangling bonds, originally present at the particle surface, can be passivated by the interaction with their neighbors. Cross-linking can change the particle's bandgaps and other features in the electron density of states. This is seen in the peak at 2 V, which seems to be related to interparticle interaction, as it has not been observed for free silicon particles.

11. APPLICATIONS

11.1. Photonic Devices

The potential value of quantum-confined particles for nonlinear optical and electrooptical applications has long been anticipated [237, 488, 489]. In fact, there are plenty of possible applications for quantum dots in nanoelectronics [490–494] and for photonic devices [495–502]. Nonlinear optical response has for instance been found for gold particles with 25-, 90-, and 150-Å radius [503].

Nanomaterials with nonlinear properties find use as optical limiters, for eye protection and switching applications. Carbon black (particle) suspensions (CBSs) have been extensively investigated as optical limiters [504, 505]. A strong optical

limiting effect was found for 56-Å Ag particles, while Ni (58 Å), CdS (50 Å), and PbS (66 Å) show poor limiting performance [506]. Gold particles show a size-dependent optical limiting effect in the range 25–150 Å [503].

The field of nanoelectronics is often considered as the key technology in the twenty-first century [507–509]. The required nanometer-sized structures however are often too small for the currently used industrial methods [510]. Technology such as new patterning methods have to be developed [511].

The tunability of the energy gap can be used to make light sources and detectors for specific use. In addition, when discrete energy level are formed with decreasing particle size, third-order optical nonlinearities are observed, which can be used in optical switches, waveguides, shutters, or information processors [265, 488]. Nonlinear optical response occurs for metal particles [512, 513] and semiconductor particles. For CdSe nanocrystal quantum dots, for example, the second harmonic generation (SHG) response shows a pronounced size dependence [514]. Additionally, third-harmonic linearities were found for nanocrystals and were discussed in relation to quantum confinement [8, 515, 516].

Further use of the particles has been demonstrated for metal-insulator-semiconductor field-effect-transistors (MISFET) [371, 517], photodetectors [518, 519], quantum dot lasers [520–523], solar cells [524], single-electron transistors [525], infrared detectors [518], or optical memory devices [526].

Silicon single-electron transistors (SETs) [368] have the potential of very low power consumption devices [527]. Often, SETs need to be operated at 4.2 K [366]. To make the devices however practical for circuits application, the room temperature operation and the integration into silicon are essential. Additionally, an Si dot size of less than 10 nm is required. This is the size range where both the electronic and Coulomb energy gaps become large and strongly dependent on the particle sizes. The carrier transport properties through the dots [382, 528–530] needs to be known for such applications. It critically depends on the bandgap.

A silicon nanocrystal-based single-electron memory [531, 532] could well be embedded in integrated circuits. It would allow using techniques of the silicon industry to incorporate the memory function in silicon chips.

Semiconductor nanoparticles were also used as probes in biological diagnostics [533, 534]. Nanobiology and nanochemistry are large fields where clusters and nanoparticles can be used for novel processes and materials [495].

Metal particles find many applications in fields such as photocatalysis, ferrofluids, chemisorption, aerosols, and powder metallurgy. The heterogeneous catalysis by metal particles has been studied extensively [535] and is widely used in industry. The linear and nonlinear optical properties [536–538] of metal clusters have attracted a great deal of interest and may be used in future applications.

Carbon clusters are important species in astrophysics, materials science, and combustion processes. They play a key role in the preparation of thin diamond films via chemical vapor deposition or cold plasma techniques [539–544].

A type of material with potential applications is composed of organic ligand stabilized metal clusters. The metal core of a particle is encapsulated by an insulating organic monolayer. The insulating layer is a conductivity barrier through which electron tunneling or hopping occurs. Both components, the core and the encapsulant, can exert strong influences on the macroscopic electrical conductivity. A size-induced metal to semiconductor transition was reported for dodecanethiol-stabilized gold clusters [545]. Thiol-protected Au particles have been found to assemble in highly ordered two- and three-dimensional superlattices [546].

11.2. Cluster-Assembled Materials

Assembling clusters and nanoparticles can form a new class of materials and structures. Such so-called cluster-assembled materials [355, 470, 547–549], nanophase [79], nanocomposite materials [550] have novel mechanical, electrical, and optical properties. A hypothetical cluster assembled crystal with six atomic gold cluster units is shown in Figure 52.

The particles can be assembled in the form of mono- or multilayers on solid supports [551]. Such nanoparticle films have many uses for mechanical protection as well as thermal and electrical shielding.

Cross-linking of clusters may be an important effect for future cluster assembled materials. For carbon, crystals with C_{20} and C_{22} fullerene units have been postulated [552]. The clusters can be arranged in a face-centered cubic lattice. Electronic structure calculations predict for these hypothetical

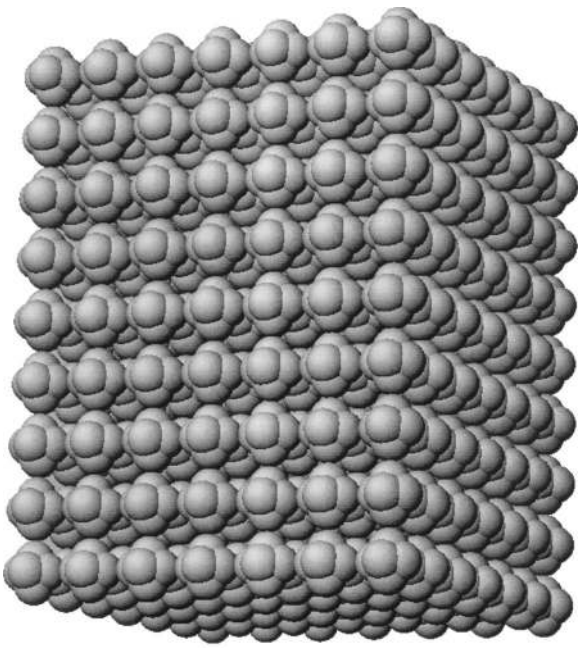

Fig. 52. Model for a hypothetical cluster assembled material consisting of Au_6 clusters in a simple cubic lattice [475]. Reproduced with permission from [475], unpublished.

crystals large bandgaps of up to 6 eV. Porous carbon structures such as hollow diamonds [553] could be very strong and light materials.

From the work on porous silicon [265, 488] and silicon nanosize films [518], one can conclude that silicon nanoparticles have the potential for use in silicon-based photonic and optoelectronic devices [554–556]. While III–V semiconductor quantum dots show interesting optical properties [520], they may eventually be replaced by silicon dots. One of the greatest challenges is the integration of such dots into serviceable architectures such as electroluminescent (EL) devices [557]. Their efficiency not only depends on the optical but also on the electrical (carrier transport) properties.

Light-emitting silicon particles may be integrated into microelectronic circuits [558]. Charge transport in nanostructures [559] is becoming an important issue as miniaturization of devices proceeds. One needs to know the detailed atomic structure of the sample at the nanoscale to fully understand the type of transport. The energy gap dependence on size and structure needs to be known for crystallites and grain boundaries. A silicon-based single electron tunneling transistor has been realized but at a temperature of 4.2 K [560], much to low for technical applications. Room-temperature single-electron tunneling can be achieved for the transport of carriers through smaller nanostructures such as a few nanometer-sized quantum dots.

A size-dependent opening of the bandgap for nanoparticles gives numerous new opportunities for their use in industrial applications. Powders of such particles can be assembled and compacted leading to nanogranular solids with new functions. If GaAs, for example, can be replaced by Si in light-emitting devices, it is an advantage as the silicon-based junction is easier to prepare and is environmentally much friendlier. Most two-component semiconductor materials are poisonous and can lead to severe health problems for exposed humans. Nanoparticle films of silicon may therefore replace intermediate and large bandgap bulk semiconductors.

11.3. Nanolithography

Optical nanolithography is limited to structures whose sizes are comparable to the wavelength of the used radiation. For nanoscale structures, X-rays can be used, but the techniques require extensive setups of special lenses and mirror systems. Alternative ways to produce small nanosized features are neutral atom lithography [561] or nanoimprint lithography [562].

A different approach is the use of STM and AFM [563]. The decomposition of organic gases in the gap between the tip and the sample was used to fabricate nanosized structures [564–568]. For instance, aluminum features were produced on silicon surfaces, using tunneling and field emission modes [569]. Using the STM, nanowires of silicon were generated by the decomposition of silane [570].

Electroluminescent devices, using silicon nanowires [441] are based on the intergration of quantum optics and silicon. Electric-field assisted AFM can also be used for nanofabrication [571]. Pits have been formed with the STM tip on gold [572], graphite [573], sputtered carbon [574], and metal oxide layers [575]. Nanometer scale rings on a thin Si-oxide layer were fabricated [576]. Another approach is the nanooxidation of hydrogen-passivated Si surfaces using an STM [577–579].

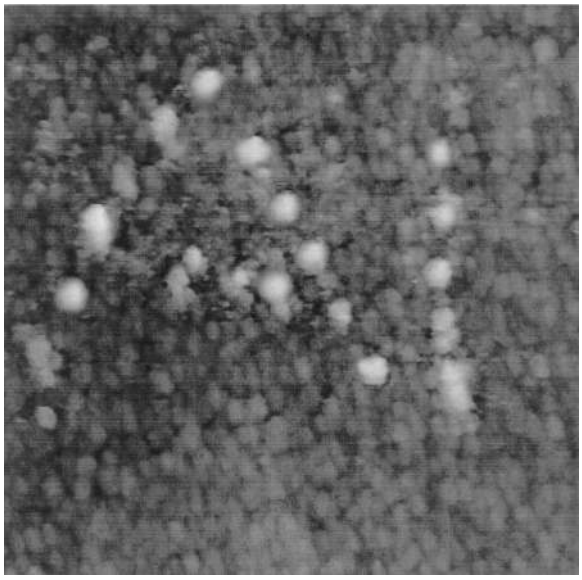

Fig. 53. A 250×250-nm STM image: The letters A and I were written on a thin film of silicon particles using the STM tip and high tunneling currents. For obtaining a white dot, two to three particles of the substrate where fused together [487]. Reproduced with permission from [487], unpublished.

In Figure 53 an STM image is shown where the letters A I are written on a thin film of silicon particles [487]. The indi-

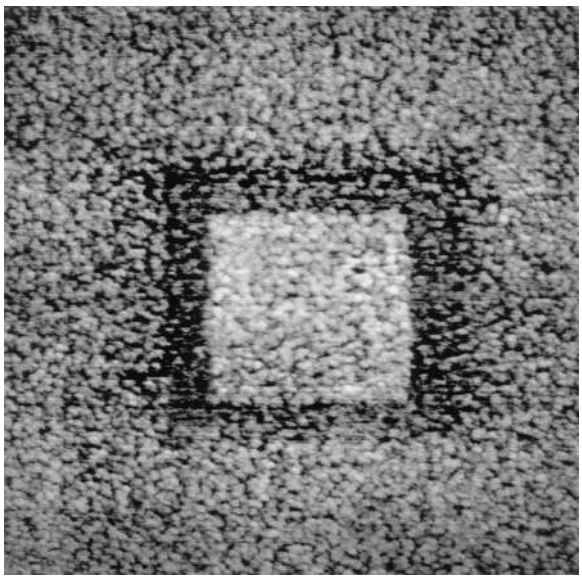

Fig. 54. A 600×600-nm STM image: A three level terrace structure was produced on a silicon particle film by fusion of clusters in of a small square with subsequent vaporization of a surrounding square. The white square in the center is stabilized in the first process and does not vaporize in the second [487]. Reproduced with permission from [487], unpublished.

vidual points, making up the letters, are produced by scanning over a few particles with an enhanced tunneling current. This leads to the fusion of two to three silicon particles, which then appear white with respect to the gray background.

The STM can also be used to vaporize particles. This occurs when a high bias voltage is temporarily applied. In this case, nanostructures can be formed which appear black on a gray background of the silicon particle film. The combination of fusion and vaporization can be used to shape a silicon particle film [487]. This is demonstrated in Figure 54. A square-shaped terrace, higher than the substrate level, is surrounded by a trench, separating the inner terrace from the particle film.

Both the fusion and the vaporization are possible due to the large bandgap of the silicon particles forming the thin films. For the low-conducting layer, the separation between the tip and silicon surface is very small and the electric field is very high. A combination of both, very high tunneling current and very high bias voltage, and their variation, allows the formation of shapes as shown in the preceding figures.

REFERENCES

1. T. van Buuren, L. N. Dinh, L. L. Chase, W. J. Siekhaus, and L. J. Terminello, *Phys. Rev. Lett.* 80, 3803 (1998).
2. S. Hayashi and H. Abe, *Jpn. J. Appl. Phys.* 23, L824 (1984).
3. Y. Kanemitsu, H. Uto, Y. Masumoto, and Y. Maeda, *Appl. Phys. Lett.* 61, 2187 (1992).
4. V. Cracium, I. W. Boyd, A. H. Reader, and D. E. W. Vandenhoudt, *Appl. Phys. Lett.* 65, 3233 (1994).
5. M. R. Zachariah, M. J. Carrier, and E. Blaisten-Barijas, *J. Phys. Chem.* 100, 14,856 (1996).
6. D. J. Norris, A. Sacra, C. B. Murray, and M. G. Bawendi, *Phys. Rev. Lett.* 72, 2612 (1994).
7. D. J. Norris and M. G. Bawendi, *Phys. Rev. B* 53, 16338 (1996).
8. U. Banin, J. C. Lee, A. A. Guzelian, A. V. Kadavanich, A. P. Alivisatos, W. Jaskolski, G. W. Bryant, A. L. Efros, and M. Rosen, *J. Chem. Phys.* 109, 2306 (1998).
9. U. Banin, J. C. Lee, A. Guzelian, A. V. Kadavanich, and A. P. Alivisatos, *Superlattices Microstruct*. 22, 559 (1997).
10. M. Leon, P. M. Petroff, D. Leonard, and S. Fafard, *Science* 267, 1966 (1995).
11. S. A. Empedocles, D. J. Norris, and M. G. Bawendi, *Phys. Rev. Lett.* 77, 3873 (1996).
12. A. I. Ekimov, F. Hache, M. C. Schanne-Klein, D. Ricard, C. Flytzanis, I. A. Kudryavtsev, T. V. Yazeva, A. V. Rodina, and A. L. Efros, *J. Opt. Soc. Am. B* 10, 100 (1993).
13. H. Fu and A. Zunger, *Phys. Rev. B* 57, R15064 (1998).
14. H. Fu, L. W. Wang, and A. Zunger, *Phys. Rev. B* 57, 9971 (1998).
15. L.-W. Wang and A. Zunger, *J. Phys. Chem.* 98, 2158 (1994).
16. B. Garrido, A. Perez-Rodrigues, J. R. Morante, A. Achiq, F. Gourbilleau, R. Madelon, and R. Rizk, *J. Vac. Sci. Technol. B* 16, 1851 (1998).
17. J. P. Wilcoxon, G. A. Samara, and P. N. Provencio, *Phys. Rev. B* 60, 2704 (1999).
18. A. K. Dutta, *Appl. Phys. Lett.* 68, 1189 (1996).
19. V. S. Veerasamy, G. A. J. Amaratunga, W. I. Milne, P. Hewitt, P. J. Fallon, D. R. McKenzie, and C. A. Davis, *Diamond Relat. Mater.* 2, 782 (1993).
20. U. Stephan, T. Frauenheim, P. Blaudeck, and G. Jingnickel, *Phys. Rev. B* 49, 1489 (1994).
21. D. R. McKenzie, D. A. Muller, and B. A. Pailthorpe, *Phys. Rev. Lett.* 67, 773 (1991).
22. D. A. Drabold, P. A. Fedders, and M. P. Grumbach, *Phys. Rev. B* 54, 5480 (1996).
23. D. Kwon, C.-C. Chen, J. D. Cohen, H.-C. Jin, E. Hollar, I. Robertson, and J. R. Abelson, *Phys. Rev. B* 60, 4442 (1999).
24. M. Yamamoto, R. Hayashi, K. Tsunemoto, K. Kohno, and Y. Osaka, *Jpn. J. Appl. Phys.* 30, 136 (1991).
25. D. J. DiMaria, J. R. Kirtley, E. J. Pakulis, D. W. Dong, T. S. Kuan, F. L. Pesavento, T. N. Theis, and J. A. Cutro, *J. Appl. Phys.* 56, 401 (1984).
26. M. O'Neil, J. Marohn, and G. McLendon, *J. Phys. Chem.* 94, 4356 (1990).
27. J. A. Eychmuller, A. Hasselbrath, L. Katsikas, and H. Weller, *Ber. Bunsen-Ges. Phys. Chem.* 95, 79 (1991).
28. A. Hasselbarth, A. Eychmuller, and H. Weller, *Chem. Phys. Lett.* 203, 271 (1993).
29. M. G. Bawendi, P. J. Carroll, and W. L. Wilson, *J. Chem. Phys.* 96, 946 (1992).
30. M. Nirmal, C. B. Murray, and M. G. Bawendi, *Phys. Rev. B* 50, 2293 (1994).
31. V. Petrova-Koch, T. Muschik, A. Kux, B. K. Meyer, and F. Koch, *Appl. Phys. Lett.* 61, 943 (1992).
32. W. Hoheisel, Y. L. Colvin, C. S. Johnson, and A. P. Alivisatos, *J. Chem. Phys.* 101, 845 (1994).
33. M. Nirmal, D. J. Norris, M. Kuno, M. G. Bawendi, A. L. Efros, and M. Rosen, *Phys. Rev. Lett.* 75, 3728 (1995).
34. A. L. Efros, M. Rosen, M. Kuno, M. Nirmal, D. J. Norris, and M. Bawendi, *Phys. Rev. B* 54, 4843 (1996).
35. D. J. Norris, A. L. Efros, M. Rosen, and M. G. Bawendi, *Phys. Rev. B* 53, 16,347 (1996).
36. M. Chamarro, C. Gourdon, P. Lavallard, O. Lublinskaya, and A. I. Ekimov, *Phys. Rev. B* 53, 1336 (1996).
37. M. Chamarro, C. Gourdon, and P. Lavallard, *J. Lumin.* 70, 222 (1996).
38. U. Woggon, F. Gindele, O. Wind, and C. Klingshirn, *Phys. Rev. B* 54, 1506 (1996).
39. I. Giaever, *Phys. Rev. Lett.* 5, 147 (1960).
40. R. M. Feenstra, W. A. Thompson, and A. P. Fein, *Phys. Rev. Lett.* 56, 608 (1986).
41. R. M. Feenstra, J. A. Stroscio, and A. P. Fein, *Surf. Sci.* 181, 295 (1987).
42. R. M. Feenstra, *J. Vac. Sci. Technol. B* 7, 925 (1989).
43. P. Avouris and I. Lyo, *Surf. Sci.* 242, 1 (1991).
44. R. J. Hamers, R. M. Tromp, and J. E. Demuth, *Phys. Rev. Lett.* 56, 1972 (1986).
45. H. F. Hess, R. B. Robinson, R. C. Dynes, J. Valles, J. M., and J. V. Waszczak, *J. Vac. Sci. Technol. A* 8, 450 (1990).
46. L. C. Davis, M. P. Everson, R. C. Jaklevic, and W. Shen, *Phys. Rev. B* 43, 3821 (1991).
47. R. M. Feenstra, *Phys. Rev. B* 60, 4478 (1999-I).
48. B. Marsen, M. Lonfat, P. Scheier, and K. Sattler, *Phys. Rev. B* 62, 6892 (2000).
49. O. Millo, D. Katz, Y. W. Cao, and U. Banin, *Phys. Rev. B* 61, 16,773 (2000-II).
50. D. Porath, Y. Levi, M. Tarabiah, and O. Millo, *Phys. Rev. B* 56, 9829 (1997-I).
51. X. Yao, T. G. Ruskell, R. K. Workman, D. Sarid, and D. Chen, *Surf. Sci.* 366, L743 (1996).
52. W. Mizutani, M. Shigeno, and Y. Sakakibara, *J. Vac. Sci. Technol.* 8, 675 (1990).
53. A. Okumura, K. Miyamura, and Y. Gohshi, *J. Vac. Sci. Technol.* 8, 625 (1990).
54. A. Okumura, H. Nakagawa, and Y. Gohshi, *Jpn. J. Appl. Phys.* 34, 2055 (1995).
55. S. Ogawa, F.-R. F. Fan, and A. J. Bard, *J. Phys. Chem.* 99, 11,182 (1995).
56. B. Alperson, I. Rubinstein, G. Hodes, D. Porath, and O. Millo, *Appl. Phys. Lett.* 75, 1751 (1999).

57. B. Alperson, S. Cohen, I. Rubinstein, and G. Hodes, *Phys. Rev. B* 52, R17,017 (1995).
58. L. I. Halaoui, R. L. Wells, and J. Coury, L. A., *Chem. Mater.* 12, 1205 (2000).
59. U. Banin, Y. W. Cao, D. Katz, and O. Millo, *Nature (London)* 400, 542 (1999).
60. D. L. Klein, R. Roth, A. K. L. Lim, A. P. Alivisatos, and P. L. McEuen, *Nature (London)* 389, 699 (1997).
61. D. L. Klein, P. L. McEuen, J. E. Bowen Katari, R. Roth, and A. P. Alivisatos, *Appl. Phys. Lett.* 68, 2574 (1996).
62. U. Sivan, R. Berkovits, Y. Aloni, O. Prus, A. Auerbach, and G. BenYoseph, *Phys. Rev. Lett.* 77, 1123 (1996).
63. S. R. Patel, S. M. Cronenwett, D. R. Stewart, A. G. Hubers, C. M. Marcus, C. I. Duruoz, J. S. Harris, K. Campman, and A. C. Gossard, *Phys. Rev. Lett.* 80, 4522 (1998).
64. J. Tersoff and D. R. Hamann, *Phys. Rev. B* 31, 805 (1985).
65. N. D. Lang, *Phys. Rev. Lett.* 55, 230 (1985).
66. N. D. Lang, *Phys. Rev. Lett.* 55, 2925 (1985).
67. C. J. Chen, *J. Vac. Sci. Technol. A* 6, 319 (1988).
68. C. R. Leavens and G. C. Aers, *Phys. Rev. B* 38, 7357 (1988).
69. E. Teckman and S. Ciraci, *Phys. Rev. B* 40, 10,386 (1989).
70. C. J. Chen, *Phys. Rev. Lett.* 65, 448 (1990).
71. G. Doyen, D. Drakova, and M. Scheffler, *Phys. Rev. B* 47, 9778 (1993).
72. N. D. Lang, *Phys. Rev. B* 34, 5947 (1986).
73. A. Selloni, P. Carnevalli, E. Tosati, and C. D. Chen, *Phys. Rev. B* 31, 2602 (1985).
74. M. Tsukada, K. Kobayashi, N. Isshiki, and H. Kageshima, *Surf. Sci. Rep.* 13, 2 (1991).
75. F. Zypman, L. F. Fonseca, and Y. Goldstein, *Phys. Rev. B* 49, 1981 (1994-I).
76. R. Tromp, *J. Phys. Condens. Matter* 1, 10,211 (1989).
77. R. J. Hamers, *Annu. Rev. Phys. Chem.* 40, 531 (1989).
78. S. Morita, Y. Sugawara, and Y. Fukano, *Jpn. J. Appl. Phys., Part 1*, R32, 2983 (1993).
79. K. Sattler, G. Raina, M. Ge, J. Xhie, N. Venkateswaran, Y. X. Liao, and R. W. Siegel, *J. Appl. Phys.* 76, 546 (1994).
80. J. Bardeen, *Phys. Rev. Lett.* 6, 57 (1960).
81. K. Makoshi, N. Shima, and T. Mii, *Surf. Sci.* 386, 335 (1997).
82. H. Matsuoka and S. Kimura, *Jpn. J. Appl. Phys.* 34, 1326 (1995).
83. K. A. Matveev, L. I. Glazman, and H. U. Baranger, *Phys. Rev. B* 54, 5637 (1996).
84. B. Wang, X. Xiao, X. Huang, P. Sheng, and J. G. Hou, *Appl. Phys. Lett.* 77, 1179 (2000).
85. H. Nejo, M. Aono, and V. A. Tkachenko, *J. Vac. Sci. Technol.* 14, 2399 (1996).
86. R. O. Jones, *J. Chem. Phys.* 99, 1194 (1993).
87. V. Bonacic-Koutecky, L. Cespiva, P. Fantucci, J. Pittner, and J. Koutecky, *J. Chem. Phys.* 100, 490 (1994).
88. C.-Y. Cha, G. Ganteför, and W. Eberhardt, *J. Chem. Phys.* 100, 995 (1994).
89. W. A. de Heer, *Rev. Mod. Phys.* 65, 611 (1993).
90. K. Clemenger, *Phys. Rev. B* 32, 1359 (1985).
91. W. Ekardt and Z. Penzar, *Phys. Rev. B* 43, 1322 (1991).
92. S. Frauendorf and V. V. Pashkevich, *Z. Phys. D* 26, S98 (1993).
93. A. Bulgac and C. Lewenkopf, *Phys. Rev. Lett.* 71, 4130 (1993).
94. C. Yannouleas and U. Landman, *Phys. Rev. B* 51, 1902 (1995).
95. G. Lauritsch, P.-G. Reinhard, J. Meyer, and M. Brack, *Phys. Lett. A* 160, 179 (1991).
96. J. Martins, J. Buttet, and R. Car, *Phys. Rev. B* 31, 1804 (1985).
97. U. Roetlisberger and W. Andreoni, *J. Chem. Phys.* 94, 8129 (1991).
98. V. Bonacic-Koutecky, P. Fantucci, and J. Koutecky, *Chem. Rev.* 91, 1035 (1991).
99. D. M. Lindsay, Y. Wang, and T. F. George, *J. Chem. Phys.* 86, 3500 (1987).
100. A. Yoshida, T. Dossing, and M. Manninen, *J. Chem. Phys.* 101, 3041 (1994).
101. F. Chandezon, S. Bjornholm, J. Borggreen, and K. Hansen, *Phys. Rev. B* 55, 5485 (1997-II).
102. U. Lammers and G. Borstel, *Phys. Rev. B* 49, 17,360 (1994-II).
103. H. Häkkinen and M. Manninen, *Phys. Rev. B* 52, 1540 (1995).
104. C. Lueder and K. H. Meiwes-Broer, *Chem. Phys. Lett.* 294, 391 (1998).
105. P. B. Balbuena, P. A. Derosa, and M. J. Seminario, *J. Phys. Chem.* 103, 2830 (1999).
106. O. Cheshnovsky, K. J. Taylor, J. Conceicao, and R. E. Smalley, *Phys. Rev. Lett.* 64, 1785 (1990).
107. K. J. Taylor, C. L. Pettiette-Hall, O. Cheshnovsky, and R. E. Smalley, *J. Chem. Phys.* 96, 3319 (1993).
108. C. Y. Cha, G. Ganteför, and W. Eberhardt, *J. Chem. Phys.* 99, 6308 (1993).
109. O. B. Christensen, *Phys. Rev. B* 50, 1844 (1994-I).
110. C. Massobrio, A. Pasquarello, and R. Car, *Phys. Rev. B* 54, 8913 (1996-II).
111. C. Massobrio, A. Pasquarello, and R. Car, *Phys. Rev. Lett.* 75, 2104 (1995).
112. H. Akeby, I. Panas, L. G. M. Pettersson, P. Siegbahn, and U. Wahlgren, *J. Chem. Phys.* 94, 5471 (1990).
113. O. B. Christensen, K. W. Jacobsen, J. K. Norskov, and M. Manninen, *Phys. Rev. Lett.* 66, 2219 (1991).
114. J. Demuynck, M.-M. Rohmer, A. Strich, and A. Veillard, *J. Chem. Phys.* 75, 3443 (1981).
115. H. Tekewaki, E. Miyoshi, and T. Nakamura, *J. Chem. Phys.* 76, 5073 (1982).
116. G. L. Estiu, M. G. Cory, and M. C. Zerner, *J. Phys. Chem.* 104, 233 (2000).
117. A. L. Efros and A. L. Efros, *Sov. Phys. Semicond.* 16, 772 (1982).
118. L. E. Brus, *J. Chem. Phys.* 79, 5566 (1983).
119. L. E. Brus, *J. Chem. Phys.* 80, 4403 (1984).
120. P. F. Trwoga, A. J. Kenyon, and C. W. Pitt, *J. Appl. Phys.* 83, 3789 (1998).
121. D. B. T. Thoai, Y. Z. Hu, and S. W. Koch, *Phys. Rev. B* 42, 11,261 (1990).
122. J. P. Proot, C. Delerue, and G. Allan, *Appl. Phys. Lett.* 61, 1948 (1992).
123. M. V. Rama Krishna and R. A. Friesner, *Phys. Rev. Lett.* 67, 629 (1991).
124. M. V. Rama Krishna and R. A. Friesner, *J. Chem. Phys.* 96, 873 (1992).
125. M. V. Rama Krishna and R. A. Friesner, *J. Chem. Phys.* 95, 8309 (1992).
126. V. L. Colvin and A. P. Alivisatos, *J. Chem. Phys.* 97, 730 (1992).
127. P. E. Lippens and M. Lannoo, *Phys. Rev. B* 39, 10,935 (1989).
128. J. C. Phillips, *J. Chem. Phys.* 83, 3330 (1985).
129. S. Saito, S. Ohnishi, and S. Sugano, *Phys. Rev. B* 33, 7036 (1986).
130. K. Raghavachari, *J. Chem. Phys.* 84, 5672 (1986).
131. G. Pacchioni and J. Koutecky, *J. Chem. Phys.* 84, 3301 (1986).
132. R. Biswas and D. R. Hamann, *Phys. Rev. B.* 36, 6434 (1987).
133. U. Roethlisberger, W. Andreoni, and P. Giannozzi, *J. Chem. Phys.* 96, 1248 (1992).
134. U. Roethlisberger, W. Andreoni, and M. Parrinello, *Phys. Rev. Lett.* 72, 665 (1994).
135. K. Balasubramanian, *Chem. Phys. Lett* 125, 400 (1986).
136. K. Balasubramanian, *Chem. Phys. Lett.* 135, 283 (1987).
137. P. Ballone, W. Andreoni, R. Car, and M. Parrinello, *Phys. Rev. Lett.* 60, 271 (1988).
138. C. H. Patterson and R. P. Messmer, *Phys. Rev. B* 42, 7530 (1990).
139. K. Raghavachari, *J. Chem. Phys.* 83, 3520 (1985).
140. K. Raghavachari and V. Logovinsky, *Phys. Rev. Lett.* 55, 2853 (1985).
141. K. Raghavachari and C. M. Rohlfing, *J. Chem. Phys.* 89, 2219 (1988).
142. D. Tomanek and M. A. Schlueter, *Phys. Rev. Lett.* 56, 1055 (1986).
143. D. Tomanek and M. A. Schlüter, *Phys. Rev. B* 36, 1208 (1987).
144. N. Binggeli and J. R. Chelikowsky, *Phys. Rev. B* 50, 11,764 (1994).
145. M. R. Hunt and R. E. Palmer, *Philos. Trans. R. Soc. London, Ser. A* 356, 231 (1998).
146. C. Brechignac, P. Cahuzac, F. Carlier, M. de Frutos, and J. Leygnier, *Chem. Phys. Lett.* 189, 28 (1992).

147. V. Bonacic-Koutecky, J. Pittner, C. Fuchs, P. Fantucci, M. F. Guest, and J. Koutecky, *J. Chem. Phys.* 104, 1427 (1996).
148. V. Bonacic-Koutecky, J. Jellinek, M. Wiechert, and P. Fantucci, *J. Chem. Phys.* 107, 6321 (1997).
149. U. Roethlisberger and W. Andreoni, *J. Chem. Phys.* 94, 8129 (1991).
150. J. M. Pacheco and W. D. Schoene, *Phys. Rev. Lett.* 79, 4989 (1997).
151. R. A. Broglia and J. M. Pacheco, *Phys. Rev. B* 44, 5901 (1991).
152. Z. Penzar and W. Ekardt, *Z. Phys. D* 19, 109 (1991).
153. O. Genzken, M. Brack, and E. Chabanat, *Ber. Bunsen-Ges. Phys. Chem.* 96, 1217 (1992).
154. W. Eberhardt, P. Fayet, D. M. Cox, Z. Fu, A. Kaldor, R. Sherwood, and D. Sondericker, *Phys. Rev. Lett.* 64, 780 (1990).
155. A. Bettac, L. Koeler, V. Rank, and K. H. Meiwes-Broer, *Surf. Sci.* 402, 475 (1998).
156. B. V. Reddy, S. K. Nayak, S. N. Khanna, B. K. Rao, and P. Jena, *J. Phys. Chem.* 102, 1748 (1998).
157. H. Wu, S. R. Desai, and L.-S. Wang, *Phys. Rev. Lett.* 77, 2436 (1996).
158. L. Lian, C.-X. Su, and P. B. Armentrout, *J. Chem. Phys.* 96, 7542 (1992).
159. G. L. Estiu and M. C. Zerner, *J. Phys. Chem.* 100, 16,874 (1996).
160. S. K. Nayak, B. K. Rao, and P. Jena, *J. Phys.: Condens. Matter* 10, 10,863 (1998).
161. Q. Sun, X. G. Gong, Q. Q. Zheng, D. Y. Sun, and G. H. Wang, *Phys. Rev. B* 54, 10,896 (1996-I).
162. B. K. Rao and P. Jena, *J. Chem. Phys.* 111, 1890 (1999).
163. S. H. Yang, D. A. Drabold, J. B. Adams, and A. Sachdev, *Phys. Rev. B* 47, 1567 (1993-I).
164. R. C. Baetzold, *J. Phys. Chem.* 101, 8180 (1997).
165. J. E. Fowler and J. M. Ugalde, *Phys. Rev. A* 58, 383 (1998).
166. V. Kumar, *Phys. Rev. B* 57, 8827 (1998).
167. J. Akola, M. Manninen, H. Hakkinen, U. Landman, X. Li, and L.-S. Wank, *Phys. Rev. B* 60, R11,297 (1999-II).
168. Y. Q. Cai, A. M. Bradshaw, Q. Guo, and D. W. Goodman, *Surf. Sci.* 399, L357 (1998).
169. H. Wu, S. R. Desai, and L.-S. Wang, *Phys. Rev. Lett.* 76, 212 (1996).
170. C. P. Vinod, G. U. Kulkarni, and C. N. R. Rao, *Chem. Phys. Lett.* 289, 329 (1998).
171. H. Poppa, R. D. Moorhead, and M. Avalos-Borja, *J. Vac. Sci. Technol. A* 7, 2882 (1989).
172. P. A. Montano, G. K. Shenoy, E. E. Alp, W. Schulze, and J. Urban, *Phys. Rev. Lett.* 56, 1285 (1983).
173. S. Ijima and T. Ichihashi, *Phys. Rev. Lett.* 56, 616 (1986).
174. H.-P. Cheng and R. S. Berry, *Phys. Rev. B* 43, 10,647 (1991).
175. M. E. Geusic, M. D. Morse, and R. E. Smalley, *J. Chem. Phys.* 82, 590 (1985).
176. M. D. Morse, M. E. Geusic, J. R. Heathm, and R. E. Smalley, *J. Chem. Phys.* 83, 2293 (1985).
177. R. L. Whetten, M. R. Zakin, D. M. Cox, D. J. Trevor, and A. Kaldor, *J. Chem. Phys.* 85, 1697 (1986).
178. J. L. Elkind, F. D. Weiss, J. M. Alford, R. T. Laaksonen, and R. E. Smalley, *J. Chem. Phys.* 88, 5215 (1988).
179. P. Fayet, A. Kaldor, and D. M. Cox, *J. Chem. Phys.* 92, 254 (1990).
180. J. L. Persson, M. Andersson, and A. Rosen, *Z. Phys. D* 23, 1 (1992).
181. J. Ho, L. Zhu, E. K. Parks, and S. J. Riley, *J. Chem. Phys.* 99, 140 (1993).
182. Y. M. Hamrick and M. D. Morse, *J. Chem. Phys.* 93, 6494 (1989).
183. C. Q. Jiao and B. S. Freiser, *J. Phys. Chem.* 99, 10,723 (1995).
184. C. Berg, T. Schindler, G. Niedern-Schatteburg, and V. E. Bondybey, *J. Chem. Phys.* 104, 4770 (1995).
185. R. L. Whetten, D. M. Cox, D. J. Trevor, and A. Kaldor, *Phys. Rev. Lett.* 54, 1494 (1985).
186. J. Conceicao, R. T. Laaksonen, L.-S. Wang, T. Guo, P. Nordlander, and R. E. Smalley, *Phys. Rev. B* 51, 4668 (1995).
187. M. B. Knickelbein and S. Yang, *J. Chem. Phys.* 93, 1476 (1990).
188. K. Athanassenas, D. Kreisle, B. A. Collings, D. M. Rayner, and P. A. Hackett, *Chem. Phys. Lett.* 213, 105 (1993).
189. M. R. Zakin, R. O. Brickman, D. M. Cox, and A. Kaldor, *J. Chem. Phys.* 88, 6605 (1988).
190. J. Y. Saillard and R. Hoffman, *J. Am. Chem. Soc.* 106, 2006 (1984).
191. M. A. Nygren, P. Siegbahn, C. Jin, T. Guo, and R. E. Smalley, *J. Chem. Phys.* 95, 6181 (1991).
192. M. B. Knickelbein and W. J. C. Menezes, *J. Phys. Chem.* 96, 1992 (1992).
193. S. K. Nayak, B. K. Rao, S. N. Khanna, and P. Jena, *Chem. Phys. Lett.* 259, 588 (1996).
194. J. Zhao, X. Chen, and G. Wang, *Phys. Lett. A* 214, 211 (1996).
195. H. Kietzmann, J. Morenzin, P. S. Bechthold, G. Ganteför, and W. Eberhardt, *J. Chem. Phys.* 109, 2275 (1998).
196. P. Calaminici, A. M. Koster, N. Russo, and D. R. Salahub, *J. Chem. Phys.* 105, 9546 (1996).
197. H.-J. Fan, C.-W. Liu, and M.-S. Liao, *Chem. Phys. Lett.* 273, 353 (1997).
198. G. D. Geske, A. I. Boldyrev, X. Li, and L.-S. Wang, *J. Chem. Phys.* 113, 5130 (2000).
199. S. Kümmel, M. Brack, and P.-G. Reinhard, *Phys. Rev. B* 62, 7602 (2000-I).
200. C. Barreteau, D. Spanjaard, and M. C. Desjonquères, *Phys. Rev. B* 58, 9721 (1998-I).
201. S. K. Nayak, S. N. Khanna, B. K. Rao, and P. Jena, *J. Phys. Chem. A* 101, 1072 (1997).
202. E. Z. D. Silva and A. Antonelli, *Phys. Rev. B* 54, 17,057 (1996).
203. H.-G. Fritsche, *Z. Phys. Chem.* 191, 219 (1995).
204. H.-G. Fritsche, *Z. Phys. Chem.* 192, 21 (1995).
205. S. Krüger, S. Vent, and N. Rösch, *Ber. Bunsen-Ges. Phys. Chem. Int. Ed.* 101, 1640 (1997).
206. S. A. Nepijko, M. Klimenkov, M. Adelt, H. Kuhlenbeck, R. Schlögl, and H.-J. Freund, *Langmuir* 15, 5309 (1999).
207. M. Klimenkov, S. Nepijko, H. Kuhlenbeck, M. Bäumer, R. Schlögel, and H.-J. Freund, *Surf. Sci.* 391, 27 (1997).
208. S. A. Nepijko, M. Klimenkov, H. Kuhlenbeck, D. Zemlyanov, D. Herein, R. Schögel, and H.-J. Freund, *Surf. Sci.* 413, 192 (1998).
209. A. V. Matveev, K. M. Neyman, G. Pacchioni, and N. Rösch, *Chem. Phys. Lett.* 299, 603 (1999).
210. V. Musolino, A. Selloni, and R. Car, *Surf. Sci.* 402–404, 413 (1998).
211. J. T. Lau, A. Achleitner, and W. Wurth, *Chem. Phys. Lett.* 317, 269 (2000).
212. F. J. Palacios, M. P. Iniguez, M. J. López, and J. A. Alonso, *Phys. Rev. B* 60, 2908 (1999-II).
213. Q. Ma and R. A. Rosenberg, *Surf. Sci.* 391, L1224 (1997).
214. A. Bifone, L. Casalis, and R. Riva, *Phys. Rev. B* 51, 11,043 (1995).
215. J. Xhie, K. Sattler, U. Mueller, G. Raina, and N. Venkateswaran, *Phys. Rev. B* 43, 8917 (1991).
216. N. Nilius, N. Ernst, and H.-J. Freund, *Phys. Rev. Lett.* 84, 2000 (2000).
217. Y. S. Gordeev, M. V. Gomoyunova, A. K. Grigorev, V. M. Mikushin, I. I. Pronin, S. E. Sysoev, V. V. Shnitov, and N. S. Faradzhev, *Fiz. Tverd. Tela* 36, 8 (1994).
218. C. Goyhenex, M. Croci, C. Claeys, and C. R. Henry, *Surf. Sci.* 352, 5 (1996).
219. J. G. A. Dubois, J. W. Gerritsen, and H. van Kempen, *Physica B* 218, 262 (1996).
220. D. A. Handley, in "Colloidal Gold: Principles, Methods, and Applications" (M. A. Hayat, Ed.), Vol. 1, pp. 13–32. Academic Press, San Diego, CA, 1989.
221. Y. N. C. Chan, G. S. W. Craig, R. R. Schrock, and R. E. Cohen, *Chem. Mater.* 4, 885 (1992).
222. D. Tomanek, S. Mukherjee, and K. H. Bennemann, *Phys. Rev. B* 28, 665 (1983).
223. K. Rademann, B. Kaiser, U. Even, and F. Hensel, *Phys. Rev. Lett.* 59, 2319 (1987).
224. C. Brechignac, M. Broyer, P. Cahuzac, G. Delacretaz, P. Labastie, and L. Woeste, *Chem. Phys. Lett.* 120, 55 (1985).
225. R. Busani, M. Folkers, and O. Cheshnovsky, *Phys. Rev. Lett.* 81, 3836 (1998).

226. J. Pedersen, S. Bjornholm, J. Borggreen, K. Hansen, T. P. Martin, and H. D. Rasmussen, *Nature* 353, 733 (1991).
227. T. P. Martin, S. Bjornholm, J. Borggreen, C. Brechignac, P. Cahuzac, K. Hansen, and J. Pedersen, *Chem. Phys. Lett.* 186, 53 (1991).
228. H. Ito, T. Sakurai, T. Matsuo, T. Ichihara, and I. Katakuse, *Phys. Rev. B* 48, 4741 (1993-I).
229. A. I. Ekimov, A. L. Efros, and A. A. Onushchenko, *Solid State Commun.* 56, 921 (1985).
230. H. Weller, U. Koch, M. Gutierez, and A. Henglein, *Ber. Bunsen-Ges. Phys. Chem.* 88, 649 (1984).
231. A. P. Alivisatos, *J. Phys. Chem.* 100, 13,226 (1996).
232. N. A. Hill and K. B. Whaley, *Chem. Phys.* 210, 117 (1996).
233. S. V. Gaponenko, "Optical Properties of Semiconductor Nanocrystals," Cambridge Univ. Press, New York, 1998.
234. L. Brus, *J. Phys. Chem.* 98, 3575 (1994).
235. C. B. Murray, D. J. Norris, and M. G. Bawendi, *J. Am. Chem. Soc.* 115, 8706 (1993).
236. N. Chestnoy, T. D. Harris, R. Hull, and L. E. Brus, *J. Phys. Chem.* 90, 3393 (1986).
237. S. Schmitt-Rink, D. S. Miller, and D. S. Chemla, *Phys. Rev. B* 35, 8113 (1987).
238. A. Kornowski, R. Eichberger, M. Giersig, H. Weller, and A. Eychmuller, *J. Phys. Chem.* 100, 12,467 (1996).
239. K. W. Berryman, S. A. Lyon, and M. Segev, *J. Vac. Sci. Technol.* 15, 1045 (1997).
240. H. Fu and A. Zunger, *Phys. Rev. B* 56, 1496 (1997).
241. M. Kuno, J. K. Lee, B. O. Dabbousi, F. V. Mikulec, and M. G. Bawendi, *J. Chem. Phys.* 106, 9869 (1997).
242. O. I. Micic, J. R. Sprague, C. J. Curtis, K. M. Jones, J. L. Machol, A. J. Notik, H. Giessen, B. Fluegel, G. Mohs, and N. Peyghambarian, *J. Phys. Chem.* 99, 7754 (1995).
243. L. M. Ramaniah and S. V. Nair, *Physica B* 212, 245 (1995).
244. J.-Y. Marzin, J.-M. Gerard, A. Izrael, D. Barrier, and G. Bastard, *Phys. Rev. Lett.* 73, 716 (1994).
245. M. Lannoo, *Mater. Sci. Eng. B* 9, 485 (1991).
246. C. Sikorski and U. Merkt, *Phys. Rev. Lett.* 62, 2164 (1989).
247. P. N. Brounkov, A. Polimeni, S. T. Stoddart, M. Henini, L. Eaves, P. C. Main, A. R. Kovsh, Y. G. Musikhin, and S. G. Konnikov, *Appl. Phys. Lett.* 73, 1092 (1998).
248. D. Gammon, E. S. Snow, B. V. Shanabrook, D. S. Katzer, and D. Park, *Phys. Rev. Lett.* 76, 3005 (1996).
249. T. R. Taylor, K. R. Asmis, C. Xu, and D. M. Neumark, *Chem. Phys. Lett.* 20, 133 (1998).
250. K. R. Asmis, T. R. Taylor, and D. M. Neumark, *Chem. Phys. Lett.* 308 (1999).
251. I. Kang and F. W. Wise, *J. Opt. Soc. Am.* 14, 1632 (1997).
252. V. N. Soloviev, A. Eichhöfer, D. Fenske, and U. Banin, *J. Am. Chem. Soc.* 122, 2673 (2000).
253. O. I. Micic, H. M. Cheong, H. Fu, A. Zunger, J. R. Sprague, A. Mascarenhas, and A. J. Nozik, *J. Phys. Chem. B* 101, 4904 (1997).
254. O. I. Micic, K. M. Jones, A. Cahill, and A. J. Nozik, *J. Phys. Chem. B* 102, 9791 (1998).
255. I. Kang and F. W. Wise, *J. Opt. Soc. Am. B* 14, 1632 (1997).
256. J.-Y. Yi, *Chem. Phys. Lett.* 325, 269 (2000).
257. A. J. Williamson, A. Franceschetti, H. Fu, L. W. Wang, and A. Zunger, *J. Electron. Mater.* 28, 414 (1999).
258. A. Tomasulo and M. V. Ramakrishna, *J. Chem. Phys.* 105, 3612 (1996).
259. M. V. Ramakrishna and R. A. Friesner, *J. Chem. Phys.* 95, 8309 (1991).
260. J. P. Zheng and H. S. Kwok, *J. Opt. Soc. Am. B* 9, 2047 (1992).
261. S. Nomura and T. Kobayashi, *Phys. Rev. B* 45, 1305 (1992).
262. A. Olkhovets, R.-C. Hsu, A. Lopovskii, and F. W. Wise, *Phys. Rev. Lett.* 81, 3539 (1998).
263. M. S. El-Shall, S. Li, and I. Germanenko, "Abstracts of Papers of the American Chemical Society," 1999, Vol. 217, p. 1.
264. W. H. Jiang, X. L. Ye, B. Xu, H. Z. Xu, D. Ding, J. B. Liang, and Z. G. Wang, *J. Appl. Phys.* 88, 2529 (2000).
265. B. L. Justus, R. J. Tonucci, and A. D. Berry, *Appl. Phys. Lett.* 61, 3152 (1992).
266. L. T. Canham, *Appl. Phys. Lett.* 57, 1046 (1990).
267. H. Takagi, H. Ogawa, Y. Yamazaki, A. Ishizaki, and T. Nakagiri, *Appl. Phys. Lett.* 56, 2379 (1990).
268. V. G. Baru, S. Bayliss, L. Zaharov, and Yu, *Microelectron. Eng.* 36, 111 (1997).
269. K. A. Littau, P. J. Szajowski, A. J. Muller, A. R. Kortan, and L. E. Brus, *J. Phys. Chem.* 97, 1224 (1993).
270. X.-N. Liu, X.-W. Wu, X.-M. Bao, and Y.-L. He, *Appl. Phys. Lett.* 64, 220 (1994).
271. P. D. Milewski, D. J. Lichtenwalner, P. Mehta, A. I. Kingon, D. Zhang, and R. M. Kolbas, *J. Electron Mater.* 23, 57 (1994).
272. H. Morizaki, F. W. Ping, H. Ono, and K. Yazawa, *J. Appl. Phys.* 70, 1869 (1991).
273. S. Nozaki, S. Sato, H. Ono, and H. Morisaki, *Mater. Res. Soc. Symp. Proc.* 351, 399 (1994).
274. A. A. Seraphin, S.-T. Ngiam, and K. D. Kolenbrander, *J. Appl. Phys.* 80, 6429 (1996).
275. J. R. Heath, *Science* 258, 1131 (1992).
276. R. Bley, A. Kauzlarich, and M. Susan, *J. Am. Chem. Soc.* 118, 12,461 (1996).
277. A. Frojtik, H. Weller, S. Fiechter, and A. Henglein, *Chem. Phys. Lett.* 134, 477 (1987).
278. M. F. Jarrold, *Science* 252, 1085 (1991).
279. J. M. Hunter, J. L. Fye, M. F. Jarold, and J. E. Bower, *Phys. Rev. Lett.* 73, 2063 (1994).
280. S. Iijima, *Jpn. J. Appl. Phys.* 26, 365 (1987).
281. S. Iijima, *Jpn. J. Appl. Phys.* 26, 357 (1987).
282. J. L. Heinrich, C. L. Curtis, G. M. Credo, K. L. Kavamagh, and M. J. Sailor, *Science* 255, 66 (1992).
283. R. A. Bley, S. M. Kauzlarich, and H. W. H. Lee, *Chem. Mater.* 8, 1881 (1996).
284. G. Allan, C. Delerue, and M. Lannoo, *Phys. Rev. Lett.* 78, 3161 (1997).
285. L.-W. Wang and A. Zunger, *J. Chem. Phys.* 100, 2394 (1994).
286. M. O. Watanabe, T. Miyazaki, and T. Kanayama, *Phys. Rev. Lett.* 81, 5362 (1998).
287. M. Hirao and T. Uda, *Surf. Sci.* 306, 87 (1994).
288. S. Oeguet, J. R. Chelikowsky, and S. G. Louie, *Phys. Rev. Lett.* 79 (1997).
289. G. Onida and W. Andreoni, *Chem. Phys. Lett.* 243 (1995).
290. B. Delley and E. F. Steigmeier, *Appl. Phys. Lett.* 67, 2370 (1995).
291. Y. Kanemitsu, S. Okamoto, M. Otobe, and S. Oda, *Phys. Rev. B* 55, R7375 (1997).
292. A. B. Filonov, A. N. Kholod, F. d'Avitaya, and X. Arnaud, *Phys. Rev. B* 57, 1394 (1998).
293. W. L. Wilson, P. F. Szajowski, and L. E. Brus, *Science* 262, 1242 (1993).
294. D. Zhang, R. M. Kolbas, and J. M. Zavada, *Appl. Phys. Lett.* 65, 2684 (1994).
295. L.-W. Wang and A. Zunger, *J. Phys. Chem.* 98, 2158 (1994).
296. H. Yorikawa, H. Uchida, and S. Muramatsu, *J. Appl. Phys.* 79, 3619 (1996).
297. A. Kux and M. B. Chorin, *Phys. Rev. B* 51, 17,535 (1995).
298. L. E. Brus, P. F. Szajowski, W. L. Wilson, T. D. Harris, S. Schuppler, and P. H. Citrin, *J. Am. Chem. Soc.* 117, 2915 (1995).
299. L. N. Dinh, L. L. Chase, M. Balooch, W. J. Siekhaus, and F. Wooten, *Phys. Rev. B* 54, 5029 (1996).
300. S. S. Iyer and Y. H. Xie, *Science* 260, 40 (1993).
301. B. Delley and E. F. Steigmeier, *Phys. Rev. B* 47, 1397 (1993).
302. X. G. Gong, Q. Q. Zheng, and Y.-Z. He, *J. Phys. Condens. Matter* 7, 577 (1995).
303. J. R. Chelikowsky, *Phys. Rev. Lett.* 60, 2669 (1988).
304. C. M. Rohlfing and K. Raghavachari, *Chem. Phys. Lett.* 167, 559 (1990).
305. N. Binggeli, J. L. Martins, and J. R. Chelikowsky, *Phys. Rev. Lett.* 68, 2956 (1992).

306. X. Jing, N. Troullier, and Y. Saad, *Phys. Rev. B* 50, 12,234 (1994).
307. M. Menon and K. R. Subbaswamy, *Phys. Rev. B* 47, 12,754 (1993).
308. E. C. Honea, A. Ogura, C. A. Murray, K. Raghavachari, W. O. Sprenger, M. F. Jarrold, and W. L. Brown, *Nature* 366, 42 (1993).
309. C. Xu, T. R. Taylor, and D. M. Neumark, *J. Chem. Phys* 108, 1395 (1998).
310. T. van Buuren, T. Tiedje, and J. R. Dahn, *Appl. Phys. Lett.* 63, 2911 (1993).
311. K. Murayama, H. Komasu, S. Miyazaki, and M. Hirose, *Solid State Commun.* 103, 155 (1997).
312. D. J. Wales, *Phys. Rev. A* 49, 2195 (1994).
313. H. Kimura, S. Imanaga, Y. Hayafuji, and H. Adachi, *J. Phys. Soc. Jpn.* 62, 2663 (1993).
314. B.-L. Gu, Z.-Q. Li, and J.-L. Zhu, *J. Phys.: Condens. Matter* 5, 5255 (1993).
315. X. G. Gong, *Phys. Rev. B* 52, 14,677 (1995).
316. E. Kaxiras, in "Cluster Assembled Materials" (K. Sattler, Ed.), Vol. 232, p. 67. Trans Tech Publications, Zurich, 1996.
317. S. Saito, in "Cluster Assembled Materials" (K. Sattler, Ed.), Vol. 232, p. 233. Trans Tech Publications, Zurich, 1996.
318. S. Saito, *Phys. Rev. B* 51, 51 (1995).
319. K. M. Ho, A. A. Shvartsburg, B. Pan, Z.-Y. Lu, C.-Z. Wang, J. G. Wacker, J. L. Fye, and M. F. Jarrold, *Nature* 392, 582 (1998).
320. D. A. Jelski, B. L. Swift, and T. T. Rantala, *J. Chem. Phys.* 95, 8552 (1991).
321. E. Kaxiras and K. Jackson, *Phys. Rev. Lett.* 71, 727 (1993).
322. A. M. Mazzone, *Phys. Rev. B* 54, 5970 (1996).
323. R. Fournier, S. B. Sinnott, and A. E. DePristo, *J. Chem. Phys.* 97, 414 (1992).
324. J. R. Chelikowsky, K. Glassford, and J. C. Phillips, *Phys. Rev. B* 44, 1538 (1991).
325. M. F. Jarrold and V. A. Constant, *Phys. Rev. Lett.* 67, 2994 (1991).
326. K. Fuke, K. Tsukamoto, and F. Misaizu, *J. Chem. Phys.* 99, 7807 (1993).
327. K. Jackson, M. Pederson, and K.-M. Ho, *Phys. Rev. A* 59, 3685 (1999).
328. J. Müller, B. Liu, A. A. Shvartsburg, S. Ögut, J. R. Chelikowsky, K. W. M. Siu, K.-M. Ho, and G. Ganteför, *Phys. Rev. Lett.* 85, 1666 (2000).
329. J. A. Cogordan, L. E. Sansores, and A. A. Valladares, *J. Non-Cryst. Solids* 181, 135 (1995).
330. Y. M. Niquet, G. Allan, C. Delerue, and M. Lannoo, *Appl. Phys. Lett.* 77, 1182 (2000).
331. Y. Maeda, N. Tsukamoto, Y. Yazawa, Y. Kanemitsu, and Y. Masumoto, *Appl. Phys. Lett.* 59, 3168 (1991).
332. D. C. Paine, C. Caragiania, T. Y. Kim, Y. Shigesto, and T. Ishahara, *Appl. Phys. Lett.* 62, 2842 (1993).
333. M. H. Ludwig, R. E. Hummel, and S.-S. Chank, *J. Vac. Sci. Technol. B* 12, 3023 (1994).
334. M. Nogami and Y. Abe, *Appl. Phys. Lett.* 65, 2545 (1994).
335. Y. Maeda, *Phys. Rev. B* 51, 1658 (1995).
336. S. Okamoto and Y. Kanemitsu, *Phys. Rev. B* 54, 16,421 (1996).
337. V. Cracium, C. Boulmer-Leborgne, and I. W. Boyd, *Appl. Phys. Lett.* 69, 1506 (1996).
338. A. Saito and T. Suemoto, *Phys. Rev. B* 56, R1688 (1997).
339. M. Zacharias and P. M. Fauchet, *Appl. Phys. Lett.* 71, 380 (1997).
340. W. K. Choi, V. Ng, S. P. Ng, H. H. Thio, Z. X. Shen, and W. S. Li, *J. Appl. Phys.* 86, 1398 (1999).
341. S. Takeoka, M. Fujii, S. Hayashi, and K. Yamamoto, *Phys. Rev. B* 58, 7921 (1998).
342. Y. Negishi, H. Kawamata, F. Hayakawa, A. Nakajima, and K. Kaya, *Chem. Phys. Lett.* 294, 370 (1998).
343. M. F. Crommie, C. P. Lutz, and D. M. Eigler, *Phys. Rev. B* 48, 2851 (1993).
344. B. Marsen and K. Sattler, *Phys. Rev. B* 60 (1999).
345. P. M. St. John and R. L. Whetten, *Chem. Phys. Lett.* 196, 330 (1992).
346. P. E. Batson and J. R. Heath, *Phys. Rev. Lett.* 71, 911 (1993).
347. Y. Kanemitsu, H. Uto, Y. Masumoto, T. Matsumoto, T. Futagi, and H. Mimura, *Phys. Rev. B* 48, 2827 (1993).
348. C. Delerue, E. Martin, J.-F. Lampin, G. Allan, and M. Lannoo, *J. Phys. IV* 3, 359 (1993).
349. A. Sieck, D. Porezag, T. Frauenheim, M. R. Pederson, and K. Jackson, *Phys. Rev. A* 56, 4890 (1997).
350. E. Kaxiras, *Phys. Rev. B* 56, 13,455 (1997).
351. J. L. Gavartin and C. C. Matthai, *Mater. Sci. Eng.* 35, 459 (1995).
352. J. A. Stroscio, R. M. Feenstra, and A. P. Fein, *Phys. Rev. Lett.* 57, 2579 (1986).
353. R. J. Hamers, P. Avouris, and F. Bozso, *Phys. Rev. Lett.* 59, 2071 (1987).
354. R. J. Hamers, *Annu. Rev. Phys. Chem.* 40, 531 (1989).
355. P. Melinon, P. Keghelian, B. Prevel, A. Perez, G. Guiraud, J. LeBrusq, J. Lerme, M. Pellarin, and M. Broyer, *J. Chem. Phys.* 107, 10,278 (1997).
356. S. G. Louis and M. L. Cohen, *Phys. Rev. B* 13, 2461 (1976).
357. R. Matz, H. Lueth, and A. Ritz, *Solid State Commun.* 46, 343 (1983).
358. K. C. Pandey, *Phys. Rev. Lett.* 47, 1913 (1981).
359. R. S. Becker, J. A. Golovchenko, D. R. Hamann, and B. S. Swartzentruber, *Phys. Rev. Lett.* 55, 2032 (1985).
360. F. J. Himpsel and T. Fauster, *J. Vac. Sci. Technol. A* 2, 815 (1984).
361. E. Kaxiras, *Chem. Phys. Lett.* 163, 323 (1989).
362. E. Kaxiras, *Phys. Rev. Lett.* 64, 551 (1990).
363. M. F. Jarrold, U. Ray, and M. Creegan, *J. Chem. Phys.* 93, 224 (1990).
364. M. F. Jarrold and E. C. Honea, *J. Phys. Chem.* 95, 9181 (1991).
365. M. Maus, G. Ganteför, and W. Eberhardt, *Appl. Phys. A* 70, 535 (2000).
366. A. Nakajama, T. Futatsugi, K. Kosemura, T. Fukano, and N. Yokoyama, *J. Vac. Sci. Technol.* 17, 2163 (1999).
367. K. Kim, *Phys. Rev. B* 57, 13,072 (1998).
368. E. Leobandung, L. Guo, Y. Wang, and S. Y. Chou, *Appl. Phys. Lett.* 67, 938 (1995).
369. F. G. Pikus and K. K. Likharev, *Appl. Phys. Lett.* 71, 3661 (1997).
370. S. K. Zhang, H. J. Zhu, F. Lu, Z. M. Jiang, and X. Wang, *Phys. Rev. Lett.* 80, 3340 (1998).
371. H. Ishikuro, T. Fujii, T. Saraya, G. Hashiguchi, T. Hiramoto, and T. Ikoma, *Appl. Phys. Lett.* 68, 3585 (1996).
372. A. E. Hanna and M. Tinkham, *Phys. Rev. B* 44, 5919 (1991).
373. "Single Charge Tunneling" (H. Grabert and M. H. Devoret, Eds.), Vol. X. Plenum, New York, 1992.
374. E. Bar-Sadeh, Y. Goldstein, B. Abeles, and O. Millo, *Phys. Rev. B* 50, R8961 (1994).
375. C. Schonenberger, H. van Houten, and H. C. Donkersloot, *Europhys. Lett.* 20, 249 (1992).
376. R. Wilkins, E. Ben-Jacob, and R. C. Jaklevic, *Phys. Rev. Lett.* 63, 801 (1989).
377. G. Markovich, D. V. Leff, S. W. Chung, H. M. Soyez, B. Dunn, and J. R. Heath, *Appl. Phys. Lett.* 70, 3107 (1997).
378. D. C. Ralph, C. T. Black, and M. Tinkham, *Phys. Rev. Lett.* 74, 3241 (1995).
379. O. Agam, N. S. Wingreen, B. L. Altshuler, D. C. Ralph, and M. Tinkham, *Phys. Rev. Lett.* 78, 1956 (1997).
380. J. G. A. Dubois, J. W. Geritsen, S. E. Shafranjuk, E. J. G. Boon, G. Schmid, and H. van Kempen, *Europhys. Lett.* 33, 279 (1995).
381. R. S. Ingram, J. M. Hostetler, and R. W. Murray, *J. Am. Chem. Soc.* 119, 9175 (1997).
382. R. Tsu, X.-L. Li, and E. H. Nicollian, *Appl. Phys. Lett.* 65, 842 (1994).
383. K. Yano, T. Ishii, T. Hashimoto, T. Kobayashi, F. Murai, and K. Seki, *IEEE Trans. Electron Devices* ED-41, 1628 (1994).
384. Y. Takahashi, M. Nagase, H. Namatsu, K. Kurihara, K. Iwadate, Y. Nakajima, S. Horiguchi, K. Murase, and M. Tabe, *Electron. Lett.* 31, 136 (1995).
385. T. Hiramoto, H. Ishikuro, T. Fujii, T. Saraya, G. Hashiguchi, and T. Ikoma, *Physica B* 227, 95 (1996).
386. H. Ishikuro and T. Hiramoto, *Appl. Phys. Lett.* 71, 3691 (1997).
387. L. Zhuang, G. L., and S. Y. Chou, *Appl. Phys. Lett.* 72, 1205 (1998).
388. N. Takahashi, H. Ishikuro, and T. Hiramoto, (2000). *Appl. Phys. Lett*. 76, 209 (2000).
389. B. Marsen, Ph.D. thesis, University of Hawaii, Honolulu, 2000.

390. M.-S. Ho, I.-S. Hwang, and T. T. Tsong, *Phys. Rev. Lett.* 94, 5792 (2000).
391. S. Furukawa and T. Miyasato, *Phys. Rev. B* 38, 5726 (1988).
392. G. R. Gupte and R. Prasad, *Int. J. Mod. Phys.* 12, 1737 (1998).
393. G. R. Gupte and R. Prasad, *Int. J. Mod. Phys.* 12, 1607 (1998).
394. V. Meleshko, X. Xu, and Q. Zhang, *Chem. Phys. Lett.* 300, 118 (1999).
395. T. Miyazaki, T. Uda, and K. Terakura, *Chem. Phys. Lett.* 261, 346 (1996).
396. H. K. T. Murakami, *Appl. Phys. Lett.* 67, 2341 (1995).
397. M. T. Swihart and S. L. Girshick, *Chem. Phys. Lett.* 307, 527 (1999).
398. T. Uda, *Surf. Rev. Lett.* 3, 127 (1996).
399. A. M. Saitta, F. Buda, G. Fiumara, and P. V. Giaquinta, *Phys. Rev. B* 53, 1446 (1996).
400. S. Y. Ren, *Phys. Rev. B* 55, 4665 (1997).
401. S. V. Gaponenko, I. N. Germanenko, E. P. Petrov, A. P. Stupak, V. P. Bondarenko, and A. M. Dorofeev, *Appl. Phys. Lett.* 64, 85 (1994).
402. S. Schuppler, S. L. Friedmann, M. A. Marcus, D. L. Adler, Y.-H. Xie, F. M. Ross, T. D. Harris, W. L. Brown, Y. J. Chabal, L. E. Brus, and P. H. Citrin, *Phys. Rev. Lett.* 72, 2648 (1994).
403. J. L. Gole and D. A. Dixon, *J. Appl. Phys.* 83, 5985 (1998).
404. J. L. Gole and S. M. Prokes, *Phys. Rev. B* 58, 4761 (1998).
405. J. L. Gole and D. A. Dixon, *Phys. Rev. B* 57, 12,002 (1998).
406. J. L. Gole and D. A. Dixon, *J. Phys. Chem. B* 102, 33 (1998).
407. G. B. Amisola, R. Behrensmeier, J. M. Galligan, and F. A. Otter, *Appl. Phys. Lett.* 61, 2595 (1992).
408. L. Tsybeskov, S. P. Duttagupta, and P. M. Fauchet, *Solid State Commun.* 95, 429 (1995).
409. Buda, F., J. Kohanoff, and M. Parrinello, *Phys. Rev. Lett.* 69, 1272 (1992).
410. Z. C. Feng and R. Tsu, "Porous Silicon," World Scientific, Singapore, 1994.
411. K. Ito, S. Ohyama, Y. Uehara, and S. Ushioda, *Appl. Phys. Lett.* 67, 2536 (1995).
412. R. Laiho, A. Pavlov, and Y. Pavlova, *Thin Solid Films* 297, 138 (1997).
413. Y. Xiao, M. J. Heben, J. M. McCullough, Y. S. Tsuo, J. I. Pankove, and S. K. Deb, *Appl. Phys. Lett.* 62, 1152 (1993).
414. H. Sakaki, *Jpn. J. Appl. Phys.* 19, L735 (1980).
415. S. Mori and T. Ando, *J. Phys. Soc. Jpn.* 48, 865 (1980).
416. J. Bloch, U. Bockelmann, and F. Laruelle, *Europhys. Lett.* 28, 501 (1994).
417. H. Akiyama, T. Someya, and H. Sakaki, *Phys. Rev. B* 53, R4229 (1996).
418. F. Vouilloz, D. Y. Oberli, M.-A. Dupertuis, A. Gustafsson, F. Reinhardt, and E. Kapon, *Phys. Rev. Lett.* 78, 1580 (1997).
419. R. Cingolani, M. Lepore, R. Tommasi, I. M. Catalano, H. Lage, D. Heitmann, K. Ploog, A. Shimizu, H. Sakaki, and T. Ogawa, *Phys. Rev. Lett.* 69, 1276 (1992).
420. A. R. Goni, A. Pinczuk, J. S. Weiner, B. S. Dennis, L. N. Pfeiffer, and K. W. West, *Phys. Rev. Lett.* 70, 1151 (1993).
421. G. W. Zhou, Z. Zhang, and D. P. Yu, *Appl. Phys. Lett.* 73, 677 (1998).
422. V. Ng, H. Ahmed, and T. Shimada, *Appl. Phys. Lett.* 73, 972 (1998).
423. D. Papadimitriou and A. G. Nassiopoulos, *J. Appl. Phys.* 84, 1059 (1998).
424. D. P. Yu, Z. G. Bai, and S. Q. Geng, *Phys. Rev. B* 59, R2498 (1999).
425. N. T. Bagraev, E. T. Chaikina, and A. M. Malyarenko, *Solid-State Electron.* 42, 1199 (1998).
426. B. Li, D. Yu, and S.-L. Zhang, *Phys. Rev. B* 59, 1645 (1999).
427. H. Namatsu, K. Kurihara, and T. Makino, *Appl. Phys. Lett.* 70, 619 (1997).
428. M. Ge and K. Sattler, *Science* 260, 515 (1993).
429. H. I. Liu, D. K. Biegelsen, F. A. Ponce, N. M. Johnson, and R. F. W. Pease, *Appl. Phys. Lett.* 64, 1383 (1994).
430. H. Namatsu, Y. Takahashi, M. Nagase, and K. Murase, *J. Vac. Sci. Technol. B* 13, 2166 (1995).
431. Y. Shi, J. L. Liu, F. Wang, Y. Lu, R. Zhang, S. L. Gu, P. Han, L. Q. Hu, Y. D. Zheng, C. Y. Lin, and D. A. Du, *J. Vac. Sci. Technol. A* 14, 1194 (1996).
432. G. S. Chen, C. B. Boothroyd, and C. J. Humphreys, *Appl. Phys. Lett.* 62, 1949 (1993).
433. V. Lehmann and U. Goesele, *Appl. Phys. Lett.* 58, 856 (1991).
434. J. L. Liu, Y. Shi, and Y. D. Zheng, *Appl. Phys. Lett.* 68, 352 (1996).
435. M. Gotza, B. Saint-Cricq, and P.-H. Jouneau, *Microelectron. Eng.* 27, 129 (1995).
436. G. Hashiguchi and H. Mimura, *Jpn. J. Appl. Phys. Part 2* 33, L1649 (1994).
437. J. L. Liu, Y. Shi, and Y. D. Zheng, *J. Vac. Sci. Technol. B* 13, 2137 (1995).
438. A. M. Morales and C. M. Lieber, *Science* 279, 208 (1998).
439. T. Ono, H. Saitoh, and M. Esashi, *Appl. Phys. Lett.* 70, 1852 (1997).
440. G. D. Sanders and Y.-C. Chang, *Appl. Phys. Lett.* 60, 2525 (1992).
441. A. G. Nassiopoulos, S. Grigoropoulos, and D. Papadimitriou, *Thin Solid Films* 297, 176 (1997).
442. J. Westwater, D. P. Gosain, and H. Ruda, *J. Vac. Sci. Technol. B* 15, 554 (1997).
443. J. Westwater, D. P. Gosain, and S. Usui, *Phys. Status Solidi A* 165, 37 (1998).
444. S. Yanagiya, S. Kamimura, and H. Koinuma, *Appl. Phys. Lett.* 71, 1409 (1997).
445. D. P. Yu, Z. G. Bai, Y. Ding, Q. L. Hang, H. Z. Zhang, J. J. Wang, Y. H. Zou, W. Qian, G. C. Xiong, H. T. Zhou, and S. Q. Feng, *Appl. Phys. Lett.* 72, 3458 (1998).
446. J. J. P. Stewart, *J. Comput. Chem.* 10, 221 (1989).
447. H. Kawaji, H. Horie, S. Yamanaka, and M. Ishikawa, *Phys. Rev. Lett.* 74, 1427 (1995).
448. P. L. McEuen, *Nature* 393, 15 (1998).
449. M. Kasper, K. Siegmann, and K. Sattler, *J. Aerosol Sci.* 28, 1569 (1997).
450. M. Kasper, K. Sattler, K. Siegmann, U. Matter, and H. C. Siegmann, *J. Aerosol Sci.* 30, 217 (1999).
451. P. Dugourd, R. R. Hudgins, and M. F. Jarrold, *Phys. Rev. Lett.* 80, 4197 (1998).
452. F. Jensen, *Chem. Phys. Lett.* 209, 417 (1993).
453. M. T. Bowers, P. R. Kemper, G. von Helden, and P. A. M. van Koppen, *Science* 260, 1446 (1993).
454. T. Frauenheim, G. Jungnickel, T. Koehler, and U. Stephan, *J. Non-Cryst. Solids* 182, 186 (1995).
455. R. Kubo, *J. Phys. Soc. Jpn.* 17, 975 (1962).
456. C. Liang and H. F. Schaefer III, *Chem. Phys. Lett.* 169, 150 (1990).
457. G. P. Lopinski, V. I. Merkulov, and J. S. Lannin, *Phys. Rev. Lett.* 80, 4241 (1998).
458. S. Saito, S. Okada, S. Sawada, and N. Hamada, *Phys. Rev. Lett.* 75, 685 (1995).
459. S. Saito and A. Oshiyama, *Phys. Rev. B* 44, 11,532 (1991).
460. S. J. Woo, E. Kim, and Y. H. Lee, *Phys. Rev. B* 47, 6721 (1993).
461. B. L. Zhang, C. Z. Wang, K. M. Ho, C. H. Xu, and J. Chan, *J. Chem. Phys.* 97, 5007 (1992).
462. H. Wang, C. Zeng, Q. Li, B. Wang, J. Yang, J. G. Hou, and Q. Zhu, *Surf. Sci.* 442, L1024 (1999).
463. P. G. Collins, J. C. Grossman, M. Cote, M. Ishigami, C. Piskoti, S. G. Louie, M. L. Cohen, and A. Zettl, *Phys. Rev. Lett.* 82, 165 (1999).
464. H. Kietzmann, R. Rochow, G. Gantefor, W. Eberhardt, K. Vietze, G. Seifert, and P. W. Fowler, *Phys. Rev. Lett.* 81, 1998 (1998).
465. M. Lonfat, B. Marsen, and K. Sattler, *Chem. Phys. Lett.* 313, 539 (1999).
466. J. W. G. Wildoer, L. C. Venema, A. G. Rinzler, R. E. Smalley, and C. Dekker, *Nature* 391, 59 (1998).
467. M. R. C. Hunt, P. J. Durston, and R. E. Palmer, *Surf. Sci.* 364, 266 (1996).
468. Z. Y. Li, K. M. Hock, and R. E. Palmer, *Phys. Rev. Lett.* 67, 1562 (1991).
469. W. A. de Heer, P. Milani, and A. Chatelain, *Phys. Rev. Lett.* 63, 2834 (1989).
470. P. C. Ohara, D. V. Leff, J. R. Heath, and W. M. Gelhart, *Phys. Rev. Lett.* 75, 3466 (1995).

471. M. J. Hostetler, S. J. Green, J. J. Stokes, and R. W. Murray, *J. Am. Chem. Soc.* 118, 4212 (1996).
472. N. Herron, J. C. Calabrese, W. Farneth, and Y. Wang, *Science* 259, 1426 (1993).
473. C. B. Murray, C. R. Kagan, and M. G. Bawendi, *Science* 270, 1335 (1995).
474. J. J. Shiang, J. R. Heath, C. P. Collier, and R. J. Saykally, *J. Phys. Chem.* 102, 3425 (1998).
475. K. Sattler, unpublished results.
476. T. A. Burr, A. A. Seraphin, and K. D. Kolenbrander, *Phys. Rev. B* 56, 4818 (1997).
477. A. B. Filinov, A. N. Kholod, V. A. Novikov, V. E. Borisenko, L. Vervoort, F. Bassani, A. Saul, and F. A. d'Avitaya, *Appl. Phys. Lett.* 70, 744 (1997).
478. M. Higo, K. Nishino, and S. Kamata, *Appl. Surf. Sci.* 51, 61 (1991).
479. M. Higo, M. Isobata, and S. Kamata, *J. Phys. Chem.* 97, 4491 (1993).
480. F. Huisken, B. Kohn, and V. Paillard, *Appl. Phys. Lett.* 74, 3776 (1999).
481. M. Ehbrecht, B. Kohn, and V. Paillard, *Phys. Rev. B* 56, 6958 (1997).
482. M. A. Laguna, V. Paillard, and H. Hofmeister, *J. Lumin.* 80, 223 (1998).
483. S. Kerdiles, R. Rizk, and J. R. Morante, *Solid-State Electron* 42, 2315 (1998).
484. M. Tzolov, Y. Jeliazova, and N. Tzenov, *Solid state Phenomena* 67–68, 107 (1999).
485. J. R. Heath, S. M. Gates, and C. A. Chess, *Appl. Phys. Lett.* 64, 3569 (1994).
486. R. Cherfi, G. Farhi, and M. Aoucher, *Solid state Phenomena* 67–68, 113 (1999).
487. P. Scheier, B. Marsen, and K. Sattler, to be published.
488. E. Hanamura, *Phys. Rev.* 37, 1273 (1988).
489. L. Banyai, Y. Z. Hu, M. Lindberg, and S. W. Koch, *Phys. Rev. B* 38, 8142 (1988).
490. S. Bandyopadhyay and V. P. Roychowdhury, *IEEE Potentials* 15, 8 (1996).
491. R. T. Bate, *Solid State Technol.* 32, 101 (1989).
492. F. A. Buot, *Phys. Rep.* 234, 1 (1993).
493. A. Schenk, U. Krumbein, and W. Fichtner, *IEICE Trans. Electron.* 77, 148 (1994).
494. B. Sweryda-Krawiec, T. Cassagneau, and J. H. Fendler, *Adv. Mater.* 11, 659 (1999).
495. G. D. Stucky, *Naval Res. Rev.* 43, 28 (1991).
496. J. H. Sinfelt and G. D. Meitzner, *Acc. Chem. Res.* 26, 1 (1993).
497. M. L. Steigerwald and L. E. Brus, *Acc. Chem. Rev.* 23, 183 (1990).
498. H. Weller, *Angew. Chem. Int. Ed. Engl.* 32, 41 (1993).
499. H. Weller, *Adv. Mater.* 5, 88 (1993).
500. L. Brus, *IEEE J. Quantum Electron.* QE-22, 1909 (1986).
501. V. Dneprovskii, A. Eev, and E. Dovidenko, *Phys. Status Solidi* 188, 297 (1995).
502. L. Pavesi and R. Guardini, *Braz. J. Phys.* 26, 151 (1996).
503. L. François, M. Mostafavi, J. Belloni, J.-F. Delouis, J. Delaire, and P. Feneyrou, *J. Phys. Chem. B* 104, 6133 (2000).
504. K. Mansour, M. J. Soileau, and E. W. Van Stryland, *J. Opt. Soc. Am. B* 9, 1100 (1992).
505. K. M. Nashold and D. P. Walter, *J. Opt. Soc. Am. B* 12, 1228 (1995).
506. Y. P. Sun, J. E. Riggs, H. W. Rollins, and R. J. Guduru, *J. Phys. Chem.* 103, 77 (1999).
507. J. N. Randall, M. A. Reed, and G. A. Frazier, *J. Vac. Sci. Technol.* 7, 1398 (1989).
508. W. M. Toiles, Nanotechnology 7, 59 (1996).
509. H. Sakaki, T. Matsusue, and M. Tsuchiya, *IEEE J. Quantum Electron.* 25, 2498 (1989).
510. M. Van Rossum, *Mater. Sci. Eng.* 20, 128 (1993).
511. J. R. Tucker, C. Wang, and T. C. Shen, *Nanotechnology* 7, 275 (1996).
512. K. Puech, W. Blau, A. Grund, C. Bubeck, and G. Cardenas, *Opt. Lett.* 20, 1613 (1995).
513. H. H. Huang, F. Q. Yan, Y. M. Kek, C. H. Chew, G. Q. Xu, W. Ji, P. S. Oh, and S. H. Tang, *Langmuir* 13, 172 (1997).
514. M. Jacobsohn and U. Banin, *J. Phys. Chem.* 104, 1 (2000).
515. L. E. Brus, *Appl. Phys. A* 53, 465 (1991).
516. D. J. Norris, M. G. Bawendi, and L. E. Brus, in "Molecular Electronics," (J. Jortner and M. Ratner, Eds.), Chap. 9. Blackwell Sci. Oxford, U.K., 1997.
517. K. H. Schmidt, G. Medeiros-Ribeiro, and P. M. Petroff, *Phys. Rev. B* 58, 3597 (1998).
518. S. Maimon, E. Finkman, G. Bahir, S. E. Achacham, J. M. Garcia, and P. M. Petroff, *Appl. Phys. Lett.* 73, 203 (1998).
519. D. Pan and E. Towe, *Electron. Lett.* 34, 1883 (1998).
520. D. L. Fuffaker, G. Park, Z. Zou, O. B. Shchekin, and D. G. Deppe, *Appl. Phys. Lett.* 73, 2564 (1998).
521. Y. Arakawa and H. Sakaki, *Appl. Phys. Lett.* 40, 939 (1982).
522. F. Schafer, J. P. Reithaier, and A. Forchel, *Appl. Phys. Lett.* 74, 2915 (1999).
523. F. Heinrichsdorff, C. Ribbat, M. Grundmann, and D. Bimberg, *Appl. Phys. Lett.* 76, 556 (2000).
524. M. Tzolov, F. Finger, R. Carius, and P. Hapke, *J. Appl. Phys.* 81, 7378 (1997).
525. A. Fujuwara, Y. Takahashi, and K. Murase, *Phys. Rev. Lett.* 78, 1532 (1997).
526. K. Tamamura, Y. Sugiyama, Y. Nakata, S. Muto, and N. Yokoyama, *Jpn. J. Appl. Phys.* 34, L1445 (1995).
527. J. R. Tucker, *J. Appl. Phys.* 72, 4399 (1992).
528. R. Tsu, *Physica B* 189, 235 (1993).
529. M. Tsukada, *Z. Phys. D* 19, 283 (1991).
530. H. Grabert, G.-L. Ingord, M. H. Devoret, D. Esteve, H. Pothier, and C. Urbina, *Z. Phys. B* 84, 143 (1991).
531. S. Tiwari, F. Rana, and K. Chan, *Appl. Phys. Lett.* 68, 1377 (1996).
532. A. Nakajima, T. Futatsugi, K. Kosemura, T. Fukano, and N. Yokoyama, *Appl. Phys. Lett.* 70, 1742 (1997).
533. C. W. Chan and S. Nie, *Science* 281, 2016 (1998).
534. M. Bruchez Jr., M. Moronne, P. Gin, S. Weiss, and A. P. Alivisatos, *Science* 281, 2013 (1998).
535. H. Hirai, H. Wakabayashi, and M. Komiyama, *Bull. Chem. Soc. Jpn.* 59, 367 (1986).
536. M. J. Bloemer, J. W. Haus, and P. R. Ashley, *J. Opt. Soc. Am. B* 7, 790 (1990).
537. T. W. Roberti, B. A. Smith, and J. Z. J. Zhang, *J. Chem. Phys.* 102, 3860 (1995).
538. E. J. Heilweil and R. M. Hochstrasser, *J. Chem. Phys.* 82, 4762 (1985).
539. E. A. Bollick and D. A. Ramsey, *J. Chem. Phys.* 29, 1418 (1958).
540. E. A. Bollick and D. A. Ramsey, *Astrophys. J.* 137, 84 (1963).
541. K. H. Hinkle, J. J. Keady, and P. F. Bernath, *Science* 241, 1319 (1988).
542. F. G. Celii and J. E. Butler, *Annu. Rev. Phys. Chem.* 42, 643 (1991).
543. R. Levy Gyyer and D. E. Koshland, *Science* 250, 1640 (1990).
544. R. F. Curl, *Rev. Mod. Phys.* 69, 691 (1997).
545. A. W. Snow and H. Wohltjen, *Chem. Mater.* 10, 947 (1998).
546. R. L. Whetten, J. T. Khoury, M. M. Alvarez, S. Murthy, I. Vezmar, Z. L. Wang, P. W. Stephens, C. L. Cleveland, W. D. Luedtke, and U. Landman, *Adv. Mater.* 8, 428 (1996).
547. "Cluster Assembled Materials" (K. Sattler, Ed.), Vol. 232. Trans Tech Publications, Zurich, 1997.
548. P. Melinon, V. Paillard, and J. Lerme, *Int. J. Mod. Phys.* 9, 339 (1995).
549. L. Motte, F. Billoudet, and M. P. Pileni, *Adv. Mater.* 8, 1018 (1996).
550. S. Komarneni, "Nanophase and Nanocomposite Materials," p. 459. Materials Research Soc., Boston, MA, 1992.
551. B. Michel, E. Delamarche, and C. Gerber, *Adv. Mater.* 8, 719 (1996).
552. G. Benedek, L. Colombo, and S. Serra, *J. Chem. Phys.* 106, 2311 (1997).
553. G. Benedek, E. Galvani, and S. Serra, *Chem. Phys. Lett.* 244, 339 (1995).
554. "Light Emission in Silicon: From Physics to Devices" (D. J. Lockwood, Ed.), Vol. 49. Academic Press, San Diego, 1998.
555. L. Tsybeskov, S. P. Duttagupta, K. D. Hirschmann, and P. M. Fauchet, *Appl. Phys. Lett.* 68, 2058 (1996).
556. L. Tsybeskov, K. L. Moore, and P. M. Fauchet, *Appl. Phys. Lett*. 69, 3411 (1996).

557. N. Lalic and J. Linnros, *J. Lumin.* 80, 263 (1998).
558. K. D. Hirschman, L. Tsybeskov, S. P. Duttagupta, and P. M. Fauchet, *Nature* 384, 338 (1996).
559. D. K. Ferry and S. M. Goodnick, "Transport in Nanostructures," Cambridge Univ. Press, New York, 1997.
560. A. Ohata, H. Niiyama, and A. Toriumi, *Jpn. J. Appl. Phys.* 34, 4485 (1995).
561. A. S. Bell, B. Brezger, U. Drodofsky, S. Nowak, T. Pfau, J. Stuhler, T. Schulze, and J. Mlynek, *Surf. Sci.* 433, 40 (1999).
562. B. Faircloth, H. Rohrs, R. Tiberio, R. Ruoff, and R. R. Krchnavek, *J. Vac. Sci. Technol. B* 18, 1866 (2000).
563. K. Kragler, E. Gunther, and G. Saemann-Ischenko, *Appl. Phys. Lett.* 67, 1163 (1995).
564. S. Dong and F. Zhu, *Vac. Sci. Technol.* 10, 379 (1990).
565. F. Thibaudau, J. R. Roche, and F. Salvan, *Appl. Phys. Lett.* 64, 523 (1994).
566. E. E. Ehrichs, S. Yoon, and A. L. de-Lozanne, *Appl. Phys. Lett.* 53, 2287 (1988).
567. D. P. Adams, T. M. Mayer, and B. S. Schwartzentruber, *Appl. Phys. Lett.* 68, 2210 (1996).
568. F. Marchi, D. Tonneau, H. Dallaporta, R. Pierrisnard, V. Bouchiat, V. I. Saforov, P. Doppelt, and R. Even, *Microelectron. Eng.* 50, 59 (2000).
569. A. Laracuente, M. J. Bronikowski, and A. Gallangher, *Appl. Surf. Sci.* 107, 11 (1996).
570. T. M. H. Wong, S. J. O'Shea, A. W. McKinnon, and M. E. Welland, *Appl. Phys. Lett.* 67, 786 (1995).
571. T. Muhl, H. Bruckl, and G. Reiss, *J. Appl. Phys.* 82, 5255 (1997).
572. C. Lebreton and Z. Z. Wang, *Surf. Sci.* 382, 193 (1997).
573. T. Abe, K. Hane, and S. Okuma, *J. Appl. Phys.* 75, 1228 (1994).
574. S. C. Eagle and G. K. Feder, *Appl. Phys. Lett.* 74, 3902 (1999).
575. J. H. Chen, G. Jianian, and J. A. Switzer, *Appl. Phys. Lett.* 71, 1637 (1997).
576. L. Nan, T. Yoshinobu, and H. Iwasaki, *Appl. Phys. Lett.* 74, 1621 (1999).
577. J. A. Dagata, J. Schneier, H. H. Harary, C. J. Evans, M. T. Postek, and J. Bennet, *Appl. Phys. Lett.* 56, 2001 (1990).
578. H. C. Day and D. R. Allee, *Appl. Phys. Lett.* 62, 2691 (1993).
579. E. S. Snow and P. M. Campbell, *Appl. Phys. Lett.* 64, 1932 (1994).
580. K. S. Pitzer and E. Clementi, *J. Am. Chem. Soc.* 81, 4477 (1959).
581. C. Liang and H. F. Schaefer III, *J. Chem. Phys.* 93, 8844 (1990).
582. J. Feng, Z. Wang, and M. C. Zerner, *Int. J. Quantum Chem.* 37, 599 (1990).
583. L. Wang, P. S. Davids, A. Saxena, and A. R. Bishop, *J. Phys. Chem. Solids* 54, 1493 (1993).
584. G. Endredi and J. Ladik, *J. Mol. Struct.* 300, 405 (1993).
585. D. Tomanek, *Comments At. Mol. Phys.* 31, 337 (1995).
586. S. Schuppler, S. L. Friedmann, M. A. Marcus, D. L. Adler, Y.-H. Xie, F. M. Ross, Y. J. Chabal, T. D. Harris, L. E. Brus, W. L. Brown, E. E. Chaban, P. F. Szajowski, S. B. Christman, and P. H. Citrin, *Phys. Rev. B* 52, 4910 (1995).
587. L.-W. Wang and A. Zunger, in "Nanocrystalline Semiconductor Materials," (P. V. Kamat and D. Meisel, Eds.), Elsevier, New York, 1996.
588. Y. Osaka, K. Tsunemoto, F. Toyomura, H. Myoren, and K. Kohno, *Jpn. J. Appl. Phys.* 31, L565 (1992).
589. S. H. Risbud, L. C. Liu, and J. F. Shackelford, *Appl. Phys. Lett.* 63, 1648 (1993).
590. W. A. Saunders, P. C. Sercel, R. B. Lee, H. A. Atwater, K. J. Vahala, R. C. Flagan, and E. J. Escorcia-Aparcio, *Appl. Phys. Lett.* 63, 1549 (1993).
591. S. Iwasaki, T. Ida, and K. Kimura, *Jpn. J. Appl. Phys.* 35, L551 (1996).
592. Y. Kanemitsu, *Phys. Rev. B* 49, 16,845 (1994).
593. C. Y. Cha, G. Ganteför, and W. Eberhardt, *Z. Phys. D* 26, 307 (1993).
594. C. L. Pettiette, S. H. Yang, M. J. Craycraft, J. Conceicao, R. T. Laaksonen, O. Cheshnovsky, and R. E. Smalley, *J. Chem. Phys.* 88, 5377 (1988).
595. A. L. Rogach, A. Koronowski, M. Gao, A. Eichmüller, and H. Weller, *J. Phys. Chem.* 103, 3065 (1999).
596. S. Y. Ren and J. D. Dow, *Phys. Rev. B* 45, 6492 (1992).
597. M. Lonfat, B. Marsen, and K. Sattler, to be published.
598. B. Delley, E. F. Steigmeier, and H. Auderset, *Bull. Am. Phys. Soc.* 37, 719 (1992).
599. M. Hirao, T. Uda, and Y. Murayama, *Mater. Res. Soc. Symp. Proc.* 283, 425 (1993).
600. J. W. Mintmire, *J. Vac. Sci. Technol. A* 11, 1733 (1993).
601. A. J. Read, R. J. Needs, K. J. Nash, L. T. Canham, P. D. J. Calcott, and A. Qteish, *Phys. Rev. Lett.* 69, 1232 (1992).